Application of Signal Tracking Methods for Fringe Analysis

A thesis submitted
in partial fulfillment for the degree of

Doctor of Philosophy

by

RAHUL G WAGHMARE

Department of Avionics
INDIAN INSTITUTE OF SPACE SCIENCE AND TECHNOLOGY
Thiruvananthapuram - 695547

January 2017

to the singular location in space around which revolves my entire universe.

CERTIFICATE

This is to certify that the thesis titled **Application of Signal Tracking Methods for Fringe Analysis**, submitted by **Rahul G. Waghmare**, to the Indian Institute of Space Science and Technology, Thiruvananthapuram, for the award of the degree of **Doctor of Philosophy**, is a bona-fide record of the research work done by him under our supervision. The contents of this thesis, in full or in parts, have not been submitted to any other Institute or University for the award of any degree or diploma.

Dr. Deepak Mishra
Supervisor
Department of Avionics
IIST Trivandrum

Dr. R. K. S. Subrahmanyam Gorthi
Co-Supervisor
Department of Avionics
IIST Trivandrum

Place: Thiruvananthapuram
January 2017
.

Counter signature of Head,
Department of Avionics
with seal

DECLARATION

I declare that this thesis titled **Application of Signal Tracking Methods for Fringe Analysis** submitted in fulfilment of the Degree of Doctor of Philosophy is a record of original work carried out by me under the supervision of **Dr. Deepak Mishra** and **Dr. R. K. S. Subrahmanyam Gorthi**, and has not formed the basis for the award of any degree, diploma, associateship, fellowship or other titles in this or any other Institution or University of higher learning. In keeping with the ethical practice in reporting scientific information, due acknowledgements have been made wherever the findings of others have been cited.

Rahul G Waghmare
SC11D025

Place: Thiruvananthapuram
January 2017

ACKNOWLEDGEMENTS

Every PhD has a unique story; and while narrating mine, I cannot proceed further without acknowledging the people, who made this story interesting and presentable.

First, I express my sincere gratitude towards my research supervisors **Dr. Deepak Mishra** and **Dr. R. K. Sai Subrahmanyam Gorthi** for their valuable guidance, technical as well as moral support, immeasurable patience and continuous encouragements during entire PhD work. I am eternally indebted to them for the friendly and enthusiastic work environment that has certainly helped me during the ups and downs in my professional as well as personal life.

I take this opportunity to thank my doctoral committee members- Prof. P. J. Narayanan, Prof. R. Krishnan, Prof. N. Padmanabhan for their regular and valuable comments and suggestions, and for steering the PhD thesis along the proper path. I would like to express my gratitude towards **Dr. Sai Siva Gorthi, Asst. Prof., IISc Bangalore** and **Dr. Rakesh Kumar Singh, Asst. Prof., IIST Trivandrum** for making their labs available for experimental study, and for the meticulous review of every manuscript I worked on. I express my gratitude towards Dr. Earu Banoth, and Shri. Ram Sukumar for their collaboration and fruitful discussions.

I thank Prof. Thomas Kurian, Former Head, Dept. of Avionics, Dr. Selva Ganeshan, Former Head, Dept. of Avionics, and Prof. Manoj B. S., Head, Dept. of Avionics and Chairman, Doctoral Committee for their encouragement and suggestions towards improvement of my research. I am extremely thankful to the Director, IIST for his support and permissions to attend technical conferences and workshops during my tenure. I thank Department of Space, Government of India, for providing me IIST-ISRO Research Fellowship. I take this opportunity to acknowledge the support of all the professors for building my foundation through course work.

I am highly grateful to Dr. Litesh Sulbhewar, Dr. C. K. Muthukumaran, Shri. Gaurav Harsha, Shri. Malai Devan, Shri. Latheef Shaik, Kum. Mahima Singh, Kum. Tamanna Meena, Kum. Apoorva Kinhikar for making my PhD experience joyful and easy going. I am very much thankful to my fellow hostel mates for the late night discussions ranging from technical difficulties, current science to the very essence of life. I also thank Shri. Gopakumar G., Shri. Anurup Guha, Shri. Nidheesh Ravi, and students of M. Tech.– Digital Signal Processing (esp. 2014-16 and 2015-17 Batch) for creating joyful and friendly environment in Virtual Reality lab, my workplace.

At last, this PhD would have been just a dream without support of my relatives. I take this opportunity to thank my grandparents, late shri Narayan Waghmare and Late smt. Anasuyabai Waghmare, who blessed me through my childhood and primary education, Shri. Rajaram Waghmare (Kaka and Kaku) and Shri. Prashant Thamke for their immeasurable support during my high school education, Dr. Mahendra Bharne (Doctor Kaka and Kaku) and Capt. Milind Bhagat (and Vandana Tai) for making my dream of engineering a reality. I am grateful to Dr. S. L. Nalbalwar, Associate Prof. and Head, Dept. Electronics & Telecomm. Engg., Dr. B. A. Technological University, Lonere for his motivation, trust and encouragements during my stay at the university. I believe that all this would not have been possible without continuous blessings of my parents late Shri. Gautam Waghmare, late Sau. Mangala Waghmare and Smt. Chhaya Waghmare. At the end, I would like to express my appreciation to my brothers, sisters and beloved wife for providing peaceful environment and bearing me during my PhD research work.

Rahul G Waghmare

ABSTRACT

Simultaneous estimation of phase and its derivatives from a single record of interference field gives significant insights about properties of an object in terms of deformation, strain, curvature and twists. Current state-of-the-art methods provide either phase or phase derivatives from the fringe pattern; moreover their performance is greatly influenced by noise in the fringe pattern and the dynamic range of the phase. Thus, there exist a strong need for development of a phase estimation approach that can handle severely noisy fringe patterns and yet capable of estimating rapidly varying phase even when the phase is having larger dynamic range. This serves us a motivation for our current research work. The main objective of this thesis is to develop the unified, simple yet effective approach for simultaneous estimation of phase and phase derivatives from single record of reconstructed interference field that can handle different conditions present in the interference field like rapidly varying phase, larger dynamic range of the phase and extreme noise in the interference field.

This thesis proposes a novel approach, namely, signal tracking approach as an elegant solution for the phase estimation from reconstructed interference fringes. Signal tracking approach involves two important parts: state space model and tracking algorithm. In this work, state space model for signal tracking approach is derived using Taylor series approximation of the phase map as state model and Polar to Cartesian conversion as measurement model. We have proposed, tested and demonstrated the significance of our work through tracking algorithms that use this state space model such as extended Kalman filter (EKF), unscented Kalman filter (UKF), Particle filter (PF) and wrapped statistics based algorithm (WKF) as tracking algorithms. In order to demonstrate the utility of proposed algorithms, we performed different real-time experiments including digital holographic Interferometry (DHI) and fringe projection profilometry to measure out-off plane displacement and 3D reconstruction of an object, respectively.

It was observed that the wrapped statistics based algorithm satisfies all of our

goals providing the efficient solution of phase estimation problem when the interference fringes are extremely noisy and when underlying phase map has larger dynamic range and can be considered as better alternative for simultaneous estimation of phase and phase derivatives.

Finally, we conclude our work by showing different applications of the proposed signal tracking approach such as multi-component phase estimation in holographic moiré, 3D reconstruction of an object using fringe projection methods. Moreover, we also demonstrate that the proposed method is a suitable fringe analysis technique for practical purposes such as thermal expansion.

TABLE OF CONTENTS

LIST OF TABLES

LIST OF FIGURES

ABBREVIATIONS

MLE	Maximum Likelihood Estimation
DCFT	Discrete Chirp Fourier Transform
IHAF	Improved High-Order Ambiguity Function
CPF	Cubic Phase Function
SSA	State Space-based Approach
PF	Particle Filter
EKF	Extended Kalman Filter
UKF	Unscented Kalman Filter
WKF	Wrapped Kalman Filter
STA	Signal Tracking Approach
DHI	Digital Holographic Interferometry
CCD	Charge Coupled Device
AWGN	Additive White Gaussian Noise
SNR	Signal to Noise Ratio
RMSE	Root Mean Squared Error
WG	Wrapped Gaussian
PSWVD	Pseudo Wigner-Ville Distribution

CHAPTER 1

Introduction

In interferometric techniques, physical quantities are encoded into phase, and hence reliable phase estimation becomes the major task. These techniques include synthetic aperture radar for surface topography, magnetic resonance imaging for mapping of internal structure of the body, digital holographic interferometry and moiré for in-plane and out-off plane deformation assessment, fringe projection profilometry for 3D reconstruction of the object, digital holographic microscopy for study of microscopic biological objects, and many others. The term *phase* changes from method to method, e.g., in fringe projection profilometry, the phase means the phase of the sinusoids of the fringe pattern whereas in holography, phase means the phase of the actual light wave. However, following equation represents most general form for the interference field [Gorthi and Rastogi (2010a)].

$$\mathbf{\Gamma}(m,n) = a(m,n)exp(j\phi(m,n)) + \eta(m,n) \tag{1.1}$$

where, $\Gamma(m,n)$ represents the interference field, $a(m,n)$ is the real amplitude and $\phi(m,n)$ is the phase of the interference field. $\eta(m,n)$ is the noise, and is assumed to be white Gaussian with zero mean and variance σ_η^2. Spatial indices m and n denote the pixel location as a row and column number, respectively.

Several techniques have been proposed over last three decades for the analysis of these fringe patterns. These methods analyse the interference field via various transform domain filters such as Fourier transform [Takeda et al. (1982); Takeda and Mutoh (1983)], time-frequency analysis [Boashash (1992a,b)], local adaptive transform domain filters [Yaroslavsky (2007)] and many others [Zhou et al. (2012); Jiang et al. (2012); Paul Kumar et al. (2013); Kemao (2015)]. The fringe analysis methods developed based on local transform domain filters includes techniques such as windowed Fourier transform profilometry proposed by Kemao (2004), wavelet transform profilometry by Watkins et al. (1999) and Zhong and Weng (2004). The phase map generated by most of these methods is noisy and

wrapped. This requires careful selection of the combination of proper noise filtering [Lee et al. (1998); Palacios et al. (2004)] and phase unwrapping algorithms [Huang and Sheu (2005); Li et al. (2008); Goldstein et al. (1988); Schofield and Zhu (2003)]. Therefore it is desirable to have unified fringe analysis technique that does both the operations (noise filtering and unwrapping), simultaneously and produces continuous and accurate phase map from the fringe pattern.

In deformation analysis, phase of the reconstructed interference field provide the deformation measurement whereas first and second order derivatives of the phase give residual strain and curvature/twist in the object, respectively. Hence, estimation of phase derivatives helps in applications such as fault detection [Qian et al. (2005)], quality assurance [Steinchen et al. (1995)], strain detection in bone sections [Alvarez et al. (2014a,b)]. Phase derivatives can be calculated from the estimated phase map, which is estimated using `arctan` and unwrapping methods, by numerical differentiation. When the interference field becomes noisy, the estimated phase by such approach becomes noisy too. In the numerical differentiation of such noisy phase results in noisy phase derivatives. Thus accurate and simultaneous estimation of phase and its derivatives from the fringe pattern has become highly sought after research field in recent years.

This thesis proposes a signal tracking approach for simultaneous estimation of phase and derivatives of arbitrary order from the interference pattern. With simulation and experimental analysis of each of the algorithm, we demonstrate the real time applicability of the proposed approach in various scenarios. These scenarios include extremely noisy fringe pattern, rapidly varying phase and the phase map with larger dynamic range. Section (1.1) gives a brief review of literature in the area of fringe analysis. Section (1.2) defines objectives of the research carried out for this thesis, and finally outline of the thesis is summarized in Section (1.4).

1.1 State-of-the-art

Fringe analysis methods available in literature can be predominantly categorised into three groups.

1. Phase Unwrapping Methods
2. Piecewise Polynomial Phase Approximation Approach
3. Non-parametric Approaches

1.1.1 Phase Unwrapping Methods

The phase values retrieved by fringe analysis techniques are always limited to the principal range $(-\pi, \pi]$ and is known as wrapped phase. Continuous phase is obtained from the wrapped phase by adding or subtracting the integer multiples of 2π at each pixel value to obtain the unwrapped phase map without any induced discontinuities. This process is known as phase unwrapping. Many phase unwrapping algorithms have been developed over the past decades [Goldstein et al. (1988); Huntley (1989); Bone (1991); Lim et al. (1995); Ghiglia and Pritt (1998); Zappa and Busca (2008)]. Most of the phase unwrapping algorithms fall into two groups, namely, path following algorithms and least-squares based approach. In path following algorithms the path for unwrapping is chosen such that areas of lesser inconsistencies are processed first followed by processing of higher inconsistencies [Huntley (1989); Flynn (1996); Asundi and Wensen (1998); Xu and Cumming (1999); Gutmann and Weber (2000); Baldi (2003); Huang and Sheu (2005)]. While others use least squares based approach for phase unwrapping [Hunt (1979); Ghiglia and Romero (1996); Flynn (1997)]. The main limitation of the phase unwrapping algorithms is that their performance is influenced by the noise present in the fringe pattern making them unreliable in noisy fringes.

1.1.2 Piecewise Polynomial Phase Approximation Approach

The piecewise polynomial phase approximation approach was proposed by Gorthi and Rastogi (2009c) for direct estimation of unwrapped and continuous phase from reconstructed interference field. In this approach, each column (or row) of phase map is divided into segments. Each segment is then approximated using polynomial of sufficiently higher order. The coefficients of these phase polynomials are then estimated by analysing the respective segment of the interference

field using signal processing techniques such as Maximum Likelihood Estimation (MLE) [Gorthi and Rastogi (2009c)], Discrete Chirp-Fourier Transform (DCFT) [Gorthi and Rastogi (2009a)], Cubic Phase Function (CPF) [O'Shea (2002); Gorthi and Rastogi (2010b)], High-order Ambiguity Function (HAF) [Barbarossa and Petrone (1997); Gorthi and Rastogi (2009b)], Polynomial phase transform [Peleg and Friedlander (1995)], State Space Based Approach (SSA) [Rajshekhar and Rastogi (2013)] and others. These methods are useful in digital holographic interferometry provided that the phase maps can be approximated with piecewise low order polynomials. If the order of polynomial increases, number of data points required per segment also increases. This makes piecewise polynomial approximation approach less reliable for rapidly varying phase. In addition, as the phase map generated by these methods is discontinuous at the end points of each segment, phase stitching becomes an essential part of the algorithm.

1.1.3 Non-parametric Approaches

The non-parametric approaches are mostly based on time-frequency distributions of the complex fringe pattern [Katkovnik (1997)]. This approach is generally applied for phase derivative estimation [Boashash (1992a,b)]. In this approach, each column (or row) of the complex interference field is treated as arbitrary function. This function is then analysed using different time-frequency resolution distribution functions like 1D pseudo Wigner-Ville distribution [Barkat and Boashash (1999); Rajshekhar et al. (2009)], 2D pseudo Wigner-Ville distribution [Rajshekhar et al. (2010a)]; complex-lag distributions [Rajshekhar and Rastogi (2011)]; discrete energy separation algorithms [Kulkarni and Rastogi (2014)], adaptive window spectrogram [Rajshekhar et al. (2010b)], auto term window [Liu (2013)], least square approach [Jakob2000], transport of intensity equations [Volkov et al. (2002)], combination of enhanced phase gradient estimator and path-following strategy [Xie and Li (2014)] and many others [Gorthi and Rastogi (2009d); Rajshekhar et al. (2011a); Rajshekhar and Rastogi (2012)]. These methods provide accurate phase derivatives as long as the phase derivative values are confined to principal range of $(-\pi, \pi]$. In addition, to get the phase map, we need to integrate the phase gradients, which is computationally expensive.

We have identified discrete chirp-Fourier transform, improved high-order ambiguity function and state space approach based phase estimation algorithms as representative candidates of the piecewise polynomial approximation category, whereas Pseudo Wigner-Ville distribution method as representative example of the non-parametric phase derivative estimation approach. These methods are the best known for their accuracy and computational complexity. We discuss each of these methods, in brief, explaining the theoretical foundation which is used for estimation of phase and/or phase gradient.

Discrete Chirp-Fourier Transform [Gorthi and Rastogi (2009a)]

In DCFT, the phase is approximated by second order polynomial. Thus the complex interference field represented by equation (1.1), for arbitrary column, is rewritten as:

$$\mathbf{\Gamma}(n) = a(n)exp(j\sum_{q=0}^{2} a_q n^q) + \eta(n)$$

For piecewise polynomial approximation, row/column of the phase is divided into overlapping or non-overlapping segments of length $N_s < N$, where N is the length of a row/column. Hence, the discrete chirp-Fourier transform for a given segment is defined as [Xia (Nov 2000)]:

$$G(k_1, k_2) = \sum_{n=0}^{N_s-1} \mathbf{\Gamma}(n)exp(-j(\alpha_{k_1} n + \beta_{k_2} n^2)) \tag{1.2}$$

Where,

$$\alpha_{k_1} = \frac{2\pi}{N_s} k_1 \ \ \forall \ \ 0 \leq k_1 \leq N_s - 1$$

$$\beta_{k_2} = \frac{2\pi}{N_s^2} k_2 \ \ \forall \ \ -N_s + 1 \leq k_2 \leq N_s - 1$$

Location of the peak in DCFT-domain, in terms of α_{k_1} and β_{k_2}, indicates that the values of α_{k_1} and β_{k_2} match with the actual coefficients of the second order polynomial, which is used to approximate the phase function.

The DCFT based method produces accurate and unwrapped phase from extremely noisy interference field. However, It cannot handle rapidly varying phase

map, because the phase is being approximated by quadratic function.

Improved High-order Ambiguity Function [Gorthi and Rastogi (2009b)]

In IHAF, the phase is approximated by polynomials upto order M. M^{th} order ambiguity function for the interference field is given by:

$$PT_M(\mathbf{\Gamma}, \omega, \tau) = \sum_{n=(M-1)\tau}^{N} P_M(\mathbf{\Gamma}(n), \tau) e^{-j\omega n}$$

Where,

$$P_M(\mathbf{\Gamma}(n), \tau) = \prod_{q=o}^{M-1} [\mathbf{\Gamma}^{\dagger q}(n - q\tau_q)]^{\binom{M-1}{q}}$$

$$\binom{M-1}{q} = \frac{(M-1)!}{(M-1-q)!q!}$$

$$\mathbf{\Gamma}^{\dagger q}(x) = \begin{cases} \mathbf{\Gamma}(x) & \text{if } q \text{ is even} \\ \mathbf{\Gamma}^*(x) & \text{if } q \text{ is odd} \end{cases}$$

* denotes the complex conjugation.

Highest order coefficient of the polynomials are computed as:

$$a_M = \frac{1}{M!\tau^{M-1}} \underset{\omega}{\operatorname{argmax}} |PT_M(\mathbf{\Gamma}, \omega, \tau)|$$

Iterative frequency estimation by interpolation on Fourier coefficients (IFEIF) is used to optimize the above function, that tremendously improves the computational time of this method. This process of estimating the highest-order coefficient in each iteration and peeling off the signal to reduce its polynomial phase order is repeated until all the coefficients are estimated.

State Space based Approach [Rajshekhar and Rastogi (2013)]

The model of the variable amplitude M^{th} order polynomial phase signal $\mathbf{\Gamma}(n)$ embedded in additive white Gaussian noise $w(n)$ can be written as

$$\mathbf{\Gamma}(n) = a(n)exp(j\sum_{q=0}^{M} a_q n^q) + w(n) \tag{1.3}$$

where, n is the integer representing the pixel location along row/column

Taking, $\mathbf{F} = \begin{bmatrix} 1 & 0 & 0 & \cdots & 0 \\ 0 & 1 & \frac{1}{1!} & \cdots & \frac{1}{M!} \\ \vdots & \vdots & \vdots & \ddots & \vdots \\ 0 & 0 & 0 & \cdots & 1 \end{bmatrix}$, and $\mathbf{x}(n) = \begin{bmatrix} a & \phi & \phi^{(1)} & \phi^{(2)} & \cdots & \phi^{(M)} \end{bmatrix}^T$

the state model is written as:

$$\mathbf{x}(n+1) = \mathbf{F}\mathbf{x}(n) + G\omega(n) \tag{1.4}$$

The observation model is written as:

$$\mathbf{z}(n) = \mathbf{h}(\mathbf{x}(n)) + \nu(n) \tag{1.5}$$

where, $\mathbf{h}(\mathbf{x}(n)) = \begin{bmatrix} x(1)cos(x(2)) \\ x(1)sin(x(2)) \end{bmatrix}$

With known state estimate at $y - N_s$, the coefficients of polynomial are then computed using relation:

$$\begin{bmatrix} a_0 \\ a_1 \\ \vdots \\ a_M \end{bmatrix} = \begin{bmatrix} 1 & n & n^2 & \cdots & n^M \\ 0 & 1 & 2n & \cdots & Mn^{M-1} \\ 0 & 0 & 2 & \cdots & M(M-1)n^{M-2} \\ \vdots & \vdots & \vdots & \ddots & \vdots \\ 0 & 0 & 0 & \cdots & M! \end{bmatrix}^{-1} \begin{bmatrix} \hat{x}(2) \\ \hat{x}(3) \\ \vdots \\ \hat{x}(M+2) \end{bmatrix} \tag{1.6}$$

Pseudo Wigner-Ville distribution [Rajshekhar et al. (2009)]

Wigner-Ville distribution of the time domain signal is given by

$$\mathcal{W}(n,\omega) = \int_{-\infty}^{\infty} \mathbf{\Gamma}(n+\frac{u}{2})\mathbf{\Gamma}^*(n-\frac{u}{2})e^{-j\omega u}du \tag{1.7}$$

replacing $\frac{u}{2}$ with τ,

$$\mathcal{W}(n,\omega) = 2\int_{-\infty}^{\infty} \mathbf{\Gamma}(n+\tau)\mathbf{\Gamma}^*(n-\tau)e^{-j\omega\tau}d\tau \tag{1.8}$$

The pseudo Wigner-Ville distribution is formed by introducing a windowed function $w(\tau)$ in the original Wigner-Ville distribution and neglecting the constant outside the integration, we get:

$$\mathcal{PW}(n,\omega) = \int_{-\infty}^{\infty} w(\tau)\mathbf{\Gamma}(n+\tau)\mathbf{\Gamma}^*(n-\tau)e^{-j\omega\tau}d\tau \tag{1.9}$$

suppose the function to be analysed, $\mathbf{\Gamma}(n)$, is of the form

$$\mathbf{\Gamma}(n) = a(n)e^{j\phi(n)} + \eta(n) \tag{1.10}$$

Neglecting the noise term and assuming the amplitude variations to be small, we can represent the same function as

$$\mathbf{\Gamma}(n) = a(n)e^{j\phi(n)} \tag{1.11}$$

The pseudo Wigner-Ville distribution, then, becomes-

$$\begin{aligned} \mathcal{PW}(n,\omega) &= \int_{-\infty}^{\infty} w(\tau)a(n)e^{j\phi(n+\tau)}a(n)e^{-j\phi(n-\tau)}e^{-j\omega\tau}d\tau & (1.12)\\ &= a^2(n)\int_{-\infty}^{\infty} w(\tau)e^{j[\phi(n+\tau)-\phi(n-\tau)]}e^{-j\omega\tau}d\tau & (1.13) \end{aligned}$$

Within the window region, the phase is assumed to be slowly varying. So using second order Taylor series expansion

$$\phi(n+\tau) = \phi(n) + \tau\phi'(n) + \frac{\tau^2}{2}\phi''(n) \tag{1.14}$$

$$\phi(n-\tau) = \phi(n) - \tau\phi'(n) + \frac{\tau^2}{2}\phi''(n) \tag{1.15}$$

$\therefore$

$$\phi(n+\tau) - \phi(n-\tau) = 2\tau\phi'(n) \tag{1.16}$$

Equation 1.13 then becomes

$$\mathcal{PW}(n,\omega) = a^2(n)\int_{-\infty}^{\infty} w(\tau)e^{j2\tau\phi'(n)}e^{-j\omega\tau}d\tau \tag{1.17}$$

Using time shifting property of the Fourier transform,

$$\mathcal{PW}(n,\omega) = a^2(n)\mathcal{F}\{w(2\tau - 2\phi'(n))\} \tag{1.18}$$

Since the window is chosen to have a low pass behaviour, $\mathcal{PW}(x,\omega)$ is maximum for $\mathcal{F}\{w(0)\}$. i.e., when $\tau = \phi'(n)$

$$\therefore \phi'(n) = \arg\max_{\omega} \mathcal{PW}(n,\omega) \tag{1.19}$$

The pseudo Wigner-Ville distribution based method provides only first order phase derivative. In order to estimate the phase map, numerical integration of the phase gradient is essential. Moreover, for estimation of the higher order phase derivatives, we need to form reconstructed interference field using estimated first order phase derivatives and process it again.

1.2 Thesis objectives

We follow, from above discussion, that there exist a strong need of development of novel phase estimation approach that can handle severely noisy fringe pattern and yet capable of estimating rapidly varying phase even when the phase is having larger dynamic range. Additionally, Estimation of phase derivatives from a single

record of interference field gives significant insights about deformed object in terms of strain, curvature and twists. This serves us a motivation for our current research work.

The main objective of this thesis is to develop simple yet effective approach for simultaneous estimation of phase and phase derivatives from *single record* of reconstructed interference field that can handle different conditions present in the interference field like:

- *Larger dynamic range* of the phase map to increase the dynamic range of out-of-plane deformation,
- *Rapidly varying phase* map to meet the real time scenarios,
- *Extreme noise* in the interference field,
- *Simultaneous estimation of phase and phase derivatives* from interference fringe patterns without additional computational load.

In other objectives, our research work is intended to aid as an efficient tool for fringe analysis with following advantages.

- Deformation measurement at rough and diffusely reflecting surface, which occurs frequently in engineering, in real-time environment without worrying about noisy interference field.
- out-off plane measurement range with extended range from hundredth of wavelength to several hundreds of wavelengths, e.g., displacement from about $0.001\mu m$ to $500\mu m$
- Analysis of strain/stress, curvature, twists in the deformed objects via simultaneous estimation of phase and its derivatives.
- With proper fringe normalization algorithm, possible extension of the signal tracking approach for fringe projection profilometry for accurate calculation of 3D shape of the object.

1.3 Contributions

Following are the contributions of our research work which makes the major part of the thesis.

- We proposed a signal tracking based phase estimation from reconstructed interference field in digital holographic interferometry. We developed Extended Kalman Filter (EKF) and Unscented Kalman Filter (UKF) based algorithms to estimate accurate, continuous and unwrapped phase maps even from noisy interference field.
- We developed a novel weight calculation approach for particle filter through which we extended the performance of signal tracking approach which enables better performance even when the phase is rapidly varying and having larger dynamic range.
- We proposed a wrapped dynamical system based approach for extending the performance of signal tracking approach when the interference field is noisy as well as the phase is rapidly varying.
- We compared and proved that the signal tracking approach provides accurate estimates of phase derivatives, without additional computing requirement, when compared with state-of-the-art phase derivative estimation approaches.
- We demonstrated the possibility and potential of signal tracking approach for multicomponent phase estimation to provide an efficient tool in holographic moiré.
- We demonstrated through experimental analysis of thermal expansion and fringe projection profilometry that the developed signal tracking approach is reliable for real time scenarios.

1.4 Outline of the Thesis

The outline of the thesis is as follows:

Chapter 2 introduces basic mathematical preliminaries such that the reader can get acquainted with the methods proposed in the thesis. This chpater summarizes the numerical processing of digital holograms for the generation of reconstruction interference field. We then briefly overview the generic Kalman filter and particle filter framework followed by discussion.

Chapter 3 presents a signal tracking based phase estimation from reconstructed interference field in digital holographic interferometry. We developed Extended Kalman Filter (EKF) and Unscented Kalman Filter (UKF) based algorithms to estimate accurate, continuous and unwrapped phase maps even from noisy interference field.

Chapter 4 presents a novel weight calculation approach for particle filter through which we extended the performance of signal tracking approach which enables better performance even when the phase is rapidly varying and having larger dynamic range.

Chapter 5 proposes a wrapped dynamical system based approach for extending the performance of signal tracking approach when the interference field is noisy as well as the phase is rapidly varying.

Chapter 6 shows the possibility and potential of signal tracking approach for accurate and simultaneous estimation of phase derivatives, when compared with state-of-the-art phase derivative estimation approaches. We also discuss the multicomponent phase estimation to provide an efficient tool in holographic moiré and fringe projection profilometry.

Chapter 7 summarizes the contributions of the thesis, followed by future scope of our research work.

CHAPTER 2

Mathematical Preliminaries

In this chapter, we will discuss the background mathematical pre-requisites and generic framework of the signal tracking algorithms. First the brief overview of the numerical reconstruction of the digital hologram and formation of reconstructed interference field is explained, followed by the discussion on Kalman filter and particle filter framework in the subsequent sections. Numerical processing of the digital hologram provides a brief idea about the setup used for digital holographic interferometry experiment. In addition to this, brief review of generation of reconstructed interference field from the extracted complex optical field of the object wave is presented. This thesis deals with the signal tracking approach, where we define the state space model for estimation of unobserved variable (unwrapped phase) from the observed data (complex interference field). Two major state estimation algorithms, Kalman and particle filters, are available in literature that provides hidden state estimation. Brief overview of them with their generic framework is discussed in the consequent sections.

2.1 Numerical Processing of Digital Holograms

In this section, we provide a brief review of the process of hologram acquisition and its numerical processing. Digital Holography is a technique where the interference pattern of the reference wave with object wave (light scattered from diffuse object) is recorded by CCD sensors and then numerically processed so that the 3D information can be extracted from the object wave [Sun (2009); Fan et al. (2009)]. The experimental setup used for recording the digital holographic interferograms is shown in Figure 2.1. A Laser (HNL150L-HeNE laser, 632.8nm, 15mW, Thorlab US) has been used as the light source. The beam is split into two equal halves (BE1-object beam, BE2- reference beam) with the help of a non-polarizing beam splitter cube (BS010 Thorlab). Digital holograms are recorded with a monochrome CCD camera (DMK72BUC02 imaging source).

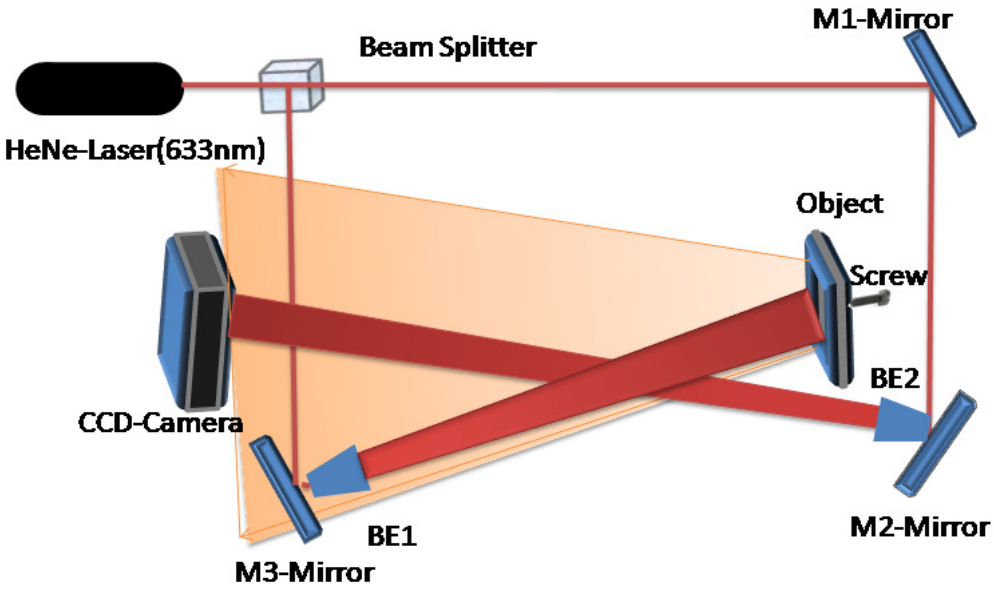

Figure 2.1: Experimental setup used for digital holographic interferometry to record the hologram on the optical bench

The test specimen was made out of aluminum (0.5 mm thickness) and held on the optical table by clamping the plate on all four sides with a custom-designed mount. A threaded bore (M4 screw thread) was created at the center on the backside of the mount, such that driving an M4-screw through this bore would induce a deformation in the object (plate). Broadband dielectric mirrors (M1, M2, M3) (BB1-E02 Thorlab) mounted onto adjustable precision kinematic mirror mounts (KS1 Thorlab) were used to adjust the direction of beams. The two beams reflected off the mirrors (M2, M3) were expanded using two concave lenses (f-80mm). The beam of light scattered by the object interferes with the reference beam in a 3D volume of space. The intensity record of the cross section of this 3D volume recorded using CCD sensor is termed as digital hologram.

let R be the reference wave, O be the object wave, then the intensity distribution due to interference of these two waves is given by

$$\begin{aligned} I &= (R+O)\cdot(R+O)^* \\ &= R\cdot R^* + R\cdot O^* + O\cdot R^* + O\cdot O^* \\ &= |R|^2 + |O|^2 + R\cdot O^* + O\cdot R^* \end{aligned} \tag{2.1}$$

where, * denotes complex conjugate. Here, the indices (m, n), which represent the location of the pixel along rows and columns, respectively, are removed for the sake of brevity. The amplitude recorded by CCD sensors, $h(m, n)$ can be written in terms of intensity distribution $I(m, n)$ as:

$$h(m, n) = \beta\tau I(m, n) \tag{2.2}$$

where, β is constant, τ is the exposure time and the function $h(m, n)$ is called as hologram function.

For hologram reconstruction, recorded amplitude have to be multiplied with reference (reconstruction) wave:

$$\begin{aligned} R \cdot h &= [\beta\tau I(m, n)] \cdot R \\ &= [\beta\tau(|R|^2 + |O|^2 + R \cdot O^* + O \cdot R^*)] \cdot R \\ &= \underbrace{\beta\tau(|R|^2 + |O|^2) \cdot R}_{} + \underbrace{\beta\tau|R|^2 \cdot O}_{} + \underbrace{\beta\tau R^2 \cdot O^*}_{} \end{aligned} \tag{2.3}$$

In equation (2.3), the first term on the right side of this equation is the reference wave, multiplied by a factor. It represents the un-diffracted wave passing through the hologram, the second term is the reconstructed object wave, forming the virtual image. The factor $\beta\tau|R|^2$ only influences the brightness of the image, while the third term produces a distorted real image of the object. These terms are separated in frequency domain, and can be separated by taking Fourier transform.

The virtual image is used for the further analysis of the object like deformation analysis, vibration analysis etc., using digital holographic interferometry. In Digital Holographic Interferometry, usually, two holograms are recorded corresponding to the object state before and after the deformation. Numerical reconstruction of these holograms provides their respective reconstructed object wave-fields. Multiplication of one reconstructed object wave-field with that of complex conjugate of the other, generates the *reconstructed interference field*. The phase of this reconstructed interference field carries the information of the full-field deformation undergone by the object. Step by step procedure is depicted in figure 2.2.

Let, the complex amplitude of object wave obtained using numerical recon-

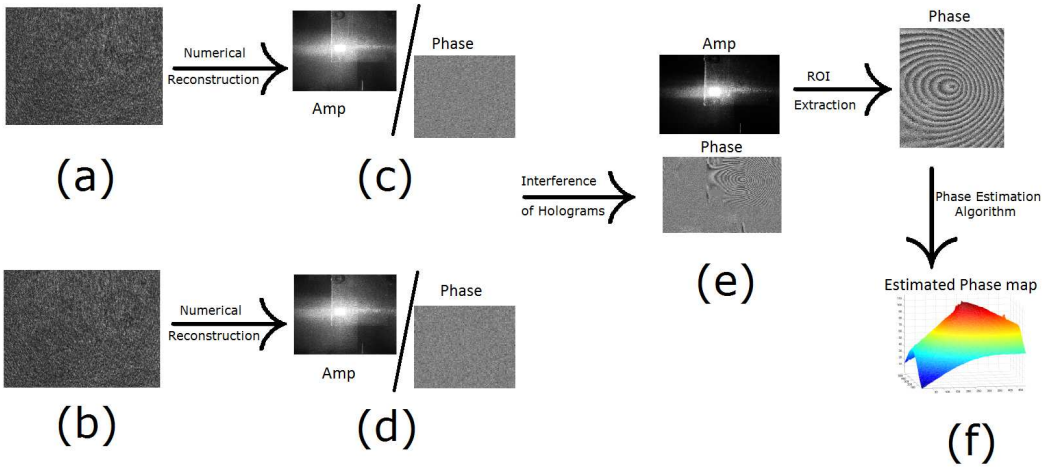

Figure 2.2: Flowchart of digital holographic interferometry. (a) and (b) represent the holograms recorded before and after the deformation. (c) and (d) represent corresponding reconstructed complex object waves. (e) represents the amplitude and phase of reconstructed interference field, while (f) shows the wrapped (top) and unwrapped phase map (Bottom) corresponding to analysis region.

struction is given by

$$O_1(m,n) = o(m,n)e^{i\varphi(m,n)} \tag{2.4}$$

where $o(m,n)$ is amplitude and $\varphi(m,n)$ is the phase of object wave. Optical path changes due to deformations on object surface can be described by variations in phase from $\varphi(m,n)$ to $\varphi(m,n) + \phi(m,n)$. $\phi(m,n)$ is called as interference phase. the complex amplitude of object wave after deformation is given by:

$$O_2(m,n) = o(m,n)e^{i[\varphi(m,n)+\phi(m,n)]} \tag{2.5}$$

The reconstructed interference field can then be obtained by multiplying two object waves from equations (2.4) & (2.5) as:

$$\Gamma(m,n) = O_2 \cdot O_1^* = o^2(m,n)e^{i\phi(m,n)}$$

Let, $a(m,n) = o^2(m,n)$ represent the real valued amplitude of the reconstructed interference field, Then the complex interference field is given by the

equation

$$\Gamma(m,n) = a(m,n)e^{i\phi(m,n)} \tag{2.6}$$

The relation between the measured interference phase and the displacement of the object surface under investigation in z direction is given by the following equation

$$d_z = \frac{\lambda}{4\pi}\phi \tag{2.7}$$

where, λ is the wavelength of the laser source.

2.2 Kalman Filter Framework

R. E. Kalman's paper [Kalman (1960)] describing a recursive solution of the discrete-data linear filtering problem was published in 1960. With the Advances in computing power and digital technology, implementation of such solution become more simple and convenient. Here, we will consider a basic mathematical derivation of various Kalman equations used in the filter implementation problem.

We start with the assumption that any random process, which follows auto-regressive model, can be modelled as:

$$\mathbf{x}_{n+1} = \mathbf{F}_n\mathbf{x}_n + \mathbf{w}_n \tag{2.8}$$

and the output of the process can occur as:

$$\mathbf{z}_n = \mathbf{H}_n\mathbf{x}_n + \mathbf{v}_n \tag{2.9}$$

The notations used in above equations are enumerated below

1. $\mathbf{x}_n = (N \times 1)$ vector as collection of state variables at time n
2. $\mathbf{F}_n = (N \times N)$ matrix relating $\mathbf{x}_n$ and $\mathbf{x}_{n+1}$ in absence of forcing function
3. $\mathbf{w}_n = (N \times 1)$ vector of process noise, assumed to be white Gaussian with known co-variance
4. $\mathbf{z}_n = (M \times 1)$ measurement or output vector at time n

5. $\mathbf{H}_n = (M \times N)$ matrix relating the measurement to the state vector at time n in noiseless condition.

6. $\mathbf{v}_n = (M \times 1)$ vector corresponding to the measurement error, assumed to be white gaussian noise with known covariance and having zero cross correlation with the $\mathbf{w}_n$ sequence.

The covariance matrices for the $\mathbf{w}_n$ and $\mathbf{v}_n$ vectors are given by

$$E[\mathbf{w}_k \mathbf{w}_i^T] = \begin{cases} \mathbf{Q}_n & i = k \\ 0 & i \neq k \end{cases} \tag{2.10}$$

$$E[\mathbf{v}_k \mathbf{v}_i^T] = \begin{cases} \mathbf{R}_n & i = k \\ 0 & i \neq k \end{cases} \tag{2.11}$$

$$E[\mathbf{w}_k \mathbf{v}_i^T] = 0, \ \forall \ k \ and \ i \tag{2.12}$$

Now let's assume that we have the initial estimate of the process at some point in time n. We call this estimate as **A priori** estimate and denote by $\hat{\mathbf{x}}_n^-$. Also let's assume that we know the error covariance matrix associated with $\hat{\mathbf{x}}_n^-$. So, let's define the estimation error as:

$$\mathbf{e}_n^- = \mathbf{x}_n - \hat{\mathbf{x}}_n^- \tag{2.13}$$

and the associated error covariance matrix is:

$$\mathbf{P}_n^- = E[\mathbf{e}_n^- \mathbf{e}_n^{-T}] = E[(\mathbf{x}_n - \hat{\mathbf{x}}_n^-)(\mathbf{x}_n - \hat{\mathbf{x}}_n^-)^T] \tag{2.14}$$

where, $E[\cdot]$ is the expectation operator. With this assumption of $\mathbf{x}_n - \hat{\mathbf{x}}_n^-$, we now try to utilize the measurement $\mathbf{z}_n$ to improve the prior estimate in accordance with the equation

$$\hat{\mathbf{x}}_n = \hat{\mathbf{x}}_n^- + \mathbf{K}_n(\mathbf{z}_n - \mathbf{H}_n \hat{\mathbf{x}}_n^-) \tag{2.15}$$

where, $\hat{\mathbf{x}}_n$ = updated estimate, and $\mathbf{K}_n$ = Blending factor or Kalman Gain.

To determine the particular blending factor $\mathbf{K}_n$ that yields an updated estimate that is optimal in some sense. We use minimization of error covariance for the estimation. Hence the error covariance matrix associated with the updated estimate can be written as

$$\mathbf{P}_n = E[\mathbf{e}_n\mathbf{e}_n^T] = E[(\mathbf{x}_n - \hat{\mathbf{x}}_n)(\mathbf{x}_n - \hat{\mathbf{x}}_n)^T] \tag{2.16}$$

Solving the above expectation value for $\mathbf{P}_n$ using matrix manipulation methods, we get

$$\begin{aligned}
\mathbf{P}_n &= E[\mathbf{e}_n\mathbf{e}_n^T] \\
&= E[(\mathbf{x}_n - \hat{\mathbf{x}}_n)(\cdots)^T] \\
&= E[(\mathbf{x}_n - \{\hat{\mathbf{x}}_n^- + \mathbf{K}_n(\mathbf{z}_n - \mathbf{H}_n\hat{\mathbf{x}}_n^-)\})(\cdots)^T] \\
&= E[(\mathbf{x}_n - \hat{\mathbf{x}}_n^- - \mathbf{K}_n(\mathbf{z}_n - \mathbf{H}_n\hat{\mathbf{x}}_n^-))(\cdots)^T] \\
&= E[(\mathbf{x}_n - \hat{\mathbf{x}}_n^- - \mathbf{K}_n(\mathbf{H}_n\mathbf{x}_n + \mathbf{v}_n - \mathbf{H}_n\hat{\mathbf{x}}_n^-))(\cdots)^T] \\
&= E[((\mathbf{x}_n - \hat{\mathbf{x}}_n^-) - \mathbf{K}_n\mathbf{H}_n\mathbf{x}_n - \mathbf{K}_n\mathbf{v}_n + \mathbf{K}_n\mathbf{H}_n\hat{\mathbf{x}}_n^-)(\cdots)^T] \\
&= E[(\mathbf{e}_n^- - \mathbf{K}_n\mathbf{H}_n\mathbf{x}_n - \mathbf{K}_n\mathbf{v}_n + \mathbf{K}_n\mathbf{H}_n\hat{\mathbf{x}}_n^-)(\cdots)^T] \\
&= E[(\mathbf{e}_n^- - (\mathbf{K}_n\mathbf{H}_n\mathbf{x}_n - \mathbf{K}_n\mathbf{H}_n\hat{\mathbf{x}}_n^-) - \mathbf{K}_n\mathbf{v}_n)(\cdots)^T] \\
&= E[(\mathbf{e}_n^- - \mathbf{K}_n\mathbf{H}_n(\mathbf{x}_n - \hat{\mathbf{x}}_n^-) - \mathbf{K}_n\mathbf{v}_n)(\cdots)^T] \\
&= E[(\mathbf{e}_n^- - \mathbf{K}_n\mathbf{H}_n\mathbf{e}_n^- - \mathbf{K}_n\mathbf{v}_n)(\cdots)^T] \\
&= E[((I - \mathbf{K}_n\mathbf{H}_n)\mathbf{e}_n^- - \mathbf{K}_n\mathbf{v}_n)(\cdots)^T] \\
&= E[\{((I - \mathbf{K}_n\mathbf{H}_n)\mathbf{e}_n^-) - (\mathbf{K}_n\mathbf{v}_n)\}\{((I - \mathbf{K}_n\mathbf{H}_n)\mathbf{e}_n^-)^T - (\mathbf{K}_n\mathbf{v}_n)^T\}]
\end{aligned} \tag{2.17}$$

Here, $(\cdots)$ is used to denote that the content of the parenthesis is same as that of adjacent one. Let's consider the error $\mathbf{e}_n^-$ and the measurement noise $\mathbf{v}_n$ are uncorrelated, hence $E(\mathbf{e}_n^-\mathbf{v}_n) = 0$. hence we can write:

$$\begin{aligned}
\mathbf{P}_n &= E[((I - \mathbf{K}_n\mathbf{H}_n)\mathbf{e}_n^-)((I - \mathbf{K}_n\mathbf{H}_n)\mathbf{e}_n^-)^T] + E[(\mathbf{K}_n\mathbf{v}_n)(\mathbf{K}_n\mathbf{v}_n)^T] \\
&= (I - \mathbf{K}_n\mathbf{H}_n)\mathbf{P}_n^-(I - \mathbf{K}_n\mathbf{H}_n)^T + \mathbf{K}_n\mathbf{R}_n\mathbf{K}_n^T
\end{aligned} \tag{2.18}$$

Optimization of Blending Factor

The above equation is a perfectly geveral expression for the updated error covariance matrix, and it applies for any gain $\mathbf{K}_n$.

But we wish to find out the particular $\mathbf{K}_n$ that minimizes the individual terms along the major diagonal of $\mathbf{P}_n$, because these terms represents the estimation error variance for the element of the state vector being estimated. Let's do the optimization using differential calculus approach.

To do so, let's rewrite the above equation in proper format, then

$$\begin{aligned}\mathbf{P}_n &= (I - \mathbf{K}_n\mathbf{H}_n)\mathbf{P}_n^-(I - \mathbf{K}_n\mathbf{H}_n)^T + \mathbf{K}_n\mathbf{R}_n\mathbf{K}_n^T \\ &= \mathbf{P}_n^- - \mathbf{P}_n^-\mathbf{H}_n^T\mathbf{K}_n^T - \mathbf{K}_n\mathbf{H}_n\mathbf{P}_n^- + \mathbf{K}_n(\mathbf{H}_n\mathbf{P}_n^-\mathbf{H}_n^T + \mathbf{R}_n)\mathbf{K}_n^T \qquad (2.19)\end{aligned}$$

Now, differentiate $tr(\mathbf{P}_n)$ w.r.t. $\mathbf{K}_n$ and equating it with 0, we get

$$\frac{dtr(\mathbf{P}_n)}{d\mathbf{K}_n} = 0 - 2(\mathbf{H}_n\mathbf{P}_n^-)^T + 2\mathbf{K}_n(\mathbf{H}_n\mathbf{P}_n^-\mathbf{H}_n^T + \mathbf{R}_n) = 0$$

$$2\mathbf{K}_n(\mathbf{H}_n\mathbf{P}_n^-\mathbf{H}_n^T + \mathbf{R}_n) = 2(\mathbf{H}_n\mathbf{P}_n^-)^T$$

$$\mathbf{K}_n = (\mathbf{H}_n\mathbf{P}_n^-)^T(\mathbf{H}_n\mathbf{P}_n^-\mathbf{H}_n^T + \mathbf{R}_n)^{-1} \qquad (2.20)$$

This particular $\mathbf{K}_n$ minimizes the mean-square estimation error, is called the Kalman Gain.

Using this, we can compute the optimized error covariance matrix as:

$$\begin{aligned}\mathbf{P}_n &= (I - \mathbf{K}_n\mathbf{H}_n)\mathbf{P}_n^-(I - \mathbf{K}_n\mathbf{H}_n)^T + \mathbf{K}_n\mathbf{R}_n\mathbf{K}_n^T \\ &= \mathbf{P}_n^- - \mathbf{K}_n\mathbf{H}_n\mathbf{P}_n^- - \mathbf{P}_n^-\mathbf{H}_n^T\mathbf{K}_n^T + \mathbf{K}_n(\mathbf{H}_n\mathbf{P}_n^-\mathbf{H}_n^T + \mathbf{R}_n)\mathbf{K}_n^T \qquad (2.21)\end{aligned}$$

Rearranging eqn 2.20, we get:

$$(\mathbf{H}_n\mathbf{P}_n^-\mathbf{H}_n^T + \mathbf{R}_n) = \mathbf{K}_n^{-1}(\mathbf{H}_n\mathbf{P}_n^-)^T = \mathbf{K}_n^{-1}\mathbf{P}_n^{-T}\mathbf{H}_n^T \qquad (2.22)$$

Substituting the value of optimum gain from eqn 2.22 into above equation to get:

$$\begin{aligned}
\mathbf{P}_n &= \mathbf{P}_n^- - \mathbf{K}_n\mathbf{H}_n\mathbf{P}_n^- - \mathbf{P}_n^-\mathbf{H}_n^T\mathbf{K}_n^T + \mathbf{K}_n\mathbf{K}_n^{-1}\mathbf{P}_n^-\mathbf{H}_n^T\mathbf{K}_n^T \\
&= \mathbf{P}_n^- - \mathbf{K}_n\mathbf{H}_n\mathbf{P}_n^- - \mathbf{P}_n^-\mathbf{H}_n^T\mathbf{K}_n^T + \mathbf{P}_n^-\mathbf{H}_n^T\mathbf{K}_n^T \\
&= \mathbf{P}_n^- - \mathbf{K}_n\mathbf{H}_n\mathbf{P}_n^- \\
&= (I - \mathbf{K}_n\mathbf{H}_n)\mathbf{P}_n^- \qquad (2.23)
\end{aligned}$$

To complete the system, yet we need to calculate $\hat{\mathbf{x}}_{n+1}^-$ and $\mathbf{P}_{n+1}^-$. the updated estimated $\hat{\mathbf{x}}_n$ is easily projected ahead via the transition matrix. Thus we have

$$\hat{\mathbf{x}}_{n+1}^- = \mathbf{F}_n\hat{\mathbf{x}}_n \qquad (2.24)$$

and the error covariance matrix associated with $\hat{\mathbf{x}}_{k+1}^-$ is obtained by hfirst forming the expression of the a priori error

$$\begin{aligned}
\mathbf{e}_{n+1}^- &= \mathbf{x}_{n+1} - \hat{\mathbf{x}}_{n+1}^- \\
&= (\mathbf{F}_n\mathbf{x}_n + \mathbf{w}_n) - \mathbf{F}_n\hat{\mathbf{x}}_n \\
&= \mathbf{F}_n\mathbf{e}_n + \mathbf{w}_n \qquad (2.25)
\end{aligned}$$

Now note that, $\mathbf{w}_n$ and $\mathbf{e}_n$ are non-correlated, hence we can write the error covariance matrix as

$$\begin{aligned}
\mathbf{P}_{n+1}^- &= E[\mathbf{e}_{n+1}^-\mathbf{e}_{n+1}^{-T}] \\
&= E[(\mathbf{F}_n\mathbf{e}_n + \mathbf{w}_n)(\mathbf{F}_n\mathbf{e}_n + \mathbf{w}_n)^T] \\
&= \mathbf{F}_n\mathbf{P}_n\mathbf{F}_n^T + \mathbf{Q}_n \qquad (2.26)
\end{aligned}$$

Finally, all the Kalman filter equations are summarized below:

1. State prediction

$$\hat{\mathbf{x}}_{n+1}^- = \mathbf{F}_n\hat{\mathbf{x}}_n$$

2. Predicted state error covariance

$$\mathbf{P}_{n+1}^- = \mathbf{F}_n\mathbf{P}_n\mathbf{F}_n^T + \mathbf{Q}_n$$

3. State updates

$$\hat{\mathbf{x}}_n = \hat{\mathbf{x}}_n^- + \mathbf{K}_n(\mathbf{z}_n - \mathbf{H}_n\hat{\mathbf{x}}_n^-)$$

4. Kalman gain

$$\mathbf{K}_n = (\mathbf{H}_n\mathbf{P}_n^-)^T(\mathbf{H}_n\mathbf{P}_n^-\mathbf{H}_n^T + \mathbf{R}_n)^{-1}$$

5. Updated state error covariance

$$\mathbf{P}_n = (I - \mathbf{K}_n\mathbf{H}_n)\mathbf{P}_n^-$$

2.3 Particle Filter Framework

Particle filter employs the sequential Bayesian estimator by Monte Carlo simulation. It offers an alternative to Kalman filter and its variants for non-linear transition functions. This section provides overview of the generic sampling importance re-sampling (SIR) particle filter for state estimation from given state space model.

There are many particle filter methods, and almost all of them follows the three basic operations: 1) Particle propagation, 2) Weights calculations, and 3) Re-sampling. Particle propagation and weights calculation helps in the generation of particle sets and assignment of the weights to them, whereas re-sampling replaces one set of particle and weights with the another set. The main objective of the particle filter is the representation of posterior density function by set of particles and associated weights and estimation of state using these particles and weights. As the number of samples becomes very large, this Monte Carlo characterization becomes an equivalent representation to the usual functional description of the posterior pdf, and the Particle filter approaches the optimal Bayesian estimate. In this section, we briefly review the particle filter algorithm presented by Arulampalam et al. (2002).

In order to formally introduce the particle filter, we need to start with the non-linear state space model. Let's denote the state space model by:

$$\mathbf{x}_n = \mathbf{f}(\mathbf{x}_{n-1}) + \boldsymbol{\omega}_{n-1} \tag{2.27}$$

$$\mathbf{z}_n = \mathbf{h}(\mathbf{x}_n) + \boldsymbol{\nu}_n \tag{2.28}$$

where, n is the spatial index (e.g., pixel location in an arbitrary row/column. for the sake of brevity, we use it as suffix), $\mathbf{x}_n$ is the state vector hidden from the observer, $\mathbf{z}_n$ is the measurement vector observed by the sensors, $\boldsymbol{\omega}_{n-1}$ and $\boldsymbol{\nu}_{n-1}$ are the process noise and measurement noise, respectively, and $\mathbf{f}(\cdot)$, $\mathbf{h}(\cdot)$ are the non-linear state and measurement transition functions. We can represent the state space model by the probability distributions of the state, $P[\mathbf{x}_n|\mathbf{x}_{n-1}]$ and of the measurements, $P[\mathbf{z}_n|\mathbf{x}_n]$. These probability distributions can be acquired using equation (2.27), (2.28), and the probability distribution of the process and measurement noises, $\boldsymbol{\omega}_{n-1}$ and $\boldsymbol{\nu}_{n-1}$. We note here that the probability distributions of the noise are not necessarily Gaussian.

Considering Markovian property and by Bayes rule, the pdf $P(\mathbf{x}_n|\mathbf{z}_{1:n})$ can be obtained recursively from the pdf $P(\mathbf{x}_{n-1}|\mathbf{z}_{1:n-1})$ calculated from $(n-1)^{th}$ pixel. It is assumed that initial pdf $P(\mathbf{x}_0|\mathbf{z}_0) = P(\mathbf{x}_0)$ is known. Next, at the current pixel n, samples are updated according to the current observation $\mathbf{z}_n$.

The complete estimation problem can be divided in to two stages: *prediction* and *update*. The other important step in PF approach is *resampling* step. The prediction stage is accomplished by the propagating each particle through the state transition model $P(\mathbf{x}_n|\mathbf{x}_{n-1})$ and generate a new set of samples. These samples obtained represent the prediction of state variable $\mathbf{x}_n$ without consideration of observation at pixel n.

To consider the effect of the current observation $\mathbf{z}_n$, the update stage is performed. The weights associated with each sample, $\boldsymbol{\omega}_n^i, i = 1, ..., N_s$ are obtained from the observation model $P(\mathbf{z}_n|\mathbf{x}_n)$. Let, $\{\mathbf{x}_n^i\}, i = 1, \cdots, N_s$ denote the N_s particles with their associated weights denoted by $\{\boldsymbol{\omega}_n^i\}, i = 1, \cdots, N_s$. The weights are normalized such that $\sum_i \boldsymbol{\omega}_n^i = 1$. The posterior density at n, then, can be

approximately represented as:

$$P(\mathbf{x}_{0:n}|\mathbf{z}_{1:n}) = \sum_{i=1}^{N_s} \boldsymbol{\omega}_n^i \delta(\mathbf{x}_{0:n} - \mathbf{x}_{0:n}^i) \tag{2.29}$$

where $\delta(.)$ represents the dirac delta function, and $(\cdot)_{0:n}$ denotes the prediction/observations corresponding to pixel values from 0 through n.

Let $\mathbf{x}_i, i = 1, ..., N_s$ be samples generated from a function $Q(.)$ called as *importance density*. The weights are chosen according to *importance resampling principle*. Suppose that $P(x)$ is a probability density function from which samples can be drawn easily, then the weighted approximation to the density $P(.)$ is given by

$$P(\mathbf{x}) \approx \sum_{i=1}^{N_s} \boldsymbol{\omega}^i \delta(\mathbf{x} - \mathbf{x}^i) \tag{2.30}$$

where

$$\boldsymbol{\omega}^i \propto \frac{P(\mathbf{x}^i)}{Q(\mathbf{x}^i)} \tag{2.31}$$

is the normalized weight of i^{th} particle drawn from $Q(.)$.

If the samples $\mathbf{x}_{0:n}^i$ are drawn from importance density $Q(\mathbf{x}_{0:n}|\mathbf{z}_{1:n})$, then weights are defined as

$$\boldsymbol{\omega}_n^i \propto \frac{P(\mathbf{x}_{0:n}^i|\mathbf{z}_{1:n})}{Q(\mathbf{x}_{0:n}^i|\mathbf{z}_{1:n})} \tag{2.32}$$

As shown by Arulampalam et al. (2002), importance density is chosen to factorize such that

$$Q(\mathbf{x}_{0:n}|\mathbf{z}_{1:n}) = Q(\mathbf{x}_n|\mathbf{x}_{0:n-1},\, \mathbf{z}_{1:n}) Q(\mathbf{x}_{0:n-1}|\mathbf{z}_{1:n-1}) \tag{2.33}$$

then samples $\mathbf{x}_{0:n}^i \sim Q(\mathbf{x}_{0:n}|\mathbf{z}_{1:n})$ are obtained by augmenting each of the existing samples $\mathbf{x}_{0:n-1}^i \sim Q(\mathbf{x}_{0:n-1}|\mathbf{z}_{1:n-1})$ with the new state $\mathbf{x}_n^i \sim Q(\mathbf{x}_n|\mathbf{x}_{0:n-1}, \mathbf{z}_{1:n})$.

After a few simplifications, numerator of Eq.2.32 can be written as

$$P(\mathbf{x}_{0:n}|\mathbf{z}_{1:n}) \propto P(\mathbf{z}_n|\mathbf{x}_n) P(\mathbf{x}_n|\mathbf{x}_{n-1}) P(\mathbf{x}_{0:n-1}|\mathbf{z}_{1:n-1}) \tag{2.34}$$

Thus by substituting Eqs.2.33 and 2.34 into weight update equation Eq.2.32, we obtain the weight update equation as

$$\begin{aligned}\boldsymbol{\omega}_n^i &\propto \frac{P(\mathbf{z}_n|\mathbf{x}_n^i)P(\mathbf{x}_n^i|\mathbf{x}_{n-1}^i)P(\mathbf{x}_{0:n-1}^i|\mathbf{z}_{1:n-1})}{Q(\mathbf{x}_n^i|\mathbf{x}_{0:n-1}^i,\mathbf{z}_{1:n})Q(\mathbf{x}_{0:n-1}^i|\mathbf{z}_{1:n-1})} \\ &= \boldsymbol{\omega}_{n-1}^i \frac{P(\mathbf{z}_n|\mathbf{x}_n^i)P(\mathbf{x}_n^i|\mathbf{x}_{n-1}^i)}{Q(\mathbf{x}_n^i|\mathbf{x}_{0:n-1}^i,\mathbf{z}_{1:n})} \end{aligned} \tag{2.35}$$

Furthermore, by considering Markovian property, $Q(\mathbf{x}_n|\mathbf{x}_{0:n-1},\mathbf{z}_{1:n}) = Q(\mathbf{x}_n|\mathbf{x}_{n-1},\mathbf{z}_n)$ the importance density becomes only dependent on $\mathbf{x}_{n-1}$ and $\mathbf{z}_n$ and weights are then given by

$$\boldsymbol{\omega}_n^i \propto \boldsymbol{\omega}_{n-1}^i \frac{P(\mathbf{z}_n|\mathbf{x}_n^i)P(\mathbf{x}_n^i|\mathbf{x}_{n-1}^i)}{Q(\mathbf{x}_n^i|\mathbf{x}_{n-1}^i,\mathbf{z}_n)} \tag{2.36}$$

The posterior filtered density $P(\mathbf{x}_n|\mathbf{z}_{1:n})$ is then given by

$$P(\mathbf{x}_n|\mathbf{z}_{1:n}) \approx \sum_{i=1}^{N_s}, \boldsymbol{\omega}_n^i \delta(\mathbf{x}_n - \mathbf{x}_n^i) \tag{2.37}$$

where weights are found according to Eq.2.36. If $N_s \to \infty$, the approximation in Eq.2.37 approaches the true pdf.

Sequential Importance Resampling (SIR) particle filter is a variant of generic particle filter in which proposal density is chosen to be same as state transition density as

$$Q(\mathbf{x}_n|\mathbf{x}_{n-1}^i,\mathbf{z}_n) = P(\mathbf{x}_n|\mathbf{x}_{n-1}) \tag{2.38}$$

then the weight equation simplifies to

$$\boldsymbol{\omega}_n^i \propto \boldsymbol{\omega}_{n-1}^i P(\mathbf{z}_n|\mathbf{x}_n^i) \tag{2.39}$$

Common problem encountered with particle filter approach is the degeneracy of samples, where after a few iterations, all but one particle has negligible weight. This implies that a considerable amount of computational work still needs to be performed to update the particles whose contribution to the approximation of posterior pdf $P(\mathbf{x}_n|\mathbf{z}_{1:n})$ is zero/negligible. Thus, for this reason, degeneracy should be avoided. Degeneracy problem can be avoided in many ways like by considering a good choice of importance density, choosing larger number of samples N_s.

However, choosing a large number of samples results in an inefficient solution. Resampling the particles is one of the most widely used solution to avoid degeneracy. There are many resampling strategies present in the literature such as Multinomial Resampling, Systematic Resampling, Residual Resampling and Stratified Resampling [Douc and Cappé (2005)]. The basic idea of resampling step is to eliminate the particles which have smaller weights and concentrate on the particles which have significantly larger weights. After resampling, all the particles have equal weights $\boldsymbol{\omega}_n^i = 1/N_s$.

In systematic resampling, the normalised weights $\boldsymbol{\omega}_n^i$ are incrementally added to form a cumulative sum of $\boldsymbol{\omega}_C^i = \sum_{j=1}^{i} \boldsymbol{\omega}^j$. A "comb" of N_s points spaced at regular intervals of $1/N_s$ is defined and the complete comb is translated by an offset chosen randomly from a uniform distribution over $[0, 1/N_s]$. The comb is then compared with cumulative sum of weights $\boldsymbol{\omega}_C^i$. We select/resample a particle more than once/delete the sample based on how many times comb values fall within CDF of that particular sample. In this way resampling is carried for N_s samples. The resampled weights of each particle is $1/N_s$ which is used in calculation of posterior for next iteration.

2.4 Discussions

In summary, Kalman filter and its variants requires the assumptions that the process and measurement noise are generated from Gaussian distribution. In addition to this Kalman filter works optimal with linear state space model and their performance gets affected by the non-linearity in the state space model. In case of particle filters, their strength lies in the fact that there is no restriction of state space model as well as on process and measurement noise. Throughout our work, we have provided additional guidelines, whenever required, for further understanding of the presented research work.

CHAPTER 3

Kalman Filter based Phase Estimation

In this chapter, we propose a novel technique, namely, signal tracking approach for simultaneous estimation of phase and its derivatives. This approach provides more accurate, unwrapped, and continuous phase directly even if the phase is rapidly varying, has a larger dynamic range, or the fringe pattern is corrupted by severe noise. In this approach, each column (or row) of the 2D phase map is considered as one dimensional arbitrary function. This function is approximated by using Taylor series expansion. We derive the state model using this approximation, whereas the measurement model is based on polar to Cartesian conversion of amplitude and phase components of state vector to real and imaginary components of the complex measurements of the reconstructed interference field.

Given a state space model for the system, estimation of the state depends solemnly on the tracking algorithm used to process the system. The choice of tracking/state estimation algorithm can be influenced by many parameters such as computational complexity, ease of implementation, efficiency towards the noise handling, etc. Our first choice of tracking algorithm was extended Kalman filter (EKF) owing to ease of implementation. It is observed that the EKF algorithm works effectively, even outperforms the state-of-the-art phase estimation algorithms, when the interference field is not corrupted by noise. It is capable of handling rapidly varying phase with larger dynamic range. Since EKF uses linearisation to linearise the non-linear measurement model, its performance gets affected when the measurements become noisy.

To overcome this issue, we used UKF as estimation algorithm that uses a deterministic sampling technique called as Unscented Transform. This transform picks a minimal set of sample points (called sigma points) around the mean such that these points capture mean and covariance of a prior random variable exactly, while approximating the mean and covariance of the transformed random variable up to the third order in Taylor series [Julier and Uhlmann (2004)]. We demonstrate, using simulation and experimental analysis, that the EKF and UKF make

suitable candidates for signal tracking algorithm to process the derived state space model.

3.1 State Space Model

The reconstructed interference field of digital holographic interferometry given by equation (2.6) with variable amplitude embedded in noise is:

$$\Gamma(m,n) = a(m,n)e^{i\phi(m,n)} + \eta(m,n) \tag{3.1}$$

for any arbitrary row, we can express it as

$$f(n) = a(n)e^{j\phi(n)} + \eta(n) \tag{3.2}$$

where $a(n)$ is the amplitude and $\phi(n)$ is the interference phase and $\eta(n)$ is the zero mean complex Additive White Gaussian Noise (AWGN) corresponding to n^{th} pixel location of any arbitrary column of the M×N complex field.

In proposed method, phase is assumed to be continuous and differentiable function. Hence, we use the Taylor series expansion for the phase function $\phi(n)$ in equation 3.2 as:

$$\phi(n+1) \;=\; \phi(n) + \frac{1}{1!}\phi^{(1)}(n) + \frac{1}{2!}\phi^{(2)}(n) + \cdots + \frac{1}{M!}\phi^{(M)}(n) + w(n) \tag{3.3}$$

Here, we choose first M terms of the Taylor series for state modelling, while considering the higher order terms as un-modelled process noise. The amplitude is modelled as random walk such that we can express,

$$a(n+1) = a(n) + w_a(n) \tag{3.4}$$

Now, equations (3.3) & (3.4) can be written in following form as:

$$\mathbf{x}(n+1) = \mathbf{F}\mathbf{x}(n) + \mathbf{w}(n) \tag{3.5}$$

where, the state vector $\mathbf{x}(n)$, state transition matrix $\mathbf{F}$ representing the relation between the present and the next state of the field, and the process noise vector $\mathbf{w}(n)$ are given as.

$$\begin{aligned}
\mathbf{x}(n) &= \begin{bmatrix} a(n) & \phi(n) & \phi^{(1)}(n) & \cdots & \phi^{(M)}(n) \end{bmatrix}^T \\
\mathbf{F} &= \begin{bmatrix} 1 & 0 & 0 & 0 & \cdots & 0 \\ 0 & 1 & \frac{1}{1!} & \frac{1}{2!} & \cdots & \frac{1}{M!} \\ 0 & 0 & 1 & \frac{1}{1!} & \cdots & \frac{1}{(M-1)!} \\ \vdots & \vdots & \vdots & \vdots & \ddots & \vdots \\ 0 & 0 & 0 & 0 & \cdots & 1 \end{bmatrix} \\
\mathbf{w}(n) &= \begin{bmatrix} w_a(n) & w_0(n) & w_1(n) & \cdots & w_M(n) \end{bmatrix}^T
\end{aligned} \tag{3.6}$$

here, $w_a(n)$ & $w_i(n), i = 0, \cdots, M$ represents noise in amplitude and the higher order terms of the Taylor series and assumed to be additive white Gaussian noise (AWGN).

From equation (3.2), we can generate the measurement signal with the relation

$$\Re[f(n)] = a(n)cos(\phi(n)) \tag{3.7}$$

$$\Im[f(n)] = a(n)sin(\phi(n)) \tag{3.8}$$

Hence, from above equations, the non-linear function $\mathbf{h}(\cdot)$ used for prediction of observation from state vector $\mathbf{x}$ can be written as:

$$\mathbf{h}(\mathbf{x}) = \begin{bmatrix} a(n)cos(\phi(n)) \\ a(n)sin(\phi(n)) \end{bmatrix} = \begin{bmatrix} x_1 cos(x_2) \\ x_1 sin(x_2) \end{bmatrix} \tag{3.9}$$

where $a(n)$ and $\phi(n)$ are the elements of the state vector $\mathbf{x}$. As the measurement signal is a complex field, the noise is also considered to be in the complex form. We assumed the measurement (observation) noise to be complex additive white Gaussian noise with zero mean and variance of σ_ν^2. the noise $\nu(n)$ has the following form

$$\nu(n) = \begin{bmatrix} \Re[\eta(n)] \\ \Im[\eta(n)] \end{bmatrix} \tag{3.10}$$

Hence observation model can be written as

$$\mathbf{z}(n) = \mathbf{h}(\mathbf{x}(n)) + \boldsymbol{\nu}(n) \tag{3.11}$$

3.2 Extended Kalman Filter

We consider EKF as our first choice of tracking algorithm, because EKF is known for handling moderate non-linearity in the state space model through linearisation of the state space model, nevertheless it's well-known for its ease of implementation. In addition to this, the computational complexity if the EKF is almost equal to that of the basic Kalman filter. The non-linear measurement function is linearised using Jacobian of the measurement function $\mathbf{h}(\cdot)$. The complete algorithm of the estimation process using EKF is summarised as follows:

Let, $\mathbf{x} = \begin{bmatrix} a(n) & \phi(n) & \phi^{(1)}(n) & \cdots & \phi^{(M)}(n) \end{bmatrix}^T$ be a state vector describing the phase map, $\mathbf{Q}$ be the process noise covariance matrix, and $\mathbf{R}$ be the measurement noise covariance.

Initialize with:

$$\begin{aligned} \hat{\mathbf{x}}_0 &= \mathbb{E}\{\mathbf{x}_0\} \\ \mathbf{P}_0 &= \mathbb{E}\{(\mathbf{x}_0 - \hat{\mathbf{x}}_0)(\mathbf{x}_0 - \hat{\mathbf{x}}_0)^T\} \end{aligned}$$

here, $\mathbb{E}\{\cdot\}$ is an expectation operator.

Now, $\forall$ k $\in \{1, 2, \cdots, N\}$, where, N is the number of pixels in a column.

Process Update Equations:

$$\begin{aligned} \hat{\mathbf{x}}_k^- &= \mathbf{F}\hat{\mathbf{x}}_{\mathbf{k-1}} \\ \mathbf{P}_{\mathbf{k}}^- &= \mathbf{F}\mathbf{P}_{\mathbf{k-1}}\mathbf{F}^{\mathbf{T}} + \mathbf{Q} \end{aligned}$$

Here, $\hat{\mathbf{x}}_k^-$ and $\mathbf{P}_{\mathbf{k}}^-$ are the predicted state vector and the predicted state error covariance matrix at k^{th} pixel, respectively.

Jacobian Matrix:

The non-linear observation function is linearised using Jacobian of the function $\boldsymbol{h}(\cdot)$, which is partial differentiation of the function with respect to all the independent variables (state vectors, in this case). The Jacobian of the function $\boldsymbol{h}(\cdot)$ is given by:

$$\begin{aligned}\mathbf{H_k} &= \left.\frac{\partial \mathbf{h}}{\partial \mathbf{x}}\right|_{\mathbf{x}=\hat{\mathbf{x}}_\mathbf{k}^-} \\ &= \begin{bmatrix} cos(x_2) & -x_1 sin(x_2) & 0 & \cdots & 0 \\ sin(x_2) & x_1 cos(x_2) & 0 & \cdots & 0 \end{bmatrix}\end{aligned}$$

where, x_i is the i^{th} element of the state vector $\hat{\mathbf{x}}_\mathbf{k}^-$

Measurement Update Equations:

$$\begin{aligned}\mathbf{K_k} &= \mathbf{P_k^-}\mathbf{H_k}^\mathbf{T}(\mathbf{P_k^-}\mathbf{H_k}\mathbf{P_k^{-T}} + \mathbf{R})^{-\mathbf{1}} \\ \hat{\mathbf{x}}_k &= \hat{\mathbf{x}}_k^- + \mathbf{K_k}(\mathbf{y_k} - \mathbf{h}(\hat{\mathbf{x}}_\mathbf{k}^-)) \\ \mathbf{P_k} &= \mathbf{P_k^-} - \mathbf{K}\mathbf{H_k}\mathbf{P_k^-}\end{aligned}$$

Here, $\mathbf{K_k}$ is the Kalman gain, $\hat{\mathbf{x}}_k$ is the updated state vector, and $\mathbf{P_k}$ is the updates state error covariance matrix.

Since the second element of state vector $\hat{\mathbf{x}}_k$ is a phase function itself, We get the unwrapped phase explicitly from the state vector. Also the state vector includes first and second derivatives of the phase, we get the direct access to phase derivatives without additional efforts like numerical differentiation. It indeed is a great advantage offered by this approach in non-destructive testing and evaluation applications where calculation of displacement (phase) as well as strain/curvature (its derivatives) are important.

3.2.1 Simulation Results

A complex interference field of size 512×512 was simulated in MATLAB. The zero-mean AWGN was then added at Signal-to-Noise-Ratio (SNR) of 20 dB using `awgn` function. For EKF, we took the process noise covariance matrix to be $\mathbf{Q} =$

$diag[10^{-1}, 10^{-1}, 10^{-3}, 10^{-5}]$, measurement noise covariance matrix to be $\mathbf{R} = k_R \times diag(\begin{bmatrix}\sigma_{re}^2 & \sigma_{im}^2\end{bmatrix})$ where, σ_{re}^2 and σ_{im}^2 are the variances estimated form uniform region of the fringe pattern and k_R is a scaling factor generally can be taken as 2.

We have compared the performance of proposed method with the state-of-the-art methods available in literature such as Discrete Chirp-Fourier Transform (DCFT) [Gorthi and Rastogi (2009a)], Improved High-order Ambiguity Function (IHAF) [Gorthi and Rastogi (2009b)], and State Space Approach (SSA) [Rajshekhar and Rastogi (2013)]. The EKF that reported in SSA based method performs parameter estimation whereas our EKF based method performs signal/state estimation. Since the state estimation involves only the 'forward problem' and parameter estimation requires the solution of an 'inverse problem' as well, proposed EKF based method provides better estimates of the phase than that of SSA based method. For the sake of distinction we are addressing the existing EKF based method as SSA based method. For IHAF and SSA based methods, order of the polynomial was taken as 4 while each column was divided into 8 segments (M = 4, Nw = 8, Nw is the number of segments). For DCFT based method, each column was divided into 8 segments (M = 2, Nw = 8).

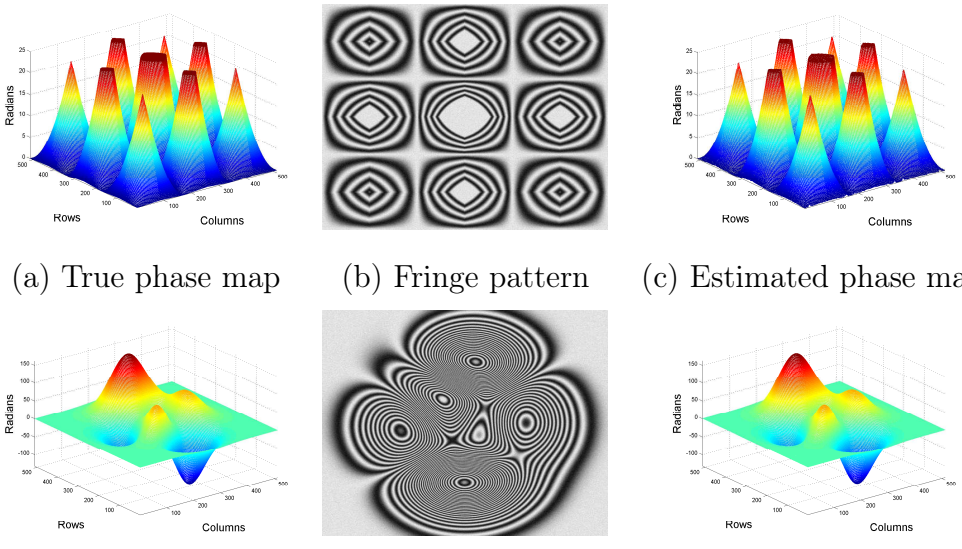

(a) True phase map (b) Fringe pattern (c) Estimated phase map

(d) True phase map (e) Fringe pattern (f) Estimated phase map

Figure 3.1: 3D mesh plot of true phase maps and corresponding fringe patterns at SNR of 20dB. (a) & (d) show the true phase map with (b) & (e) showing their corresponding fringe patterns. (c) & (f) show the estimated phase map using proposed method

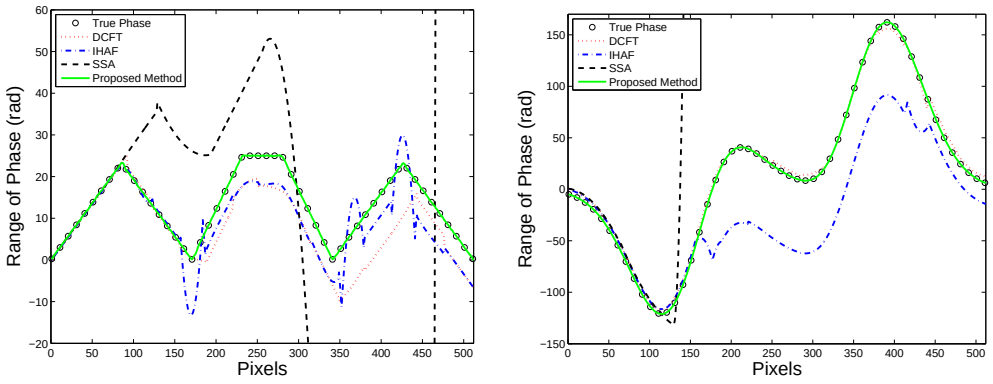

(a) (b)

Figure 3.2: Estimated Phase Comparison along 86^{th} column of a phase map shown in figure 3.1(a) and middle column of a phase map shown in figure 3.1(d) showing performance of proposed method with different methods

In order to quantify the performance variations among different methods in dealing with rapidly varying signals and signals having higher dynamic range, we generated a phase maps as shown in figure 3.1(a), and 3.1(d) respectively. The corresponding fringe patterns at 20 dB are shown in the figure 3.1(b) and 3.1(e). The phase map shown in 3.1(a) exhibit rapid changes in phase around the vertex points of triangles in the phase map. As the phase becomes rapidly varying, parameter estimation based methods under-perform producing distortion in the estimated phase, even at higher SNR values, which is evident from the figure 3.2(a). The phase map shown in 3.1(d) depicts the larger dynamic range of phase. As the dynamic range of phase increases, small error in estimation of coefficients of polynomials (parameters) leads to large change in estimated phase. This makes polynomial approximation approach less reliable for estimation of phase signals having larger dynamic range. The comparative performance of different methods for middle column of the phase map is shown in figure 3.2(b). From figure 3.2, it is observed that the parameter estimation based methods fail to estimate the parameters accurately if the phase values change rapidly.

For the purpose of comparison, we have shown the 3D mesh plot of the error in estimated phase at SNR of 20dB by different methods compared with proposed method. In figure 3.3, first row shows the error at every pixel in estimation of rapidly phase map, whereas second row shows phase map with larger dynamic

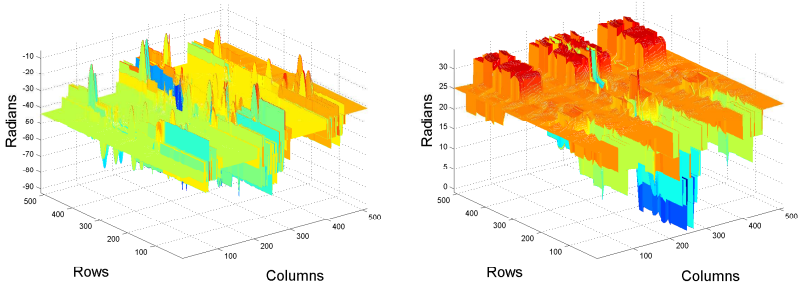

(a) IHAF based Method (b) DCFT based Method

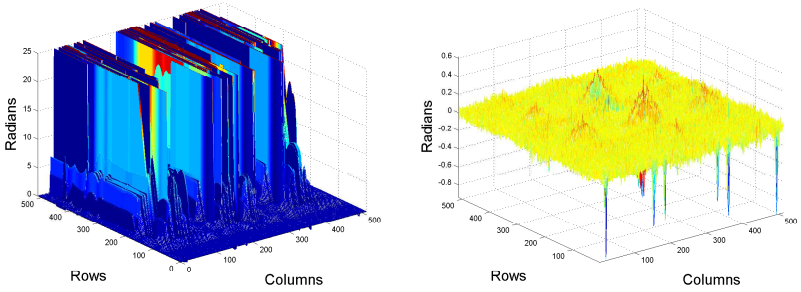

(c) SSA based Method (d) Proposed EKF Method

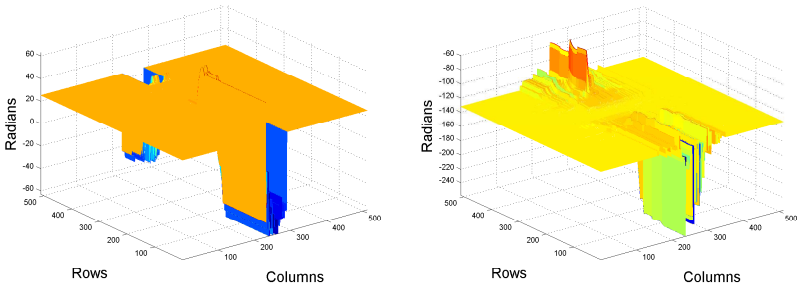

(e) IHAF based Method (f) DCFT based Method

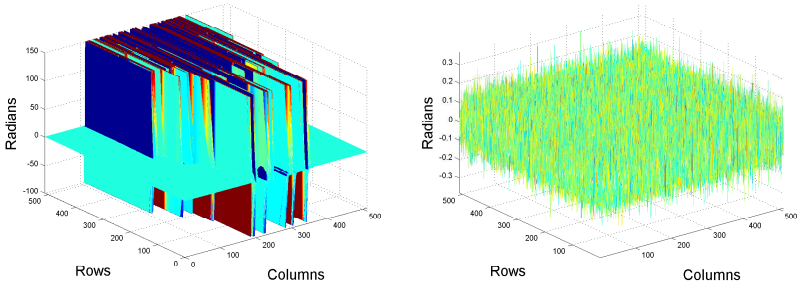

(g) SSA based Method (h) Proposed EKF Method

Figure 3.3: Phase estimation error at each pixel for the phase map showing relatively poor performance of polynomial approximation based methods for rapidly varying phase map (first two rows) and larger dynamic range of phase map (last 2 rows).

range. We note here that if the phase is rapidly varying the parametric methods proposed in literature fail to estimate the phase accurately, whereas EKF provides comparatively better estimates.

3.2.2 Experimental Results

To validate the practical applicability of the proposed method, a DHI experiment was conducted by subjecting a circularly clamped object to load, and two holograms before and after deformation using a Coherent Verdi laser(532nm) were recorded. A SONY XCL-U1000 CCD camera was used for recording the holograms. The complex amplitudes of the object wave before and after deformation were obtained by numerical reconstruction, performed using discrete Fresnel transform. The reconstructed interference field is then obtained by multiplying those two complex fields of object waves.

The real part of reconstructed interference field, which makes the fringe pattern, shown in figure 3.4(a). The estimated phase patterns using SSA based method and EKF based method are shown in figures 3.4(b) & 3.4(c), respectively. Although the phase estimated by both methods is continuous and unwrapped, fringes were generated and displayed for qualitative comparison. Figure 3.4(d) shows the 3D mesh plot of the phase estimated by proposed approach. Median filter of mask size 3×3 was applied on the SSA [Rajshekhar and Rastogi (2013)] and EKF based estimates of phase as a post processing step to eliminate few spurious estimates. Phase map estimated by SSA based methods shows distortion which corresponds to the divergence of EKF owing to inadequate process model. Divergence of EKF is avoided by the introduction of process noise covariance in the proposed state space model which is evident from figure 3.4(c). This analysis shows that the EKF can be successfully applied for phase estimation using signal tracking approach even for rapidly varying phase maps. However, its performance degrades considerably in presence of noise, owing to severe non-linearity of the measurement model. Hence, we require better approximation of the measurement model, and robust tracking algorithm for handling noisy fringes.

3.3 Unscented Kalman Filter

It is observed that the EKF algorithm works effectively, even outperforms the state-of-the-art phase estimation algorithms. But since EKF uses Jacobian to linearise the non-linear measurement model, it can handle moderate non-linearity. Its performance gets affected when the measurements function becomes highly non-linear (polar to Cartesian conversion), and when the measurements become noisy. To overcome this issue, we approximate the non-linear measurement model by using a deterministic sampling technique called Unscented Transform (UT) proposed by Julier and Uhlmann (2004).

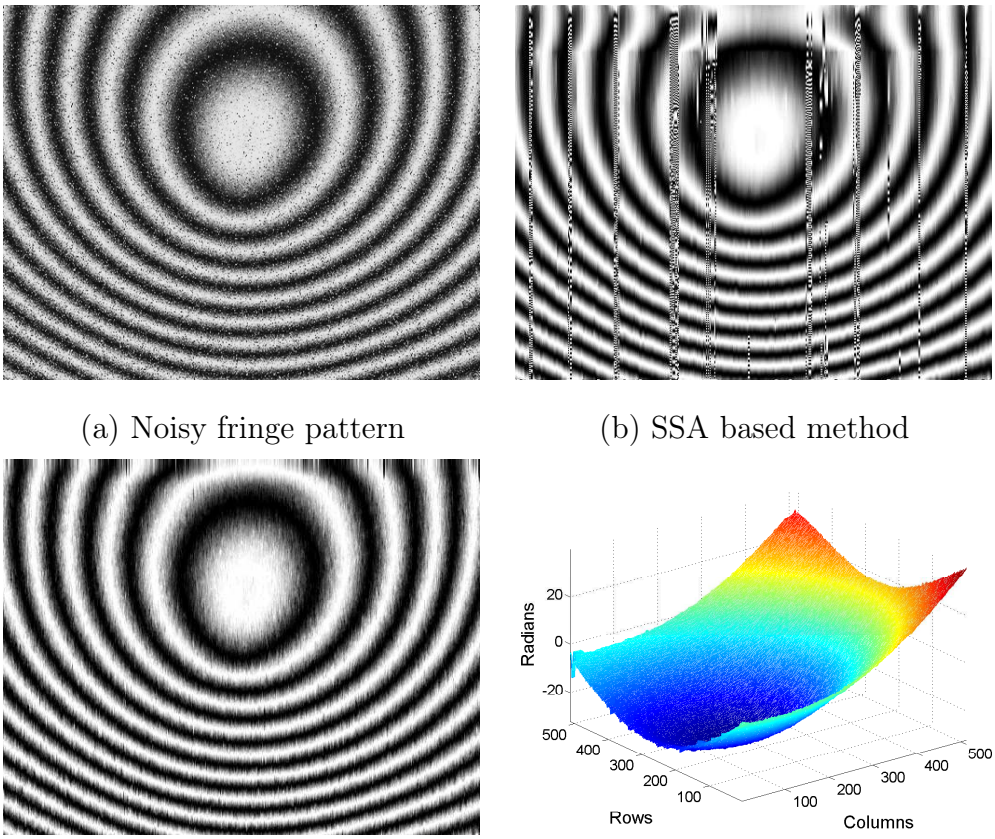

(a) Noisy fringe pattern (b) SSA based method

(c) Proposed Method (d) Est Phase by EKF

Figure 3.4: Qualitative comparison of phase estimation by SSA based method and proposed method. Distortion seen in the phase estimated by SSA based method corresponds to the divergence of EKF

3.3.1 Unscented Transformation

The UKF uses a deterministic sampling technique, Unscented Transform (UT) to pick a minimal set of sample points (called sigma points) around the mean such that these points capture mean and covariance of a prior random variable exactly, while approximating the mean and covariance of the transformed random variable up to the third order in Taylor series Julier and Uhlmann (2004). Consider, propagation of a random variable $\mathbf{x}$ (of dimension L), a state vector in our case, having mean $\bar{\mathbf{x}}$ and covariance $\mathbf{P_x}$, through a non-linear function $\mathbf{z} = \mathbf{h}(\mathbf{x})$. To calculate the first two moments of $\mathbf{z}$, we form a matrix of sigma points as follows:

$$\chi_0 = \bar{\mathbf{x}} \tag{3.12}$$

$$\chi_i = \bar{\mathbf{x}} + (\sqrt{(L+\lambda)\mathbf{P_x}})_i, \forall i = 1, \ldots, L \tag{3.13}$$

$$\chi_i = \bar{\mathbf{x}} - (\sqrt{(L+\lambda)\mathbf{P_x}})_i, \forall i = L+1, \ldots, 2L$$

$$w_0^{(\mu)} = \frac{\lambda}{(L+\lambda)} \tag{3.14}$$

$$w_0^{(c)} = \frac{\lambda}{(L+\lambda)} + (1 - \alpha^2 + \beta) \tag{3.15}$$

$$w_i^{(\mu)} = w_i^{(c)} = \frac{1}{2(L+\lambda)}, \forall i = 1, \ldots, 2L \tag{3.16}$$

where, χ_i are the sigma points, $w_i^{(\mu)}$ and $w_i^{(c)}$ are the weights to compute mean and covariance respectively. $\lambda = \alpha^2(L+k) - L$, is a scaling factor, α determines the spread of the sigma points around $\bar{\mathbf{x}}$ and is usually set to a small positive value. β is used to incorporate the prior knowledge about distribution of $\mathbf{x}$. The term $(\sqrt{(L+\lambda)\mathbf{P_x}})_i$ is the i^{th} row of the matrix square root of $(L+\lambda)\mathbf{P_x}$.

These sigma vectors are then passed through transformation function to get

$$\mathcal{Z}_i = \mathbf{h}(\chi_i), \qquad \forall i = 0, 1, 2, \cdots, 2L \tag{3.17}$$

The mean and the covariance of the posterior sigma points $\mathcal{Z}$ are approximated

as

$$\bar{\mathbf{z}} = \sum_{i=0}^{2L} w_i^{(\mu)} \mathcal{Z}_i \tag{3.18}$$

$$\mathbf{P_z} = \sum_{i=0}^{2L} w_i^{(c)} [(\mathcal{Z}_i - \bar{\mathbf{z}})(\mathcal{Z}_i - \bar{\mathbf{z}})^T] \tag{3.19}$$

These estimates in the mean are accurate upto the third order in the Taylor series, whereas the covariance estimates are accurate upto the fourth order in the Taylor series expansion [Sai Subrahmanyam (2008)].

3.3.2 Algorithm

The UKF is a straightforward extension of the UT for the recursive estimation of state vector from equations 3.5 and 3.11. The augmented state vector in UKF is redefined as the concatenation of the original state and noise variables. The UT sigma point selection scheme (Equations 3.12 through 3.16) is applied to this new augmented state vector to calculate the prior sigma points. These sigma points are then passed through state and observation functions to produce transformed sigma points. The statistics (mean and covariance) for the Kalman update equations are determined by using the transformed sigma points. Finally the Kalman updates are employed.

Let, $\mathbf{x}^a = \begin{bmatrix} \mathbf{x}^T & \mathbf{u}^T & \mathbf{v}^T \end{bmatrix}$ be an augmented state vector, λ be the composite scaling parameter, L be dimension of augmented state, $\mathbf{P}_u$ be the process noise covariance, $\mathbf{P}_v$ be the measurement noise covariance and w_i be the weights as calculated in equations 3.12 through 3.16. The complete phase estimation algorithm using UKF is as follows.

Initialize with:

$$\begin{aligned}
\hat{\mathbf{x}}_0 &= \mathbb{E}\{\mathbf{x}_0\} \\
\mathbf{P}_0 &= \mathbb{E}\{(\mathbf{x}_0 - \hat{\mathbf{x}}_0)(\mathbf{x}_0 - \hat{\mathbf{x}}_0)^T\} \\
\hat{\mathbf{x}}_0^a &= \mathbb{E}\{\mathbf{x}^a\} = \begin{bmatrix} \hat{\mathbf{x}}_0^T & \mathbf{0} & \mathbf{0} \end{bmatrix}^T \\
\mathbf{P}_0^a &= \mathbb{E}\{(\mathbf{x}_0^a - \hat{\mathbf{x}}_0^a)(\mathbf{x}_0^a - \hat{\mathbf{x}}_0^a)^T\} \\
&= \begin{bmatrix} \mathbf{P}_0 & \mathbf{0} & \mathbf{0} \\ \mathbf{0} & \mathbf{P}_u & \mathbf{0} \\ \mathbf{0} & \mathbf{0} & \mathbf{P}_v \end{bmatrix}
\end{aligned}$$

here, $\mathbb{E}\{\cdot\}$ is an expectation operator.

Now, $\forall$ k $\in \{1, 2, \cdots, N\}$, where, N is the number of pixels in a column:

Calculate the Sigma Points:

$$\chi_{k-1}^a = \begin{bmatrix} \hat{\mathbf{x}}_{k-1}^a & \hat{\mathbf{x}}_{k-1}^a + \sqrt{(L+\lambda)\mathbf{P}_{k-1}^a} & \hat{\mathbf{x}}_{k-1}^a - \sqrt{(L+\lambda)\mathbf{P}_{k-1}^a} \end{bmatrix}$$

Process Update Equations:

$$\begin{aligned}
\chi_{k|k-1}^x &= \boldsymbol{f}(\chi_{k-1}^x, \chi_{k-1}^u) \\
\hat{\mathbf{x}}_k^- &= \sum_{i=0}^{2L} w_i^{(\mu)} \chi_{i,k|k-1}^x \\
\mathbf{P}_k^- &= \sum_{i=0}^{2L} w_i^{(c)} [\chi_{i,k|k-1}^x - \hat{\mathbf{x}}_k^-][\chi_{i,k|k-1}^x - \hat{\mathbf{x}}_k^-]^T \\
\mathcal{Z}_{k|k-1} &= \boldsymbol{h}(\chi_{k|k-1}^x, \chi_{k-1}^v) \\
\hat{\mathbf{z}}_k^- &= \sum_{i=0}^{2L} w_i^{(\mu)} \mathcal{Z}_{i,k|k-1}
\end{aligned}$$

Measurement Update Equations:

$$\begin{aligned}
\mathbf{P}_{zz} &= \sum_{i=0}^{2L} w_i^{(c)} [\mathcal{Z}_{i,k|k-1} - \hat{\mathbf{z}}_k^-][\mathcal{Z}_{i,k|k-1} - \hat{\mathbf{z}}_k^-]^T \\
\mathbf{P}_{xz} &= \sum_{i=0}^{2L} w_i^{(c)} [\chi_{i,k|k-1} - \hat{\mathbf{x}}_k^-][\mathcal{Z}_{i,k|k-1} - \hat{\mathbf{z}}_k^-]^T \\
\mathbf{K} &= \mathbf{P}_{xz}\mathbf{P}_{zz}^{-1} \\
\hat{\mathbf{x}}_k &= \hat{\mathbf{x}}_k^- + \mathbf{K}(\mathbf{z}_k - \hat{\mathbf{z}}_k^-) \\
\mathbf{P}_k &= \mathbf{P}_k^- - \mathbf{K}\mathbf{P}_{zz}\mathbf{K}^T
\end{aligned}$$

We note that, unlike in EKF, no explicit calculation of Jacobian or Hessian of the nonlinear function is necessary to implement this algorithm. Also, proposed algorithm has the capability of providing directly the unwrapped phase from state vector, as the second element of state vector is a phase function itself.

3.3.3 Simulation Results

A complex interference field signal of size 512×512 was simulated in MATLAB. The zero-mean AWGN was then added at different SNRs using `awgn` function. UKF algorithm was applied to each column with initial guess taken as *arctan* of the first element of each column. With this strategy of initialization, we generate the phase map which is unwrapped for a given column, but needs post processing to avoid wrapping along the rows. Instead of this, we have used the phase value, calculated for first element of previous column as initial guess of phase for current column so that neither unwrapping nor phase stitching is required. The process noise covariance matrix is taken to be $\mathbf{Q} = diag\left(\begin{bmatrix}10^{-1} & 10^{-1} & 10^{-5} & 10^{-5}\end{bmatrix}\right)$ and measurement noise covariance matrix is taken as $\mathbf{R} = k_R \text{diag}\left(\begin{bmatrix}\sigma_{re}^2 & \sigma_{im}^2\end{bmatrix}\right)$ where, σ_{re}^2 and σ_{im}^2 are the variances estimated form uniform region of the fringe pattern and k_R is a scaling factor generally can be taken as 2.

To demonstrate the effectiveness of proposed approach, we have compared it with many other popular methods such as

1. Discrete Chirp-Fourier Transform (DCFT) [Gorthi and Rastogi (2009a)]

2. Improved High-order Ambiguity Function (IHAF) [Gorthi and Rastogi (2009b)]

3. State Space Approach (SSA) [Rajshekhar and Rastogi (2013)]

The comparison is made at three different levels. At first level we modified our signal tracking approach so that we can generate the polynomial coefficients and then reconstruct the phase. This modification is just like the piece-wise polynomial approximation approach, where we can fit second order polynomials for phase approximation in each segment. We call the estimated phase by this method as UKF_{Para}. The comparison of UKF_{Para} with different methods at slowly varying and lower dynamic range of phase maps at various noise levels are depicted. Here we have shown that the UKF_{Para} performs very well as compared to different methods. At second level, we have compared our direct signal estimation approach with existing parameter estimation methods at larger dynamic range of the same phase map. Here we have shown that the parameter estimation approach becomes unreliable for such phase maps. Finally, we have tested our algorithm for rapidly varying phase map. We compared proposed approach with the EKF based phase estimation algorithm, which shows that the UKF based phase estimation approach handles non-linearity of measurement model and noise effectively as compared to that of EKF.

Parameter Estimation Approach

A phase map [figure 3.5(a)] is generated using `peaks` function in MATLAB. The complex interference field is simulated using the generated phase map and zero mean AWGN is added to it at SNR of 20 dB. The corresponding fringe pattern is shown in figure 3.5(b).

Although the signal tracking approach is intended to estimate the phase signal directly as compared to the parameter estimation, for the fair comparison with the existing parameter estimation based methods, we have used following relation [Gal et al. (2007, 2008)] to get the coefficients of polynomials [See Appendix A for further details], which are then used to reconstruct the phase (UKF_{Para})

$$\theta(n) := \mathbf{C}\mathbf{F}^{-n}\mathbf{x}(n) \tag{3.20}$$

where, $\theta(n)$=$[\mathbf{A}(n), a_0, a_1, a_2]^T$ is a parameter vector containing amplitude as it's first element and matrix $\mathbf{C}$ is a diagonal matrix with elements 1, 1, 1, 0.5. We compared UKF$_{Para}$ with the well-known parameter estimation methods. While the number of segments is taken as 16 (Nw = 16) for all the methods, the order of polynomials for IHAF and SSA is taken as 4 (M = 4), whereas for DCFT, and UKF$_{Para}$ based methods it is taken as 2 (M = 2).

Error in estimated phase at every pixel location for the simulated pattern (figure 3.5) by different methods is shown in figure 3.6. As it can be seen from figure 3.6(a) through 3.6(d), all the methods perform equally well at SNR of 20 dB, however different methods start failing as the noise increases in the fringe pattern. Figure 3.7(a), shows the Root Mean Square Error (RMSE) produced by different method as the SNR is varied from 0 to 30 dB.

As both EKF and UKF are the variants of Kalman filters, they have the tendency to diverge due to noisy situations, inaccurate state space model, and inaccurate initial conditions, we have compared the divergence rates of both the methods in figure 3.7(b). The divergence rate is calculated as the ratio of number of columns where the phase estimation algorithm diverged to the total number of column. It can be seen from figure 3.7(b) that SSA quickly diverges below the cut-off SNR of 19dB, while UKF$_{Para}$ does not diverge even at 0 dB. Divergence in the SSA owes to the linearisation of the measurement model and absence of process noise term in the process model. Whereas our process model is based on

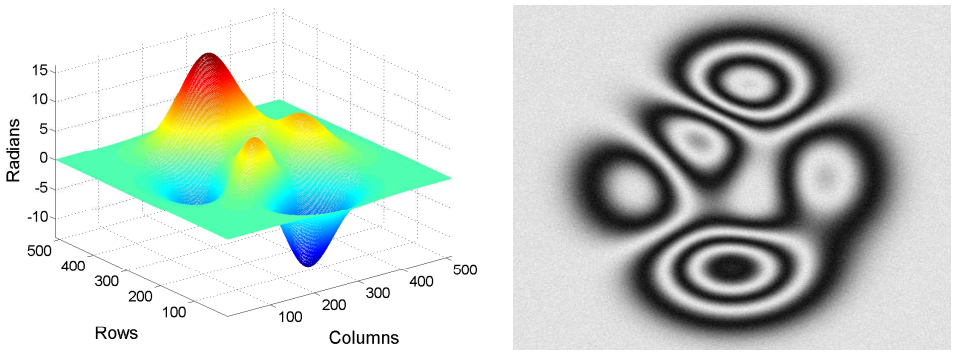

(a) Original Phase (b) Fringe Pattern

Figure 3.5: 3D mesh plot of original phase and the corresponding fringe pattern at SNR of 20 dB

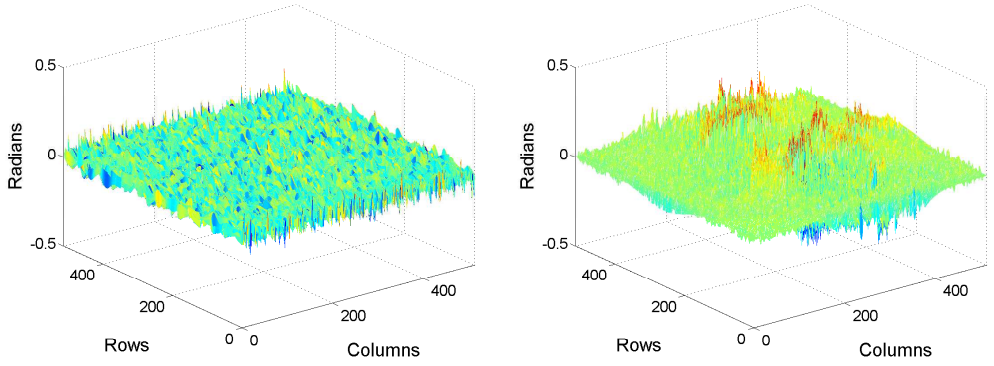

(a) IHAF based Method (b) SSA Method

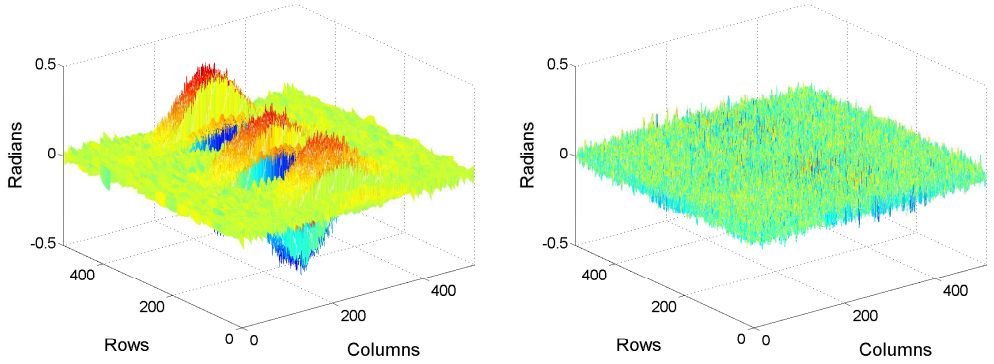

(c) DCFT based Method (d) UKF$_{Para}$ Method

Figure 3.6: Error in phase estimation with different methods at SNR 20dB.

Taylor series expansion, with additional process noise parameter for taking care of unmodelled higher order terms of the Taylor series, thus the UKF$_{Para}$ works effectively even at very low SNR levels.

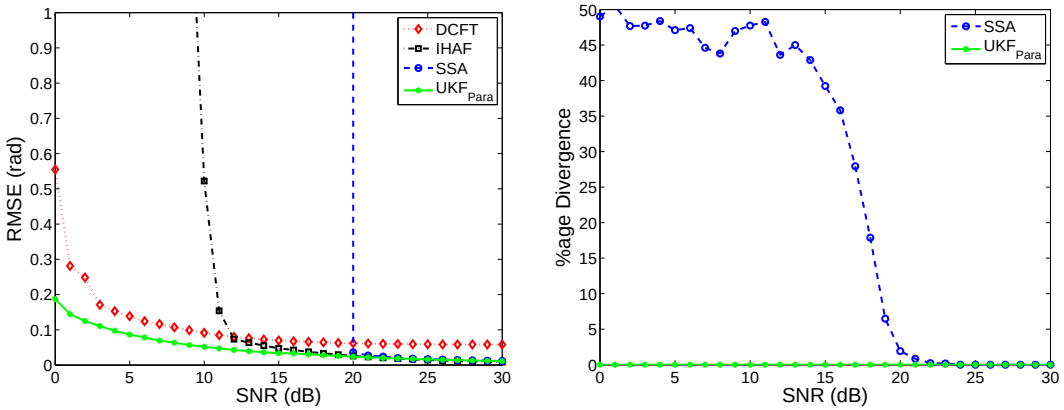

(a) RMSE versus SNR (b) Divergence rate versus SNR

Figure 3.7: Performance comparison of different methods. (a) RMSE vs SNR and (b) divergence rate vs SNR

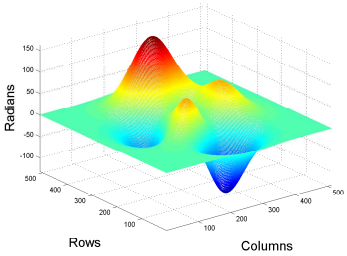

(a) Original Phase

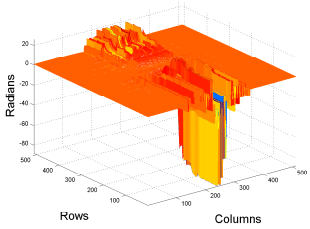

(b) IHAF based Method

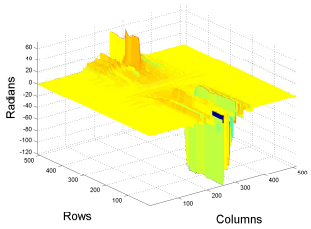

(c) DCFT based Method

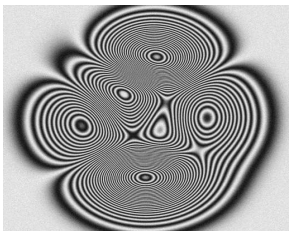

(d) Fringe Pattern

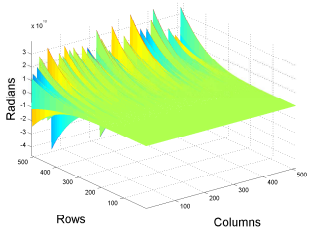

(e) SSA Method

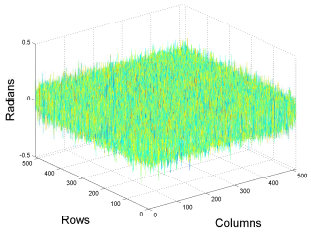

(f) UKF Method

Figure 3.8: 3D mesh plot of original phase (20×`peaks`) and corresponding fringe pattern at SNR of 20 dB. 3D mesh plots of phase estimation error maps showing relatively poor performance of polynomial approximation methods at larger dynamic range.

Table 3.1 gives the comparison of different methods based on computational time. Each method is used to process the reconstructed interference field of size 512×512. These methods were evaluated on a Windows PC with Intel(R) Xeon(R) CPU E3-1225 V2 at 3.20GHz, 16GB RAM and with MATLAB version 8.2.0.701 (R2013b).

Table 3.1: Comparison of Computational Time (in sec)

Method	DCFT	SSA	IHAF	UKF
Time	204.3605	27.0874	9.1061	38.1811

Comparison between Parameter and Signal tracking approaches

We have shown in the last section that when UKF based method applied for parameter estimation approach (UKF_{Para}), it outperforms the state-of-the-art parameter estimation methods under noisy conditions. In this section, we compared the performance of the proposed signal tracking approach (UKF) with various

parameter estimation methods. In order to quantify the performance variations among different methods in dealing with signals having higher dynamic range, we generated a phase map by using `peaks` function and up-scaled by a factor of 20, at the same resolution of 512×512. The 3D mesh plot of the simulated phase map is shown in figure 3.8(a), and the corresponding fringe pattern at SNR of 20 dB is shown in the figure 3.8(d).

Comparison for estimated phase with different methods along the middle column is shown in figure 3.9. As we increase the dynamic range (of values of the phase map), keeping same resolution, the slope of the phase increases. Hence the case of larger dynamic range can also be viewed as larger slope rate. In such cases, the parameter estimation based methods under-perform, producing distortion in the estimated phase, even at higher SNR values. The reason being, at increased dynamic range of phase, even a small error in the estimation of parameters can cause a larger variation in the overall estimated phase signal.

Figure 3.8(b,c,e,f) shows the 3D plots of error in estimated phase by IHAF, DCFT, SSA and UKF based methods. It can be noticed from figure 3.8 that if the phase has high dynamic range, the parametric methods fail to estimate the overall phase map. It is observed that the computational time for both UKF$_{Para}$ and proposed UKF based method are same.

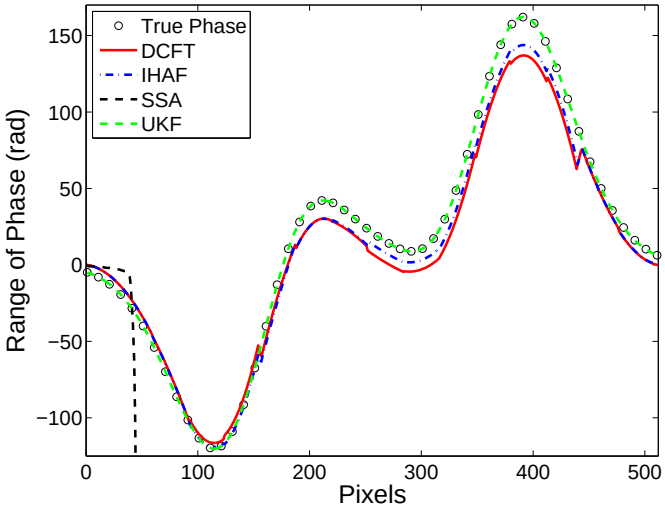

Figure 3.9: Estimated phase comparison along middle column of the phase map at SNR of 20 dB

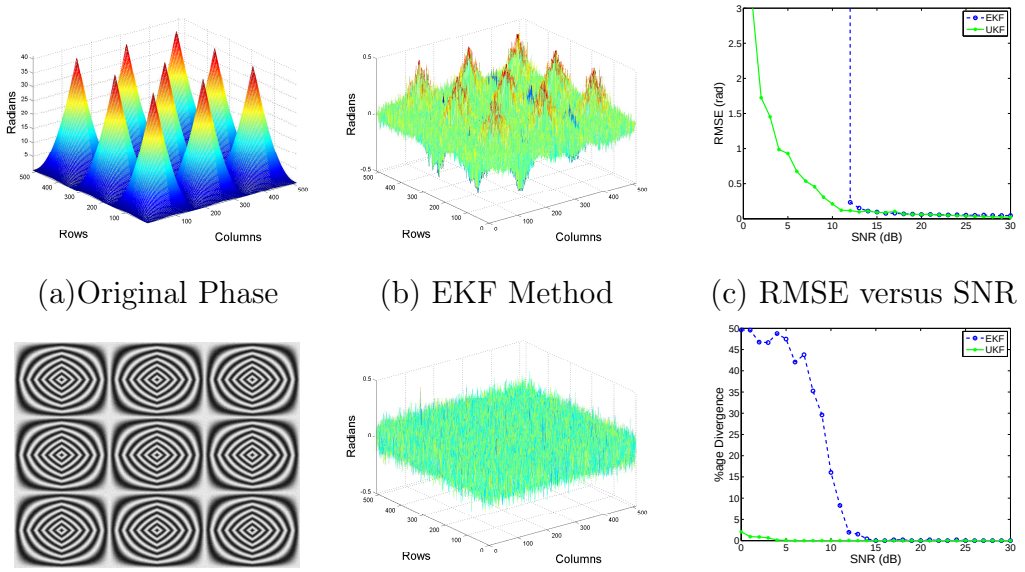

(a)Original Phase (b) EKF Method (c) RMSE versus SNR

(d) Fringe Pattern (e) UKF Method (f) Divergence versus SNR

Figure 3.10: Comparison of proposed EKF and UKF for signal tracking based phase estimation for rapidly varying phase maps at 20 dB. (a) & (d) shows 3D mesh plot of the true phase map and corresponding 2D image of fringe pattern. (b) & (e) shows error in phase estimation using EKF and UKF. (c) & (f) compares the performance of EKF and UKF for different values of SNR in terms of RMSE and divergence rate.

Dealing with rapidly varying phase signals

While deriving state space model, we used Taylor series expansion of phase function which requires an assumption of continuity and differentiability at a given point. However usually phase maps obtained in DHI may not always be well behaved functions. To verify the ability of the proposed approach in handling such cases, we generated a phase map as shown in figure 3.10(a). This phase map consists of multiple triangles in each row. As we traverse through columns, the angle between two sides of the triangle and the slope of side changes. This provides insights for the ability of the phase estimation technique to handle sudden change at the vertexes of the triangles of different shapes.

Fringe pattern shown in figure 3.10(d) is analysed with the proposed (UKF), and for the purpose of comparing its performance with already proposed EKF based method, the error plots obtained with both the methods are shown in figure

3.10(b), 3.10(e), respectively. It is found that both the filters work almost identical above SNR value of 12 dB. But under noisy conditions, EKF based method starts to diverge owing to linearisation of measurement model. Figure 3.10(c) and 3.10(f) shows the plots of RMSE and divergence rate against SNR for EKF and UKF, respectively. Figure 3.10 indicates that the UKF proves to be a better choice than EKF, in the successful realization of the proposed signal tracking approach for phase estimation in DHI. It is found that, though the process model follows Taylor series expansion, which requires the function to be continuous and differentiable, the approach works well with non-differentiable functions owing to signal tracking nature of the algorithm and the use of recent observations in Kalman update.

3.3.4 Experimental Results

Proposed method based on UKF for fringe analysis is validated using digital holographic interferometry experiment. The fringe patterns obtained under two deformation experiments are shown in Figures 3.11(a) and 3.11(d), where 3.11(a) is the representative case for rapidly varying phase signals and 3.11(d) is that of the noisy data. SSA and UKF were applied to the reconstructed interference field to estimate the phase. It is observed that SSA, by being piece-wise polynomial approximation approach, performs poorly.

Figures 3.11(b) and 3.11(e) shows fringe patterns generated using the estimated phase maps by SSA and figures 3.11(c) and 3.11(f) shows that by UKF. Estimated phase by SSA shows distortion which is due to divergence of EKF in noisy situation. Figure 3.12 shows the 3D mesh plots of the estimated phase signals by the proposed UKF method. The proposed approach is able to estimate the phase even when it is non-differentiable and rapidly varying (Figure 3.12(a)) and when the fringe pattern is severely corrupted by noise (Figure 3.12(b)).

3.4 Summary

In this chapter, we discussed a new approach, namely, the signal tracking approach, for phase estimation in DHI. Simulation and experimental results demon-

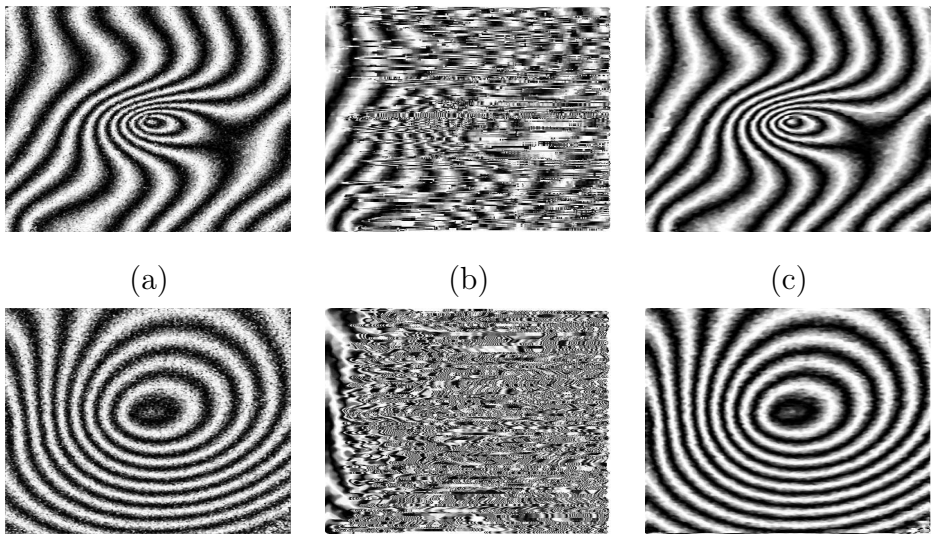

(a) (b) (c)

(d) (e) (f)

Figure 3.11: Comparison of SSA and UKF for experimental data. (a) and (d) shows the noisy fringe pattern of the reconstructed interference field. (b) and (e) are the fringes corresponding to phase estimated by SSA whereas (c) and (f) are that of proposed UKF.

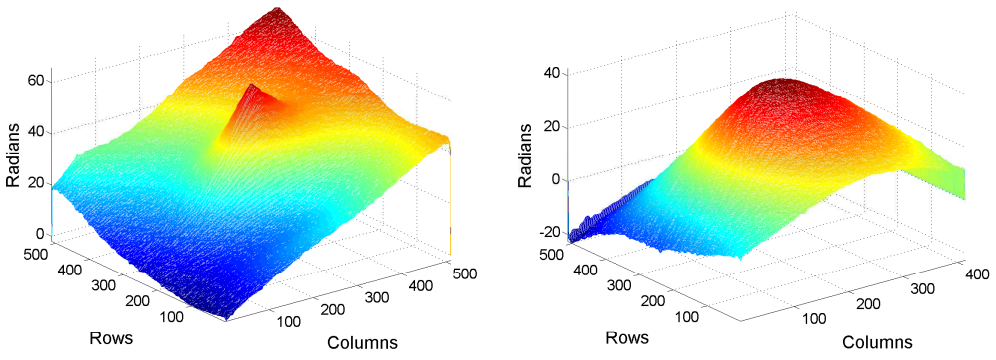

(a) (b)

Figure 3.12: 3D mesh plot of estimated phase using proposed method

strate that the signal tracking approach, realized using UKF yields more accurate phase estimates than that of the state-of-the-art approaches especially at lower SNRs. It is also observed that the proposed method produces accurate estimates even for complicated phase signals where the polynomial approximation approach based methods may have difficulty in the estimation of parameters. The analysis of the results indicate that the introduction of process noise covariance into state space model and use of UKF to estimate the state provides a significant improve-

ment in the accuracy of phase estimation, especially under noisy situation (SNR 0-20 dB). Also, since the derived state vector includes phase and derivatives of phase, it may give wide applicability of this algorithm in situations where simultaneous estimation of displacement (phase) as well as strain/curvature (derivatives of phase) are important.

CHAPTER 4

Particle Filter based Phase Estimation

The main objective of this chapter is to study the applicability of the Particle filter for continuous phase tracking under signal tracking framework. In chapter 3, we demonstrated that the signal tracking approach is a better substitute for its contemporary phase estimation methods. In this chapter, we demonstrate that the Particle filter, as against EKF and UKF, provides more accurate, unwrapped and continuous phase even when the phase is rapidly varying with larger slope range and when the fringes are corrupted by noise. Unlike Kalman filter and its variants, Particle filter is not limited by any linearity and Gaussian constraints and this fact motivates us to apply the particle filter in the present context. Here, we employ the same state model to propagate each of the Particles/Samples ahead in time/space. However, the weight updates in the Sequential Importance Re-sampling (SIR) are based on the Gaussian likelihood. This is guided by the non-linear (Polar-to-Cartesian) relationship between the state and observation and the Gaussian measurement noise. The main contribution of the work lies in formulating the likelihood based weight computations and algorithm design for phase estimation by *sequential importance sampling particle filter* framework.

4.1 Theoretical Foundation

The state space model used for particle filter based algorithm is:

$$\mathbf{x}(n) = \mathbf{F}\mathbf{x}(n-1) + \boldsymbol{\omega}(n-1) \tag{4.1}$$

$$\mathbf{z}(n) = \mathbf{h}(\mathbf{x}(n)) + \boldsymbol{\nu}(n) \tag{4.2}$$

where, state vector $\mathbf{x}(n)$, state transition matrix $\mathbf{F}$ and the non-linear function $\mathbf{h}(\mathbf{x})$ of the measurement model are given as:

$$\mathbf{x}(n) = \begin{bmatrix} a(n) & \phi(n) & \phi^{(1)}(n) & \cdots & \phi^{(M)}(n) \end{bmatrix}^T$$

$$\mathbf{F} = \begin{bmatrix} 1 & 0 & 0 & 0 & \cdots & 0 \\ 0 & 1 & \frac{1}{1!} & \frac{1}{2!} & \cdots & \frac{1}{M!} \\ 0 & 0 & 1 & \frac{1}{1!} & \cdots & \frac{1}{(M-1)!} \\ \vdots & \vdots & \vdots & \vdots & \ddots & \vdots \\ 0 & 0 & 0 & 0 & \cdots & 1 \end{bmatrix}$$

$$\mathbf{h}(\mathbf{x}) = \begin{bmatrix} a(n)cos(\phi(n)) \\ a(n)sin(\phi(n)) \end{bmatrix}$$

where $a(n)$ and $\phi(n)$ are the elements of the state vector $\mathbf{x}$. $\boldsymbol{\omega}(n) \sim \mathcal{N}(0, \boldsymbol{Q})$ is the state noise to compensate for the higher order terms of Taylor series. M is the number of terms of the Taylor series to be included into state vector, usually it can be taken from 2 to 9 depending upon the variations in the phase. $\boldsymbol{\nu}(n) \sim \mathcal{N}(0, \boldsymbol{R})$ represents the measurement noise. $\boldsymbol{Q}$ and $\boldsymbol{R}$ are the state and measurement noise covariance matrices, respectively. The stochastic representation of the used state space model can be written as

$$\mathbf{x}(n) \sim \mathcal{N}(\mathbf{F}\mathbf{x}(n-1), \boldsymbol{Q}) \tag{4.3}$$

$$\mathbf{z}(n) \sim \mathcal{N}(\mathbf{h}(\mathbf{x}(n)), \boldsymbol{R}) \tag{4.4}$$

Based on this state space model, we propose a robust particle filter based approach best suited to the phase estimation in DHI. The particle filter is a technique for recursive Bayesian estimation through Monte Carlo simulations. The key idea in Particle filter is to approximate the required posterior density by a set of random samples (particles) with associated weights and to calculate the estimates based on these samples and weights. The complete estimation process takes place into three steps: *Particle Propagation*, *Weight Computation* and *Resampling*. The particles are propagated through the state model $p(\mathbf{x}(n)|\mathbf{x}(n-1))$ (for the special case $\mathcal{N}(\mathbf{F}\mathbf{x}(n-1), \boldsymbol{Q})$) to generate a new set of predicted particles. The weights associated with each sample, $w_n^i;\ i = 1, ..., N_s$ (where, N_s is the total number of

particles) are obtained based on the observation model. An weighted average of these predicted samples using weights associated with each sample forms the final updated estimate for the state vector. The complete map of phase and it's derivatives is then formed by selecting corresponding components of the final estimate of the state vector.

The weight of each particle determines the accuracy of the state represented by that particle towards final updated estimate. The deviation of predicted observation from the actual observed values provides the information about reliability of the predicted state. As the noise present in the measurements is assumed to be Gaussian, the likelihood of the measurement is expressed in terms of standard Gaussian distribution. As the measurement taken for our experiment is in 2D, in the form of real and imaginary parts, the joint likelihood with an assumption that two components are independent is as follows:

$$\begin{aligned} w^i &= exp\left[-\frac{(\hat{z}_1^i - z_1)^2}{2\sigma^2}\right] \times exp\left[-\frac{(\hat{z}_2^i - z_2)^2}{2\sigma^2}\right] \\ &= exp\left[-\frac{(\hat{z}_1^i - z_1)^2 + (\hat{z}_2^i - z_2)^2}{2\sigma^2}\right] \end{aligned} \tag{4.5}$$

Where, $\hat{z}_k^i, k = 1, 2$ is the kth element of the predicted measurement vector corresponding to ith particle whereas $z_k, k = 1, 2$ is the kth element of the actual measurement vector at that location n.

The common problem encountered with particle filter approach is the degeneracy of samples, where after a few iterations, all but one particle has negligible weights. This implies that a considerable amount of computational work still needs to be performed to update the particles whose contribution to the approximation of posterior pdf $p(\boldsymbol{x}_k|\boldsymbol{z}_{1:k})$ is zero/negligible. Degeneracy problem can be avoided in many ways like by considering a good choice of importance density, choosing larger number of samples N_s. However, choosing a large number of samples results in an inefficient solution. Resampling the particles is one of the most widely used solution to avoid degeneracy [Li et al. (May 2015)].

The basic idea of resampling step is to eliminate the particles which have

Algorithm 1 Phase Estimation using Particle Filter

1: Initialize with

$$\hat{\mathbf{x}}(0) = \mathbb{E}\{\mathbf{x}(\mathbf{0})\}$$

2: Generate N_s samples/particles from probability density function $\mathcal{N}(\hat{\mathbf{x}}(0), Q)$

3: **for** n = 1:N **do**

4: **for** i = 1:Ns **do**

5: Propagate the particle through the state model

$$\mathbf{x}^i(n) = \mathbf{F}\mathbf{x}^i(n-1) + \boldsymbol{\omega}^i(n-1)$$

6: Generate the predicted measurements

$$\begin{bmatrix} \hat{z}_1^i \\ \hat{z}_2^i \end{bmatrix} = \begin{bmatrix} x_1^i cos(x_2^i) \\ x_1^i sin(x_2^i) \end{bmatrix}$$

Here, x_1 and x_2 are the 1^{st} and 2^{nd} components of the state vector $\boldsymbol{x}(n)$. Please note that the index (n) is dropped for the sake of brevity in step 6 and 7.

7: Compute weight for the particle

$$w^i = exp\left[-\frac{(\hat{z}_1^i - z_1)^2 + (\hat{z}_2^i - z_2)^2}{2\sigma^2}\right]$$

8: **end for**

9: **End For**

10: Normalize the weights

11: Calculate the final updated state vector

$$\hat{\mathbf{x}}(n) = \sum_{i=1}^{N_s} w^i \mathbf{x}^i(n)$$

12: Perform Systematic Resampling & update the samples and weights for next iteration

13: **end for**

14: **End For**

smaller weights and concentrate on the particles which have significantly larger weights. After resampling, all the particles have equal weights. We employed the systematic re-sampling scheme proposed by Kitagawa (1996) for our work. The normalised weights w^i are incrementally added to form a cumulative sum of $w_C^i = \sum_{j=1}^{i} w^j$. A 'comb' of N_s points spaced at regular intervals of $1/N_s$ is defined and the complete comb is translated by an offset chosen randomly from a uniform distribution over $[0, 1/N_s]$. The comb is then compared with cumulative sum of weights w_C^i. We select/re-sample a particle more than once/delete the sample based on how many times comb values fall within CDF of that particular sample. In this way re-sampling is carried for N_s samples. The re-sampled weights of each particle is $1/N_s$ which is used in calculation of posterior for next iteration. Complete phase estimation process using particle filter is summarised in the algorithm 1.

4.2 Simulation Results

A complex interference field of size 512×512 was simulated in MATLAB (R2013b) and the zero-mean additive white Gaussian noise was added at different Signal-to-Noise-Ratio (SNR) values using `awgn` function. The particle filter algorithm is then applied to individual column. The process noise covariance matrix $\mathbf{Q}$ is taken to be $\mathbf{Q}$= $K_q \times$ diag $\begin{bmatrix} 10^{-1} & 10^{-1} & 10^{-2} & \cdots & 10^{-M} \end{bmatrix}$ where K_q is the tuning parameter and takes value in range 0.1 to 10. The measurement noise covariance

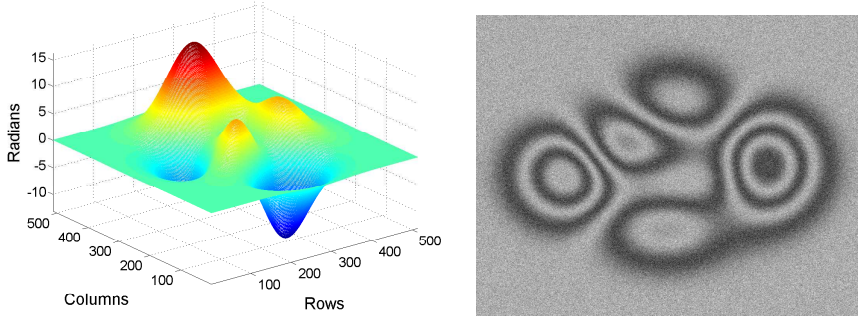

(a) Original Phase (b) Fringe Pattern

Figure 4.1: Simulated phase map ($2 \times$ `peaks`) and corresponding fringe pattern (SNR 5 dB).

$\mathbf{R}$ is estimated from a uniform region of the fringe pattern by using fast noise variance estimation method given in Immerkar (1996). Intuitively to estimate phase and phase derivatives with higher accuracy the state is modelled to include first M (usually 2 to 9) terms of the Taylor series.

Usually, initial guess of state vector is taken to be *arctan* of the first element of each column. Although this initialization produces unwrapped columns, it does not guarantee the unwrapping along the rows. In order to ensure unwrapping along rows, additional post processing like phase stitching becomes essential. We initialize the first element of the first column/row by using the values of amplitude and the wrapped phase (from the observations), and setting higher order terms of the state vector to zeros. This initialization is being refined by Particle filter updates. For rest of the columns, we initialize the state vector using the refined estimates (not the observations/wrapped phase) corresponding to the first element of the previous columns, which are already unwrapped estimates. This is based on the assumption that there will not be significant change in phase between the adjacent pixels of the first row/column. This initialization strategy along with particle filter updates produce continuous and unwrapped phase map along columns as well as rows without additional requirement of phase stitching or unwrapping.

The performance of the proposed method is compared with state-of-the-art methods such as Cubic Phase Function (CPF), Discrete Chirp-Fourier Transform (DCFT), Improved High-order Ambiguity Function(IHAF), UKF based signal tracking approach and MATLAB's (R2013b) `unwrap` function (version 5.14.4.4) with median filtering as pre- and post-processing. We simulated a phase map using `peaks` function and added moderate noise at 5 dB. The noisy fringe pattern is then processed by the state-of-the-art phase estimation methods. The true phase map along with corresponding fringe pattern at 5 dB are shown in figure 4.1 whereas error in estimation of phase by different methods are shown in figure 4.2.

It is observed that only DCFT and UKF based methods and MATLAB's `unwrap` function along with proposed approach performed well in presence of noise. Among them, DCFT based method uses second order polynomial for approximation of the phase making it unsuitable for rapidly varying phase maps. The `unwrap`

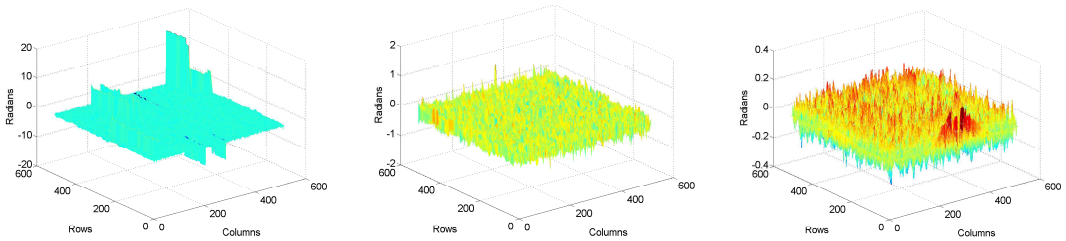

(a) CPF based method (b) DCFT based method (c) UKF based method

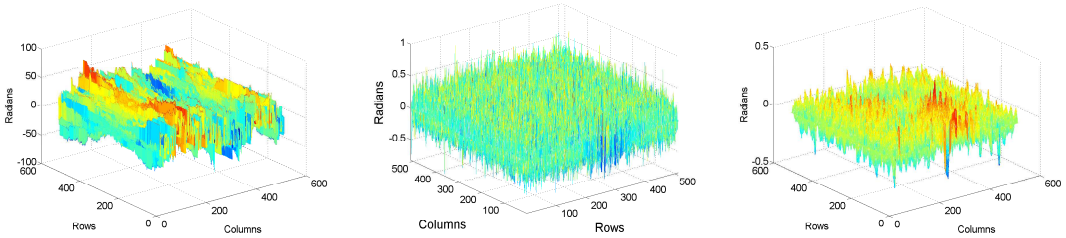

(d) IHAF based method (e) `unwrap` function (f) PF based method

Figure 4.2: Error in Phase estimation by state-of-the-art methods and the proposed particle filter approach for the simulated phase map (see fig. 4.1).

function of MATLAB R2013b performs unwrapping on the data column-wise. It uses derivative of wrapped phase map to remove the discontinuities introduced by wrapping and finally integrated them along columns to get the continuous phase map. This method works well provided that the wrapped phase has low noise and its derivative is unwrapped and continuous. This keep limitation on the performance under two conditions: (1) when the signal is corrupted by extreme noise and (2) when the underlying phase has very high dynamic range.

Table 4.1 compares the Root Mean Square Error (RMSE) values with different approaches at SNR of 5 dB and it can be seen that Particle Filter based approach outperforms all the state-of-the-art methods. Fig.4.3 shows the graph of RMS error

Table 4.1: Performance comparison in terms of RMSE in estimation of phase from the fringe pattern shown in figure 4.1(b) among proposed approach and the state-of-the-art approaches.

Approach	CPF	IHAF	DCFT	Unwrap	UKF	PF
RMSE (in radians)	1.6840	0.2226	0.1501	0.1656	0.0966	0.0797

versus SNR in the range of 0-30 dB through various state-of-the-art approaches. It can be observed that PF based approach is robust to noise and performs better when compared to all other methods even at lower SNR values, especially in the range of 0-5 dB.

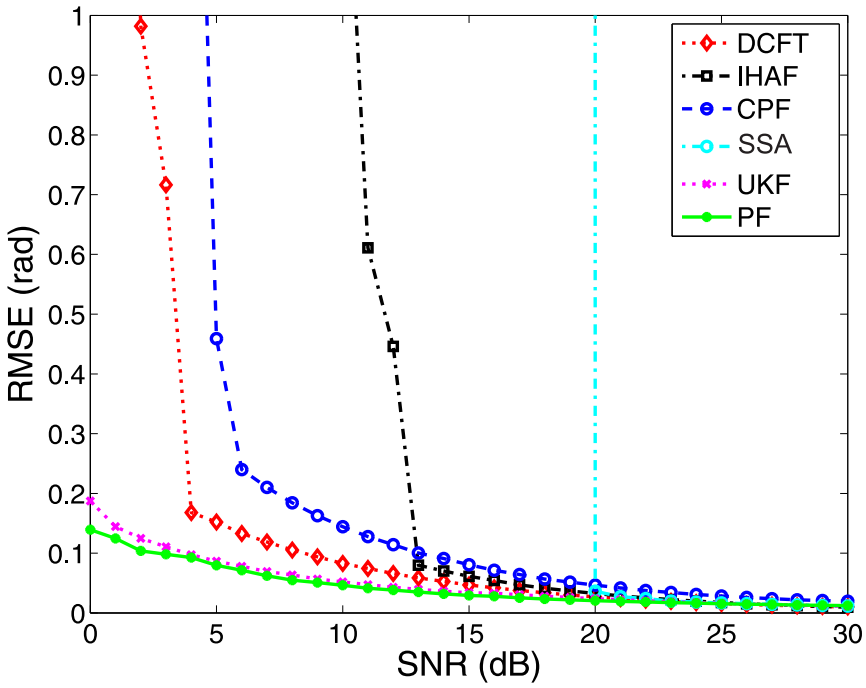

Figure 4.3: RMSE versus SNR through various approaches.

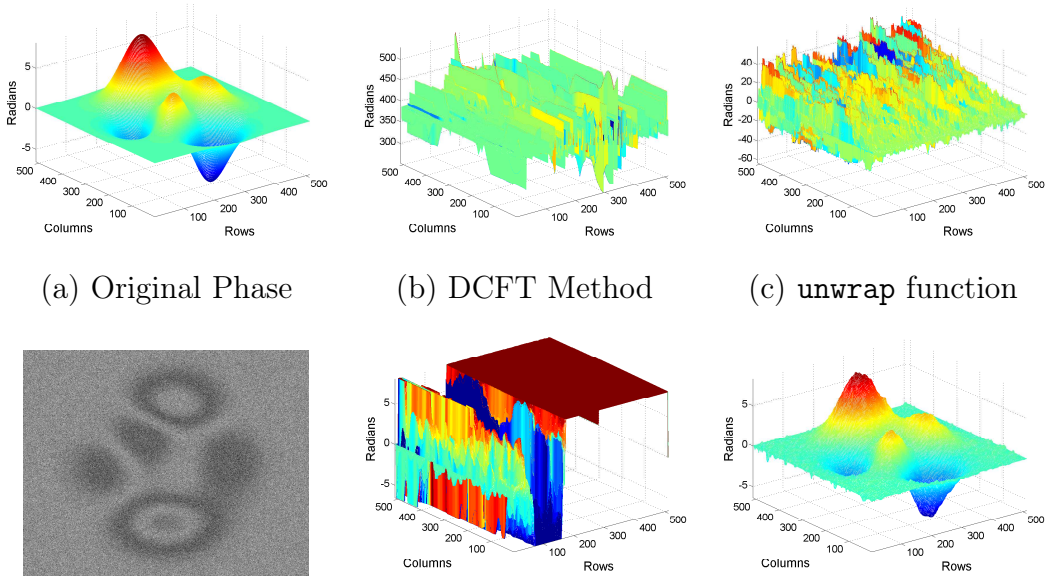

(a) Original Phase (b) DCFT Method (c) `unwrap` function

(d) Fringe Pattern (e) UKF Method (f) Proposed method

Figure 4.4: Estimated phase maps by different approaches. Condition 1: Extremely noisy fringe pattern. (SNR -5 dB).

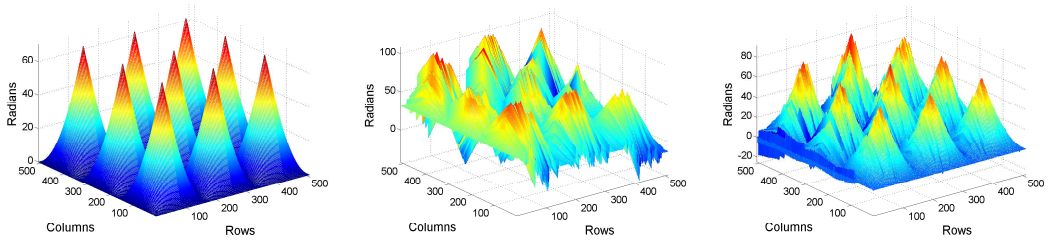

(a) Original Phase (b) DCFT Method (c) `unwrap` function

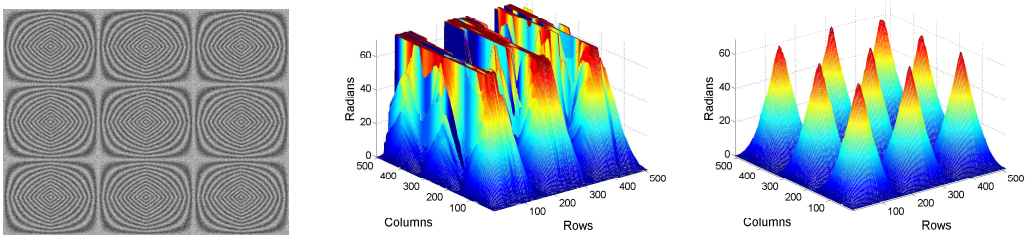

(d) Fringe Pattern (e) UKF Method (f) Proposed method

Figure 4.5: Estimated phase maps by different approaches. Condition 2: Rapidly varying phase with extremely noisy fringe pattern (SNR 2 dB).

We have tested the proposed approach under three conditions which validates the reliability of the proposed approach.

1. extremely noisy fringe pattern (Fig. 4.4)
2. rapidly varying phase (Fig. 4.5)
3. phase map with larger dynamic range (Fig. 4.6)

For first condition, we generated a simple peak function as phase map and white Gaussian noise is added to this fringe pattern at SNR of -5 dB. Second condition represents sudden changes in phase values at the vertices of the pyramids. Finally for the third condition shows we up-scaled the peaks function with a factor 20.

Figures 4.4, 4.5 and 4.6 show the comparison of estimated phase map by DCFT, UKF and MATLAB's `unwrap` function based methods with the proposed method. For MATLAB's `unwrap` function, we first unwrapped the phase map along column and then rows. The resultant unwrapped phase was then filtered by 3×3 median filter to remove the noise. The table 4.2 given the comparison of state-of-the-art

Table 4.2: Comparison of RMSE among state-of-the-art and the proposed method for different types of conditions.

Method	Extreme Noise (SNR of -5 dB)	Rapidly Varying Phase (SNR of 2 dB)	High Dynamic Range (SNR of 2 dB)
DCFT	16.4211	15.0154	16.6237
UKF	848.4214	349.2850	416.0399
`unwrap`	4.3355	20.3133	5.8828
Particle Filter	**0.2251**	**0.7390**	**0.7530**

with the proposed method in terms of root mean square error (RMSE) in the estimation of phase.

It is observed, from figures 4.4–4.6 and table 4.2, that the phase estimation becomes challenging in the presence of noise in the fringe pattern and higher dynamic range of the phase simultaneously. In such situations, where even state-of-the-art methods become unreliable, proposed method gives better estimates for the phase. Even though the state model through Taylor series expansion assumes the

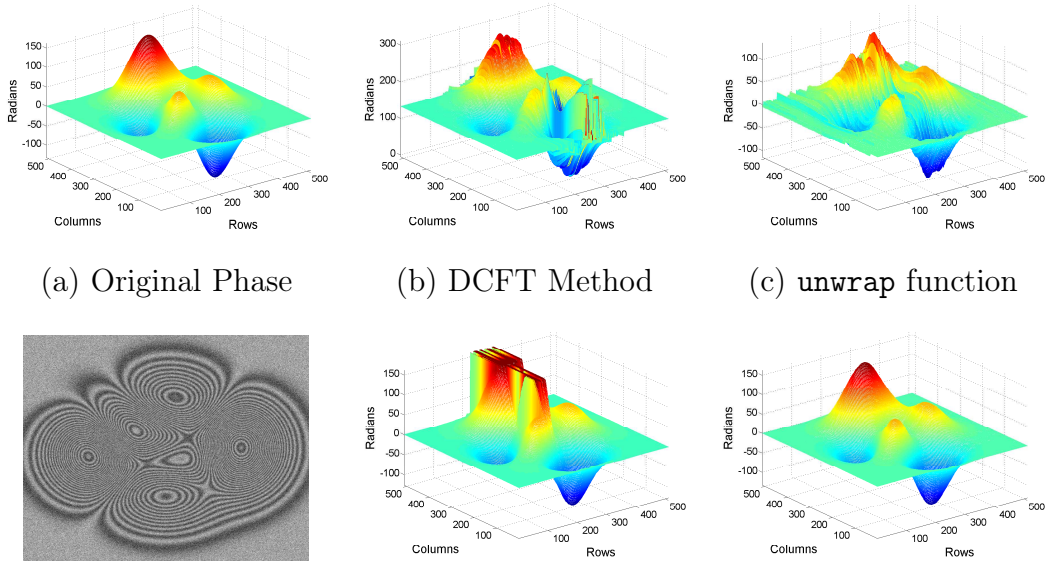

(a) Original Phase (b) DCFT Method (c) `unwrap` function

(d) Fringe Pattern (e) UKF Method (f) Proposed method

Figure 4.6: Estimated phase maps by different approaches. Condition 3: larger dynamic range with extremely noisy fringe pattern (SNR 2dB).

Table 4.3: Comparison of Computational Time through Particle filtering approach by varying number of particles for phase estimation.

Number of particles	50	100	200	350	500	600	750
Time (s)	5.12	10.4	29.7	81	160	225	352

phase to continuous and differentiable at every point, the generalization capability of particle filter based state estimation is reflected in terms of estimation of rapidly varying phase.

The performance of proposed method can be further improved by fine tuning of the parameters- scalar factor for measurement noise covariance matrix K_q, Measurement noise variance σ^2 and the number of particles. Table 4.3 summarizes the computation time required for a 512 $\times$ 512 image at SNR of 5 dB by varying the number of particles using Particle filtering approach. It can be seen that as the number of particles for phase estimation increases, time for simulation also increases.

In general, 100 particles are sufficient if phase estimation is performed at low noisy conditions (i.e., at SNR of 0-30 dB). Number of particles should be increased suitably if estimation is carried out under noisy conditions. In all the simulations 100 particles are used for phase estimation, except at SNR of -5 dB of the interference field, where 300 particles are used for phase estimation. Based on noise statistics in the image, K_q should be tuned while number of particles required for estimation is directly proportional to the noise in the underlying image. All the simulations were performed on Windows PC with Intel(R) Xeon(R) CPU X5675 (2 Processors with total 12 cores) at 3.07 GHz, 24 GB RAM with MATLAB version 8.2.0.701 (R2013b) using Parallel Computing toolbox.

4.3 Experimental Results

The performance of the proposed approach was verified on reconstructed interference field generated through real-time digital holography experiment.

The fringe pattern (real part of the complex interference field) is shown in

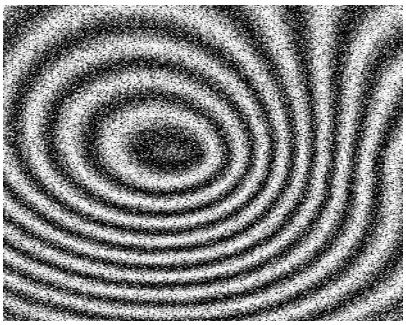

(a) Noisy Fringes

(b) Fringes with Est. Phase

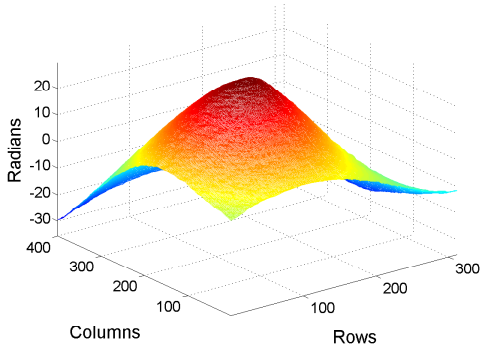

c) Est. Phase

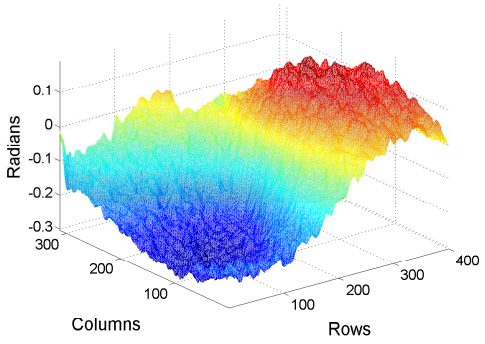

(d) Est. phase Derivatives

Figure 4.7: Experimental results. Figure (a) shows the noisy fringes, figure (b) shows the fringes generated by estimated phase for qualitative analysis, (c) and (d) show 3D mesh plot of the estimated phase and phase derivatives, respectively.

figure 4.7(a). This reconstructed interference field was then processed along individual columns using the proposed approach. The state vector for the proposed method was formed by taking 4 terms of the Taylor series ($M = 4$), which enables the accurate and simultaneous estimation of phase and phase derivative with the proposed algorithm. The estimated phase and its derivatives are shown in figure 4.7(c) & 4.7(d), respectively. We have generated the fringe pattern for qualitative analysis using estimated phase and is shown in figure 4.7(b). From the simulation and experimental results, it is evident that the proposed approach is suitable for processing of severely corrupted reconstructed interference field.

4.4 Summary

This work is a very first attempt to investigate the application of particle filter as a signal tracking approach for phase estimation in digital holographic interferometry. Simulation and experimental results demonstrate the fact that the proposed particle filter based approach accomplishes the tasks, where EKF and UKF were having trouble in estimation, especially at lower SNRs. The proposed method is able to perform phase estimation even at SNR of -5 dB and to the best of our knowledge, this is the only method which works at such lower SNR values. The robustness of the proposed approach to noise is demonstrated from very low values of RMS error. One can also estimate the phase even under SNR of -5 dB by properly tuning the parameters $\mathbf{Q}$ and number of particle N_s.

CHAPTER 5

Wrapped Statistics based Phase Estimation

In previous chapters, we presented a signal tracking approach to deal with the interferometric fringes corrupted severely by noise as well as for signals with larger dynamic range. The use of rotating vector model as measurement model in signal tracking approach leads to non-linear transformation of the state. Such systems can be analysed either by EKF or UKF. In rotating vector model, the observations are considered to be 2D vectors (i.e., real and imaginary parts of the measurement) whereas the state is truly 1D (i.e., angle of measurement). We found that, this introduces unnecessary non-linearity in the form of polar to Cartesian conversion to the system that limits the tracking capabilities.

In order to resolve this issue, we are proposing to use wrapped dynamical system [Traa and Smaragdis (2013)] as the measurement model. This, as against the earlier work [Rajshekhar and Rastogi (2013)], bypasses the 2D non-linear rotating vector model. Also, wrapped dynamical model accounts for the probability of translation of the measurement by integer multiples of 2π, and corrects the predicted state accordingly. It is observed that the proposed method produces accurate, continuous and unwrapped phase map directly even when the Signal-to-Noise Ratio (SNR) of interference fringes is around 0 dB and the underlying phase has very high dynamic range. The DCFT [Gorthi and Rastogi (2009a)] based method (polynomial approximation approach) and UKF based method (signal tracking approach) have this capability of handling noisy interference fringes provided that the phase pattern is having lower dynamic range.

The simulation results substantiate the ability of the proposed method in dealing with the complex signals, having phase maps with extended dynamic range and when corrupted by high levels of noise, whereas the experimental results demonstrates its applicability for the analysis of reconstructed interference fields in digital holographic interferometry for phase estimation.

5.1 Theoretical Foundation

In digital holographic interferometry, usually, two holograms are recorded corresponding to the object state prior to and post deformation. Numerical reconstruction of both the holograms provides their respective reconstructed object wave fields. Multiplication of one reconstructed object wave field with that of complex conjugate of the other, generates the reconstructed interference field. The reconstructed interference field in DHI, given by equation (2.6), is represented as:

$$f(m,n) = a(m,n)e^{j\phi(m,n)} + \nu(m,n) \tag{5.1}$$

where $a(m,n)$ and $\phi(m,n)$ are the amplitude and phase of the $M \times N$ complex reconstructed interference field. m and n are the rows and columns, respectively. $\nu(m,n)$ is the observation noise modelled as additive white Gaussian noise (AWGN). For an arbitrary row, we can write:

$$f_m(n) = a_m(n)e^{j\phi_m(n)} + \nu_m(n) \tag{5.2}$$

State Space Model

The phase pattern is approximated using Taylor series expansion-

$$\phi(n+1) = \phi(n) + \frac{1}{1!}\phi^{(1)}(n) + \frac{1}{2!}\phi^{(2)}(n) + \frac{1}{M!}\phi^{(M)}(n) + \text{Higher Order Terms} \tag{5.3}$$

we can write this in matrix form as follows:

$$\mathbf{x}(n+1) = \mathbf{F}\mathbf{x}(n) + \mathbf{w}(n) \tag{5.4}$$

where,

$$\mathbf{x}(n) = \begin{bmatrix} \phi(n) & \phi^{(1)}(n) & \cdots & \phi^{(M)}(n) \end{bmatrix}^T$$

$$\mathbf{F} = \begin{bmatrix} 1 & \frac{1}{1!} & \frac{1}{2!} & \cdots & \frac{1}{M!} \\ 0 & 1 & \frac{1}{1!} & \cdots & \frac{1}{(M-1)!} \\ \vdots & \vdots & \vdots & \ddots & \vdots \\ 0 & 0 & 0 & \cdots & 1 \end{bmatrix}$$

Here, the vector $\mathbf{x}(n)$ denotes the state vector, the matrix $\mathbf{F}$ is the transition matrix representing the relation between the present and the next state of the field while $\mathbf{w}(n) \sim \mathcal{N}(0, Q)$ is the process noise that compensate the discarded higher order terms.

The phase pattern obtained by taking *arctan* of the interference field, which is a wrapped phase, is limited to the range $(-\pi, \pi]$. The wrapped statistics provides a suitable tool to approximate the phenomenon of wrapping of the phase pattern. The corresponding measurement vector $\mathbf{y}(\mathbf{n})$ for the phase [i.e., angle of the $f_m(n)$], which will help us for innovation correction process, is obtained by using state vector $\mathbf{x}(n)$.

The state vector $\mathbf{x}(n)$ has the first element as $\phi(n)$, which is unwrapped phase and belong to interval $[-\infty, \infty]$, whereas the measurements are wrapped and belong to the range $(-\pi, \pi]$. Given a distribution on the line, we can wrap it inside an interval (just like wrapping around a circle of unit radius). That means, if x is random variable on the line, the corresponding random variable x_w of the wrapped distribution is given by [Mardia and Jupp (1999)]:

$$x_w = \psi(x) = mod(x + \pi, 2\pi) - \pi \tag{5.5}$$

Thus, the wrapped measurement model can be predicted from the predicted state vector using the following relation:

$$\mathbf{y}(n) = \psi[\mathbf{H}\mathbf{x}(n) + \nu(n)] \tag{5.6}$$

Here, $H = \begin{bmatrix} 1 & 0 & \cdots & 0 \end{bmatrix}$ is the measurement transition matrix. $\nu(n) \sim \mathcal{N}(0, R)$ is the measurement noise. The function $\psi(\cdot)$ is wrapping function that is defined in equation (5.5).

Wrapped Gaussian Distribution

According to Mardia and Jupp (1999), if x has distribution function F, then the distribution function F_ϕ of the corresponding wrapped random variable x_w is given by:

$$F_w(\theta) = \sum_{k=-\infty}^{\infty} \{F(\theta + 2\pi k) - F(\theta + 2\pi k)\}, \quad 0 \leq \theta \leq 2\pi \tag{5.7}$$

and similarly we can write about probability density function as:

$$f_w(\theta) = \sum_{k=-\infty}^{\infty} f(\theta + 2\pi k), \quad 0 \leq \theta \leq 2\pi \tag{5.8}$$

Now, The function $\psi(\cdot)$ in equation (5.5) transforms the Gaussian distribution to wrapped Gaussian distribution. Therefore the measurements $\mathbf{y}(n)$, which are wrapped due to `arctan` function, can be approximated by the wrapped Gaussian which is given by the following relation,

$$\mathcal{P}_w(\mathbf{y}(n); \mu, \sigma^2) = \sum_{k=-\infty}^{\infty} \mathcal{P}_l^{(k)}(\mathbf{y}(n); \mu, \sigma^2) \tag{5.9}$$

where,

$$\mathcal{P}_l^{(k)}(\theta; \mu, \sigma^2) = \frac{1}{\sqrt{2\pi\sigma^2}} e^{-((\theta+2\pi k)-\mu)^2/2\sigma^2} \tag{5.10}$$

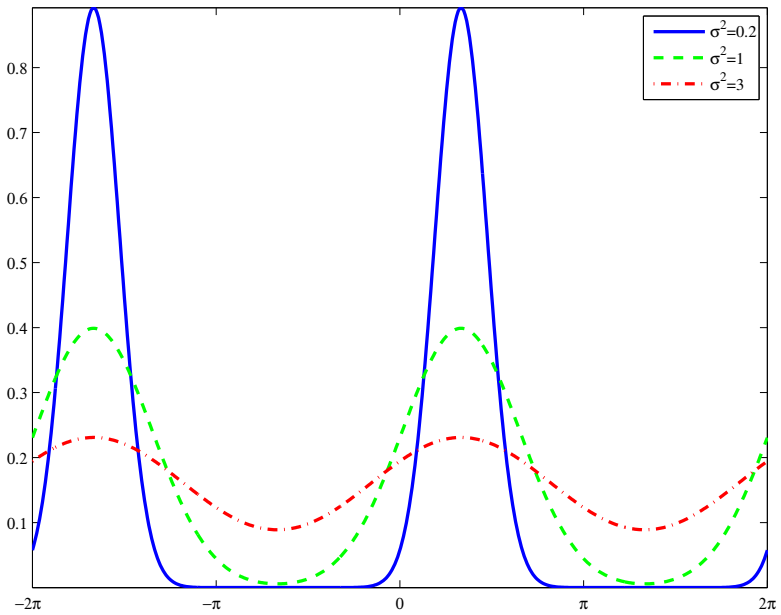

Figure 5.1: Wrapped Gaussian distribution with $\mu = \frac{\pi}{3}$ and varying σ^2.

Figure 5.1 shows the plot of the wrapped Gaussian distribution ($\mathcal{P}_w$) at $\mu = \frac{\pi}{3}$ and varying σ^2. This can be interpreted as the addition of infinite Gaussian distribution with variance σ^2 and mean μ translated by integer multiple of 2π, which is confined to the interval $\Big[-\pi \quad \pi\Big]$.

5.1.1 Wrapped Kalman Filter

The wrapped Gaussian models the wrapping function $\psi(\cdot)$. The distribution of the filtered state at pixel $n-1$ becomes:

$$\begin{aligned} P(x_{n-1}|y_{1:n-1}) &= \sum_{k=-\infty}^{\infty} P_k(x_{n-1}|y_{1:n-1}) \\ &= \sum_{k=-\infty}^{\infty} \mathcal{N}(x_{n-1}; \mu_x + 2\pi k, \sigma^2_{x_{n-1}}) \end{aligned} \tag{5.11}$$

Here, for sake of brevity, we have used indices as subscripts such as $\mathbf{x}_n$ for $\mathbf{x}(n)$ and $\mathbf{y}_{1:n}$ for $\mathbf{y}(1:n)$. As the state model (equation 5.4) is linear, prediction of the state is straightforward. The state distributions (mean and variance) is predicted by applying the state transition matrix to the present state vector. At each step, the distribution of the predicted state is given by

$$\begin{aligned} P(x_n|y_{1:n-1}) &= \int P(x_n|x_{n-1}) P(x_{n-1}|y_{1:n-1}) dx_{n-1} \\ &= \sum_{k=-\infty}^{\infty} \int P(x_n|x_{n-1}) P_k(x_{n-1}|y_{1:n-1}) dx_{n-1} \\ &= \sum_{k=-\infty}^{\infty} P_k(x_n|y_{1:n-1}) \end{aligned}$$

After predicting the state distribution, we need to correct it through innovation correction process. For that, we model the wrapping function $\psi(\cdot)$ in equation 5.6 using the wrapped Gaussian distribution. The corrected state vector is:

$$\begin{aligned} \mathcal{P}_w(\mathbf{x}_n|y_{1:n}) &\propto \mathcal{P}_w(y_n|\mathbf{x}_n) \mathcal{P}_w(\mathbf{x}_n|y_{1:n-1}) \\ &\propto \left[\sum_{m=-\infty}^{\infty} \mathcal{P}_l^{(m)}(y_n|\mathbf{x}_n) \right] \left[\sum_{k=-\infty}^{\infty} \mathcal{P}_l^{(k)}(\mathbf{x}_n|y_{1:n-1}) \right] \end{aligned} \tag{5.12}$$

As equation 5.12 is sum of infinite Gaussian components of predicted density translated by integer multiples of 2π. We approximate it by single term of predicted density and replicating the observations at interval of 2π Traa and Smaragdis (2013). The probability of the replication of the observations can be interpreted as:

$$\eta_{n,l} = \frac{\mathcal{P}_l^{(l)}(y_n; x_n, \sigma_w^2)}{\sum_{m=-\infty}^{\infty} \mathcal{P}_l^{(m)}(y_n; x_n, \sigma_w^2)} \tag{5.13}$$

Using the probability of replication of y_n, we form a weighted average of innovations due to copies of y_n. As the characteristics of the Gaussian distribution dictates that the probability value decreased exponentially as we move away from the mean value, we can safely truncate the infinite sum to L terms of translation on either side of the measurement value. The predicted state is then corrected using the resultant innovations which is given by

$$g_n = \sum_{l=-L}^{L} (y_n + 2\pi l - x_n)\eta_{n,l} \tag{5.14}$$

Algorithm: Phase retrieval using wrapped Kalman filter

The following algorithm summarizes the wrapped Kalman filter application for digital holographic interferometry

Initialize

$$\begin{aligned} \hat{\mathbf{x}}(0) &= \mathbb{E}(\mathbf{x}(0)) \\ \mathbf{P}^{+}(0) &= \mathbb{E}([\mathbf{x}(0) - \hat{\mathbf{x}}(0)][\mathbf{x}(0) - \hat{\mathbf{x}}(0)]^T) \end{aligned}$$

where, $\mathbf{P}^{+}(0)$ is the state error covariance

Predict

$$\begin{aligned}\hat{\mathbf{x}}^{-}(n) &= \mathbf{F}\hat{\mathbf{x}}(n-1)\\ \mathbf{P}^{-}(n) &= \mathbf{F}\mathbf{P}^{+}(n-1)\mathbf{F}^{T}+\mathbf{Q}\end{aligned}$$

where, $\mathbf{Q}$ being the state noise covariance.

Correct

$$\begin{aligned}\mathbf{K} &= \mathbf{P}^{-}(n)\mathbf{H}^{T}(\mathbf{H}\mathbf{P}^{-}(n)\mathbf{H}^{T}+\mathbf{R})^{-1}\\ \mathbf{P}^{+}(n) &= (\mathbb{I}-\mathbf{K}\mathbf{H})\mathbf{P}^{-}(n)\\ g_n &= \sum_{l=-L}^{L}(y_n+2\pi l-x_n)\eta_{n,l}\\ \hat{\mathbf{x}}(\mathbf{n}) &= \hat{\mathbf{x}}^{-}(n)+\mathbf{K}g_n\end{aligned}$$

where, $\mathbf{R}$ being measurement noise covariance, which can be estimated as a variance of a uniform region of the fringe pattern. $\mathbb{I}$ represent the identity matrix of appropriate order.

5.2 Simulation Results

MATLAB 2013b was used to validate the proposed method for phase estimation. The phase map representing the larger dynamic range was generated using `peaks` function. The complex reconstructed interference field was simulated using the generated phase map and the constant amplitude via equation 2.6. The complex additive white Gaussian noise with zero mean and variance σ_{ν}^{2} was simulated using `randn` function of MATLAB and added to the simulated interference field in order to generate the noisy signal. Original phase map and the noisy fringes (real part of the interference field) at $\sigma_{\eta}^{2}=0.65$ (SNR ≈ 0 dB) are shown in the figure 5.2.

The noisy complex field, shown in figure 5.2(b), was processed along individual rows/columns using proposed method to estimate the phase. The proposed approach is compared with the state-of-the-art phase estimation methods such as DCFT and UKF based method. The DCFT based method is a candidate of piecewise polynomial approximation approach, where individual column (or

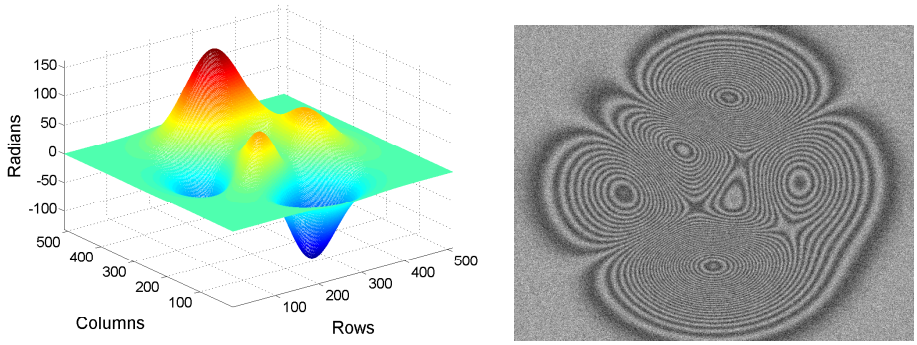

(a) True phase map (b) Noisy fringe pattern

Figure 5.2: Simulated phase map and corresponding noisy fringes

row) is divided into segments and each segment is approximated by polynomial of sufficient order. The parameters of polynomials are then estimated using signal

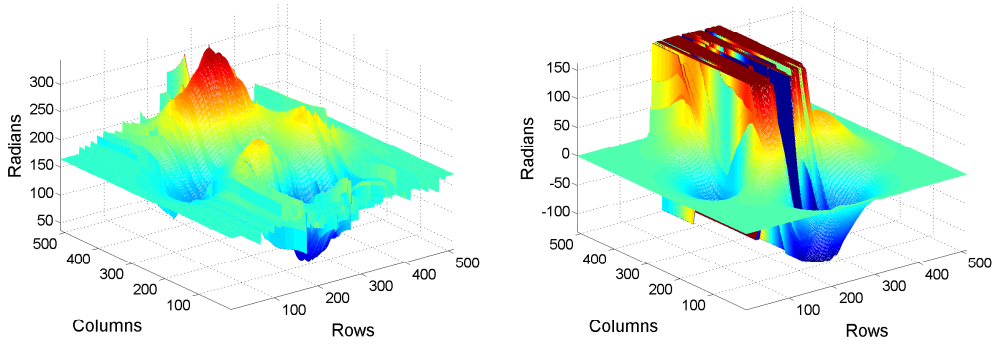

(a) DCFT approach (b) UKF approach

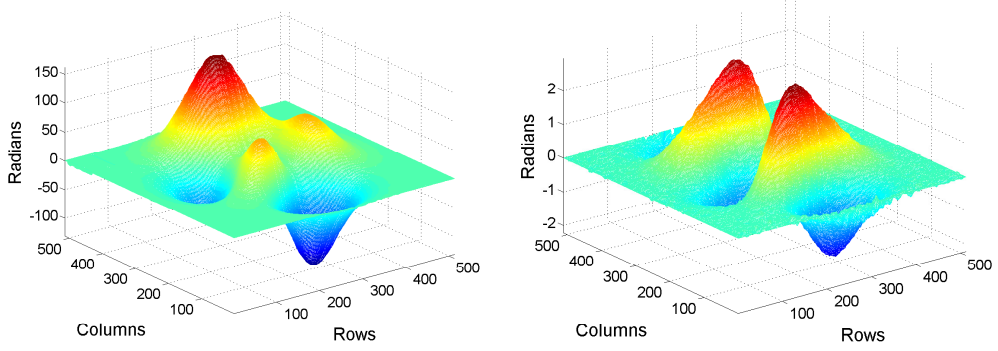

(c) WKF Approach (d) Derivatives by WKF

Figure 5.3: Comparison of phase estimation among DCFT and UKF based methods and the proposed method. Phase estimated by (a) DCFT (b) UKF and (c) proposed approach. Figure (d) shows the phase derivatives estimated by proposed approach

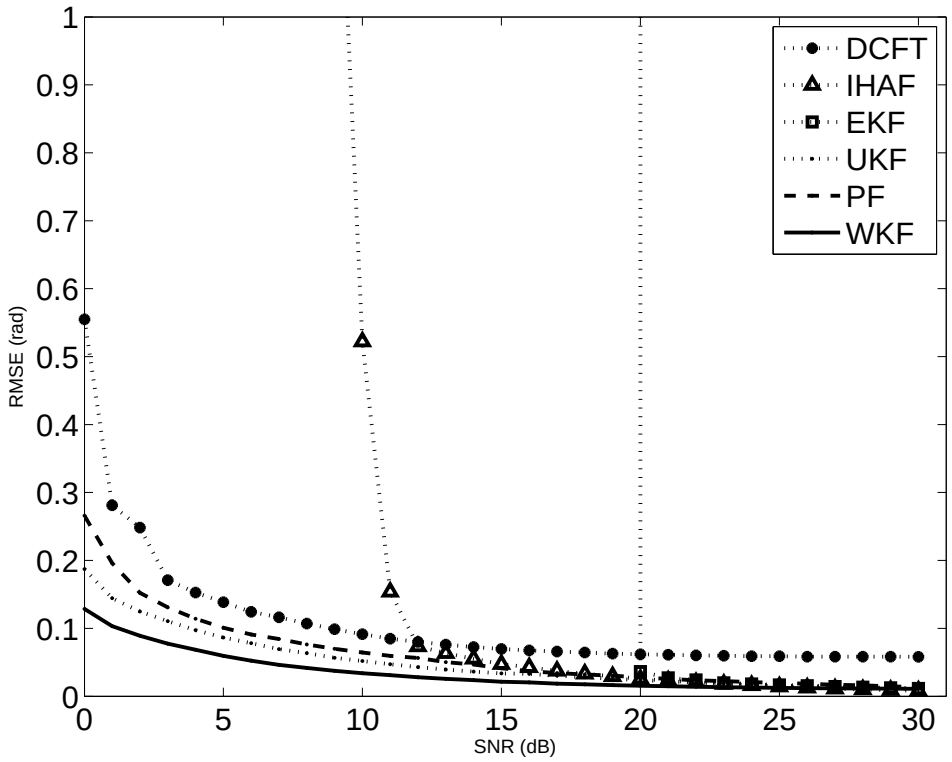

Figure 5.4: Comparison of proposed approach with state-of-the-art phase estimation approaches at different SNR values

processing algorithms. In DCFT based method, we divided each column into 16 segments (Nw = 16). Each segment was then processed by DCFT to estimate the coefficients of the second order polynomials (M = 2). The UKF based method follows the signal tracking approach which uses the rotating vector model as the measurement model.

The results of comparison for slowly varying phase are shown in figure 5.4. Figure 5.4 shows the root mean square error (RMSE) in estimated phase for different methods at varying SNR values (0-30 dB). It is observed that the Unscented Kalman filter, particle filter and wrapped statistics based filter outperforms the state of the art methods especially at lower SNR values (0-10 dB).

The estimated phase maps by parametric approach (DCFT), signal tracking approach (UKF) and the proposed method are shown in figure 5.3.

The Root Mean Square Error (RMSE) in the estimation of phase in different scenario are shown in table 5.1. From table 5.1, it can be seen that the DCFT and UKF based methods have the capability to process the noisy interference

Table 5.1: RMSE comparison of different methods

Approach	DCFT	UKF	Proposed WKF Approach
`peaks` (30 dB)	0.0099	0.0057	0.0069
`peaks` (0 dB)	0.5549	0.1872	0.1385
20×`peaks` (0 dB)	167.1835	440.8541	0.8706

fields provided that the phase pattern is having smaller dynamic range. However, these methods lacks the capability when the underlying phase pattern in having larger dynamic range of phase and severe noise in interference fringes both at the same time. DCFT under-performs because even a small error in the estimation of parameters causes a larger change in the overall estimated phase signal. In case of UKF the rotating state vector model limits the tracking capabilities when the interference field has both, larger dynamic range and severe noise, simultaneously.

Since the state vector consists of phase and phase derivative terms, the proposed approach enables the simultaneous estimation of the phase and phase derivatives from the reconstructed interference field. Figure 5.3(d) shows the estimated phase derivatives along columns using proposed approach. The errors in estimation of phase and phase derivatives are shown figure 5.5.

Finally, The RMSE values for all the proposed methods for different scenarios are summarised in the table 5.2. From the table, it is observed that the UKF and PF based approach can estimate phase when the phase map is rapidly varying

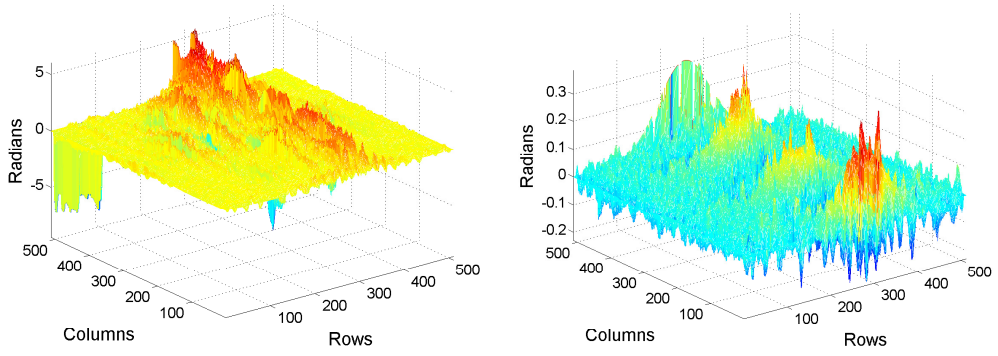

Phase Phase Derivatives

Figure 5.5: Error in estimation of phase and phase derivatives by proposed approach

Table 5.2: Comparison of performance of different proposed approaches in term of RMSE under different conditions

Phase Map	EKF	UKF	PF	WKF
Slowly Varying (30 dB)	0.0074	0.0077	0.0083	**0.0071**
Rapidly Varying Phase (30 dB)	**0.1295**	**0.1295**	0.4965	0.1399
Larger Dynamic Range (30 dB)	2.9235	0.1578	0.1517	**0.0988**
Rapidly Varying Phase (5 dB)	NA	0.9504	0.4419	**0.2076**
Slowly Varying (0 dB)	NA	0.1750	0.1442	**0.1290**
Larger Dynamic Range (0 dB)	NA	NA	NA	**0.8692**
Computational Time (sec)	**27**	38	81	97

with larger dynamic range or having extreme noise in interference fringes, but are unable to estimate phase when the interference field with larger dynamic range phase is corrupted by extreme noise. Wrapped statistics based filter found to be suitable for processing of severely corrupted reconstructed interference field even when the underlying phase had larger dynamic range.

5.3 Experimental Results

The performance of the proposed approach was verified using the reconstructed interference field, generated through real-time digital holography experiment.

The fringe pattern (real part of the complex interference field) is shown in figure 5.6(a). This reconstructed interference field was then processed along individual columns using the proposed approach. Figure 5.6(b) shows the fringe pattern generated by the estimated phase using proposed approach for qualitative analysis. The 3D mesh plot of estimated phase map and its derivatives are shown in figure 5.6(c) and 5.6(d), respectively. From the simulation and experimental results, it is clear that the proposed approach is suitable for processing of severely corrupted reconstructed interference field even when the underlying phase had larger dynamic range.

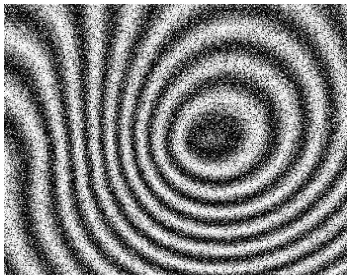

(a) Noisy Fringes

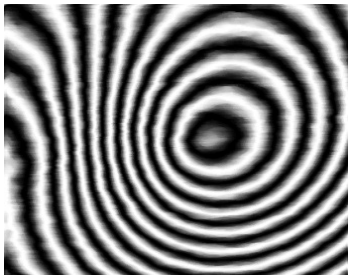

(b) Fringes with Estimated Phase

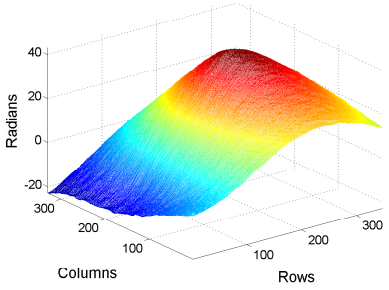

(c) Estimated Phase

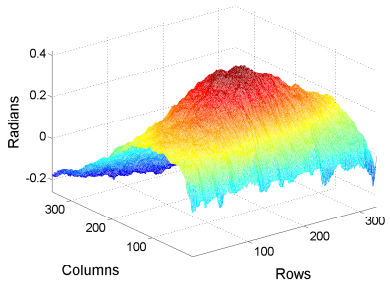

(d) Estimated phase Derivatives

Figure 5.6: Experimental results. Figure (a) shows the noisy fringe pattern (b) shows the fringe pattern generated from estimated phase for qualitative and figure (c) shows the 3D mesh plot of the estimated phase while (d) shows the estimated phase derivative

5.4 Summary

The wrapped statistics based approach estimates an accurate and direct phase from the interference fields especially when the field is having large dynamic range of the phase or severely corrupted by noise or both. Our method provides superior performance as compared to that of the existing piecewise polynomial approximation based approach and UKF based signal tracking approach in combined scenario of severely noisy fringes and larger dynamic range of phase. Also, since the state vector consists of phase and phase derivative terms, we have demonstrated that the proposed approach provides accurate and simultaneous estimation of the phase and phase derivatives from the interference field. We demonstrated, through simulation and experimental analysis, that the proposed approach is suitable for the analysis of severely corrupted fringe pattern, even when the underlying phase has a larger dynamic range.

CHAPTER 6

Applications of Signal Tracking Approach

In the previous chapters, we presented and discussed different phase estimation algorithms for the analysis of the interference fringe pattern. In this chapter, we describe the additional aspect of these algorithms such as simultaneous estimation of the phase derivatives along with phase estimation. We also discuss the potential applications of the same in different optical techniques like holographic moiré, fringe projection profilometry etc. Finally we discuss the possible fringe analysis requirements in the thermal expansion of the test object using simple holographic interferometry.

6.1 Simultaneous Estimation of Phase Derivatives

Simultaneous estimation of phase and its derivatives from the reconstructed interference field in DHI provides a vital information regarding the deformation and strain/curvature of the deformed object. The phase of the reconstructed interference field contains the information about deformation, whereas the derivatives of the phase carries information about strain/curvature of the deformed object.

Estimation of phase derivatives can be predominantly categorised into three groups. First approach uses numerical differentiation of the estimated phase map using `arctan` and unwrapping methods. When the interference field becomes noisy, the estimated phase by such approach becomes noisy too. In the numerical differentiation of such noisy phase results in noisy phase derivatives. Second approach uses parametrization techniques for phase derivative estimation which models the phase map as polynomial signals and estimation of polynomial coefficients by various signal processing techniques. Thus the problem of phase derivative estimation can be represented as parameter estimation where coefficients of the phase polynomials are the parameters. In this approach, generally, the polynomials of degree 2 to 4 are used to approximate the phase map. As the degree of

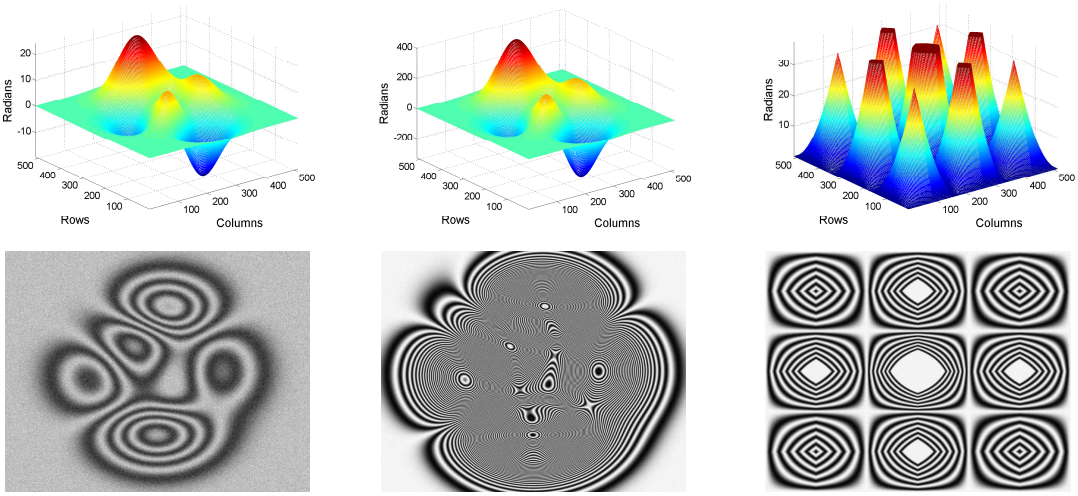

(a) Slowly varying phase (b) Larger dynamic range (c) Rapidly varying phase

Figure 6.1: Simulated phase maps (first row) along with their corresponding fringe patterns (second row)

polynomial is small, it keeps limitations on the performance of these methods, especially when the phase is rapidly varying and having larger dynamic range. Third approach is a non-parametric approach based on time-frequency distributions.

In previous chapters, we demonstrated that the signal tracking approach based methods outperform the state-of-the-art for the estimation of phase. The state vector used for signal tracking approach consists of first M terms of Taylor series, which enables estimation of phase derivatives upto order M. We now demonstrate that the signal tracking approach based method can be extended to simultaneous estimation of phase and phase derivatives by using the additional Taylor series terms and further prove that it performs better than most of the state-of-the art approaches used for phase derivative estimation, especially at low SNR levels. We use the state model based on Taylor series expansion of phase function and polar to Cartesian conversion based measurement model. Unscented Kalman filter algorithm is used for the state estimation. As the state contains the phase and derivatives terms; we can estimate the phase and derivatives of phase, simultaneously, without extra computational efforts. The estimated phase is observed to have few local spurious estimates, which are eliminated by a 3×3 median filter.

6.1.1 Simulation Analysis

The signal tracking approach is validated and compared with the state-of-the-art for three different phase maps representing slowly varying phase, rapidly varying phase and phase with larger dynamic range. These phase patterns were generated in MATLAB. The complex interference field is then generated and Additive White Gaussian Noise (AWGN) is added to it at Signal-to-Noise-ratio (SNR) of 10dB. The simulated phase maps and their corresponding fringe patterns are shown in figure 6.1.

First order phase derivatives

Noisy interference field is then analysed along each column separately using signal tracking approach. We used UKF as a signal tracking algorithm. The process noise covariance ($\mathbf{Q}$) is taken to be $k_Q \; diag\begin{bmatrix}10^{-2} & 10^{-2} & 10^{-4} & \cdots & 10^{-(2M+2)}\end{bmatrix}$. The rational behind choice of such $\mathbf{Q}$ is that the dynamic range of map of m^{th} derivative of phase is generally larger by magnitude of order 2 than that of $(m+1)^{th}$ derivative. The measurement noise covariance matrix is taken to be $\mathbf{R} = k_R \; diag\left(\begin{bmatrix}\sigma_{re}^2 & \sigma_{im}^2\end{bmatrix}\right)$ where, σ_{re}^2 and σ_{im}^2 are the variances estimated form

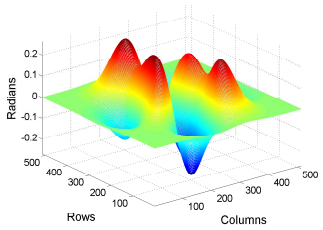

(a) True Phase derivatives

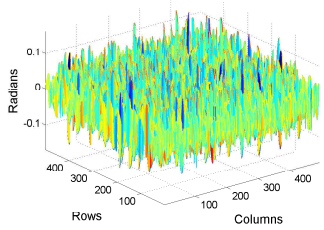

(b) DCFT based method

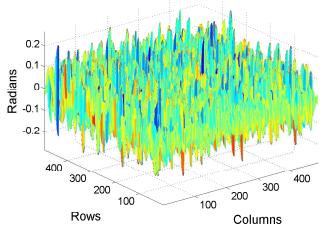

(c) CPF based method

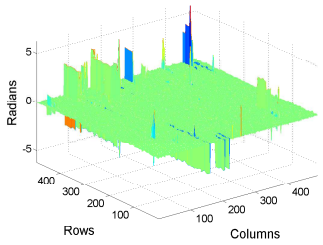

(d) IHAF Based method

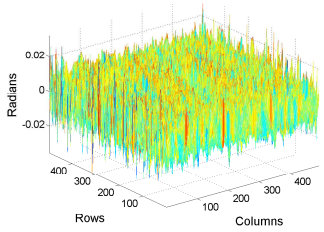

(e) PSWVD based method

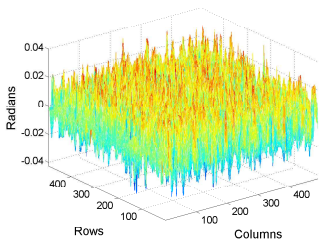

(f) Proposed method (UKF)

Figure 6.2: Error in phase derivative estimation by various methods

manually selected uniform region of the fringe pattern. This reduces the parameter tuning problem to scalar parameter tuning.

We have compared our approach with different parametric and non-parametric approaches. For class of parametric approaches we chose Discrete Chirp-Fourier Transform (DCFT) [Gorthi and Rastogi (2009a)], High-order Ambiguity Function (HAF) [Gorthi and Rastogi (2009b)] and Cubic Phase Function (CPF) [Gorthi and Rastogi (2010b)] based methods whereas Pseudo Wigner-Ville distribution (PSWVD) based methods [Rajshekhar et al. (2009)] is considered for non-parametric methods. For piecewise polynomial phase approximation based methods each column was divided into 16 segments (Nw = 16), whereas the order of polynomials for approximation was taken as 2 for DCFT based method (M=2), 3 for CPF based method (M=3) and 4 for IHAF based method (M=4).

Error in estimated of phase derivatives at SNR of 10 dB by different methods and the proposed method (UKF) are shown in figure 6.2. The proposed method (UKF) estimates the phase derivatives with almost same accuracy as that of PSWVD, whereas it outperforms the other methods. The main advantage of the proposed methods (UKF) is that it calculates phase and phase derivatives simultaneously, in single run of the algorithm, whereas PSWVD based method provides only first order phase derivative. In order to estimate the higher order

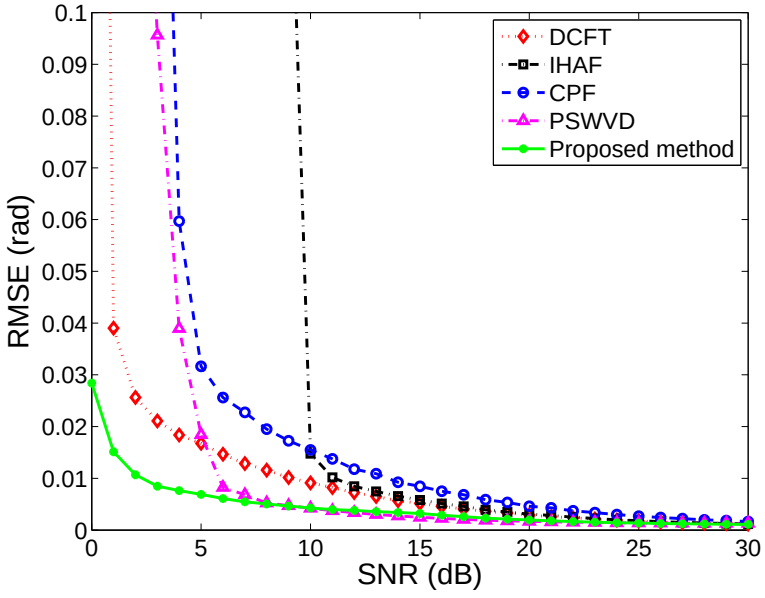

Figure 6.3: RMSE comparison of different methods for different SNR values

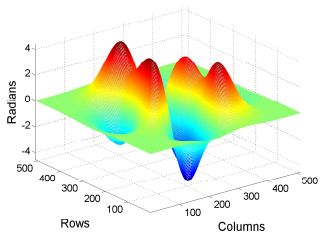

(a) True Phase derivatives

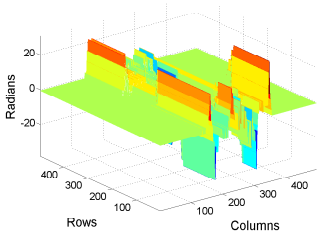

(b) DCFT based method

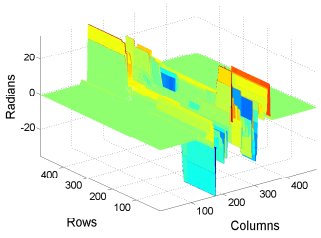

(c) CPF based method

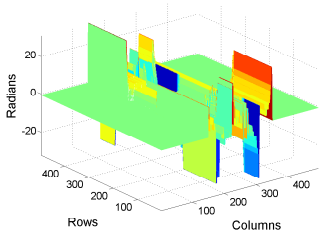

(d) IHAF Based method

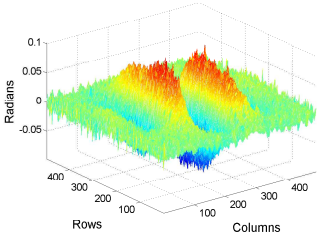

(e) PSWVD based method

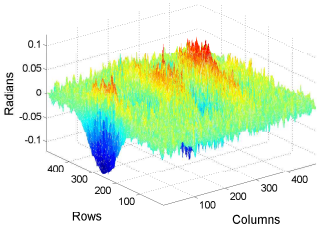

(f) Proposed method (UKF)

Figure 6.4: Error in phase derivative estimation at larger dynamic range by various methods

phase derivatives by PSWVD, we need to form reconstructed interference field using estimated first order phase derivatives and analyse it.

From figure 6.3, which shows the plot of RMSE against SNR values, we can

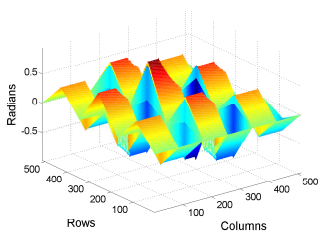

(a) True Phase derivatives

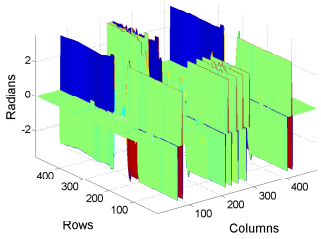

(b) DCFT based method

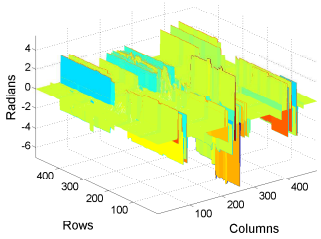

(c) CPF based method

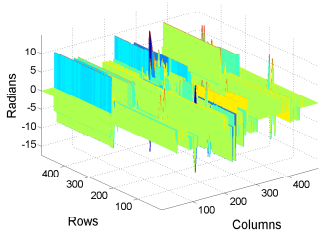

(d) IHAF Based method

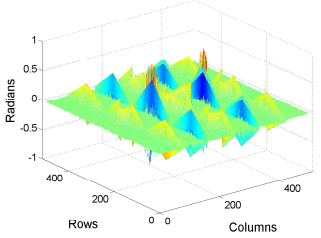

(e) PSWVD based method

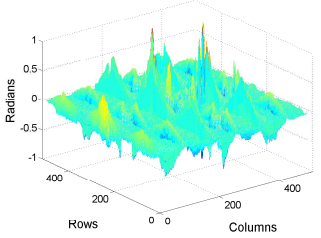

(f) Proposed method (UKF)

Figure 6.5: Error in phase derivative estimation at rapidly varying phase by various methods

infer that all these methods performs almost identical above 10 dB, but the performance of proposed method (UKF) is superior when the SNR falls below 10 dB. This can be mainly attributed to the ability of UKF to model and incorporate measurement noise and more accurate estimation of state from the measurements.

Comparison of the proposed method (UKF) with state-of-the-art methods for larger dynamic range of phase is shown in figure 6.4, whereas that of rapidly varying phase is shown in figure 6.5. It is seen from figures 6.4 and 6.5, that the parametric methods based on polynomial approximation approach provides erroneous phase derivatives estimates owing to larger error in the estimated parameters. Whereas our method agrees with the non-parametric method based on PSWVD for the interference fields with higher SNR. Our method outperforms PSWVD at lower SNR values of the interference field. The measurement noise covariance included in measurement model ensures the effective handling of noisy data.

Second order phase derivatives

The proposed method (UKF), with state vector containing M terms of Taylor series expansion, provides the second order phase derivatives, simultaneously. In this section, we will be validating the estimated second order phase derivatives by our method with that of the PSWVD method. In PSWVD based method, second derivative of phase can be obtained by running the same algorithm twice. First time, the algorithm estimates the first order derivative. Second time, the complex reconstructed field is generated using the first order derivative map and then PSWVD algorithm estimated the derivative of the first order derivative.

As we are processing rows/column independently, proposed method (UKF) estimates second order derivatives along rows (P_{xx}) and columns (P_{yy}) directly from the state vector, while cross term derivatives (P_{xy} & P_{yx}) needs to be estimated by the similar approach as that of PSWVD algorithm.

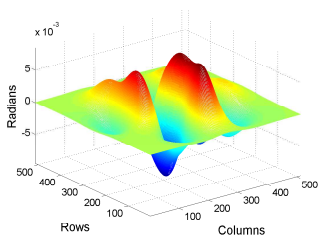

(a) True derivatives (2^{nd})

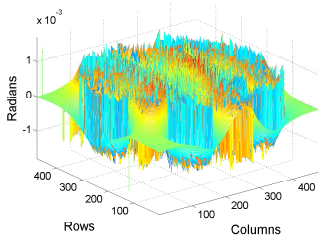

(b) PSWVD

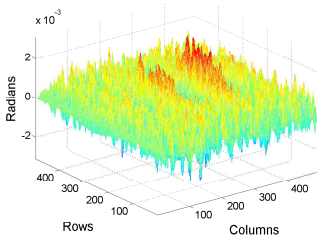

(c) Proposed method (UKF)

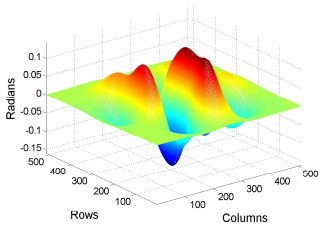

(d) True derivatives (2^{nd})

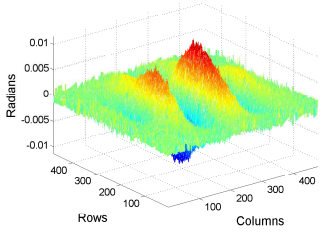

(e) PSWVD

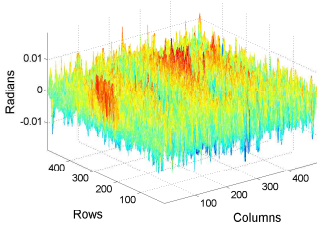

(f) Proposed method (UKF)

Figure 6.6: Error in second order phase derivative estimation at slowly varying (first row) and larger dynamic range (second row) by various methods

6.1.2 Experimental Results

For experimental analysis we have used two phase patterns representing severely corrupted by noisy (6.7(a)) and rapidly changing peak (6.7(b)). The estimated phase derivative patterns for noisy data using PSWVD based method and proposed method (UKF) are shown in figures 6.8(a), 6.8(c), respectively and that

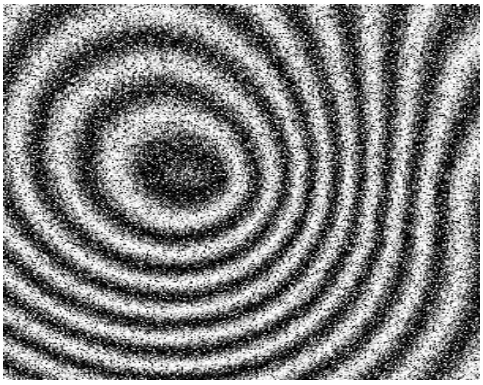

(a) Noisy

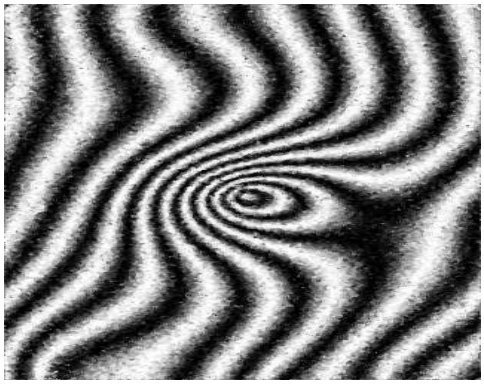

(b) Rapid Variations

Figure 6.7: Fringe patterns corresponding to noisy and rapidly varying phase maps

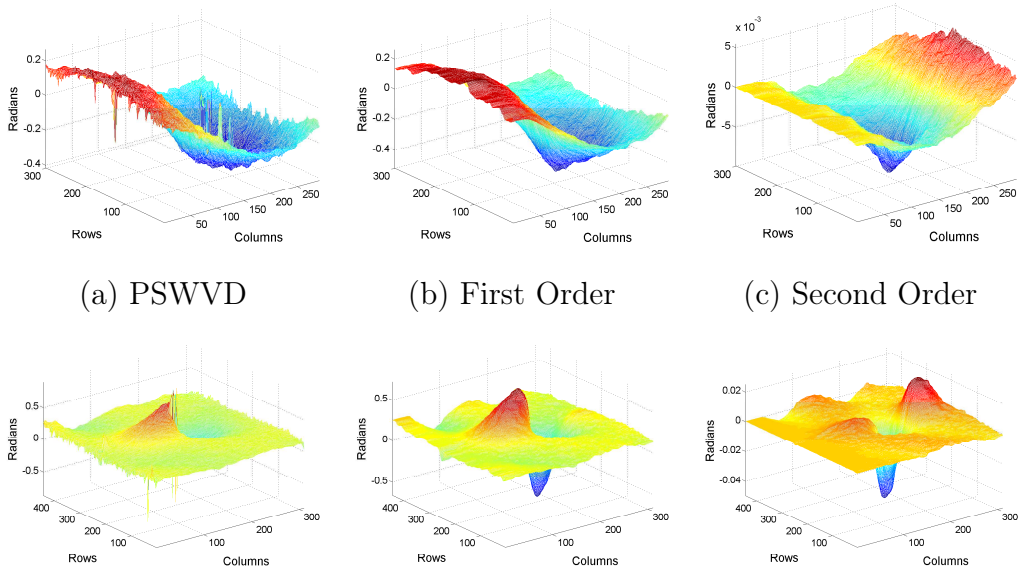

(a) PSWVD (b) First Order (c) Second Order

(d) PSWVD (e) First Order (f) Second Order

Figure 6.8: First order derivatives estimated by PSWVD based method, and first and second order derivatives by proposed method (UKF)

of rapidly varying phase are shown in figures 6.8(d), 6.8(e), respectively. Also second order derivatives estimated using proposed approach (UKF) are shown in figures 6.8(c) and 6.8(f). It is observed that the phase derivatives estimated by proposed approach (UKF) are more accurate than PSWVD. This analysis shows that the UKF based phase estimation algorithm can be successfully applied for simultaneous estimation of phase derivatives in real noisy situations.

6.2 Digital Holographic Moiré

In this section, we augment state vectors for different phase components to form a single state vector. With combined state vector, we show that the proposed signal tracking approach has the capability of the successfully tracking multiple phase maps, there by providing an aid to multi-component phase estimation. In digital holographic interferometry, interference phase corresponds to phase of the single object wave; whereas in digital holographic Moiré, multiple object beams are used to illuminate the object at different angles, Thus the Moiré pattern has phase components corresponding to each of the object wave. The intensity vari-

ation generated due to interference of scattered object beams from the surface of an object with single reference beam is recorded using CCD sensors. By numerical reconstruction of these recorded holograms after and before deformation of an object we get Moiré fringes which contains the information about multiple interference phases corresponding to different object beams. These multiple phase maps and application of sensitivity vector to there maps enables the in-plane and out-of-plane measurement [Rajshekhar et al. (2012)].

6.2.1 Theory

To analyse illumination of the object using multiple object beams, consider a figure (6.9) where the object is exposed to two object beams $\hat{s_1}$ and $\hat{s_2}$ at the same angle but from either side of the observation direction to achieve the symmetry [Rajshekhar et al. (2011b)]. A CCD sensor is used to record the interference pattern at a distance d from the object. Only one reference beam is used to create the interference pattern with the two object waves.

The interference pattern at CCD plane due to two object waves $O_1(x, y)$ &

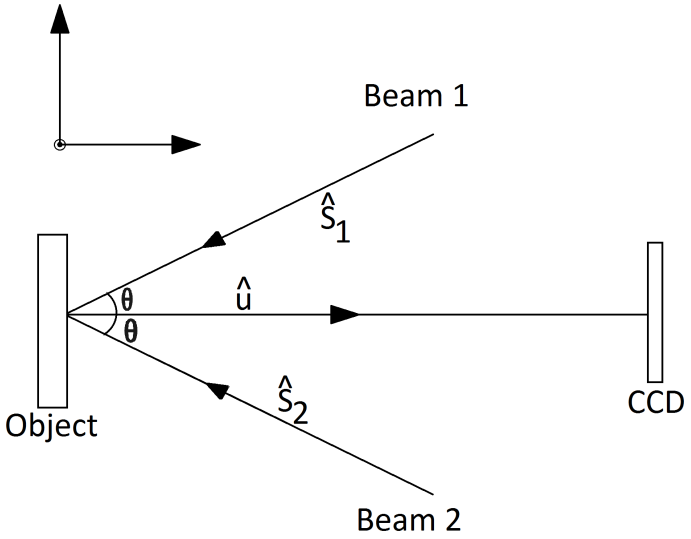

Figure 6.9: Multi beam illumination of the object

$O_2(x, y)$ and a reference wave $R(x, y)$ can be given by

$$\begin{aligned} I &= (R + O_1 + O_2)(R + O_1 + O_2)^* \\ &= I_0 + R^*(O_1 + O_2) + R(O_1 + O_2)^* \end{aligned}$$

where $I_0 = |R|^2 + |O_1|^2 + |O_2|^2 + O_1O_2^* + O_1^*O_2$ and * denotes the complex conjugate. Here the indices (x, y) are omitted just for sake of brevity.

The intensity distribution recorded using CCD sensor, called digital hologram. The hologram function can be reconstructed numerically to get the complex amplitude of object waves O_1 and O_2 [Schnars and Japtner (2002)]. The reconstructed interference field can be given as

$$\Gamma(x, y) = a_1 e^{i\varphi_1} + a_2 e^{i\varphi_2} \tag{6.1}$$

In digital holographic interferometry, two holograms are recorded corresponding before and after the deformation. These holograms are reconstructed using numerical reconstruction, and then multiplied to get the reconstructed interference field. Let ϕ_1 is the phase change of object wave O_1, and ϕ_2 is that of O_2 due to deformation. The reconstructed moiré fields for these holograms can be represented, according to Rajshekhar and Rastogi (2012), as:

$$\Gamma_1(x, y) = a_1 e^{i\varphi_1} + a_2 e^{i\varphi_2} \tag{6.2}$$

$$\Gamma_2(x, y) = a_1 e^{i(\varphi_1 + \phi_1)} + a_2 e^{i(\varphi_2 + \phi_2)} \tag{6.3}$$

The reconstructed interference moiré field is then calculated by

$$\begin{aligned} \Gamma(x, y) &= \Gamma_2 \Gamma_1^* \qquad (6.4) \\ &= a_1^2(x, y) e^{i\phi_1(x,y)} + a_2^2(x, y) e^{i\phi_2(x,y)} \\ &\quad + a_1(x, y) a_2(x, y) e^{i[\phi_1(x,y) + \varphi_1(x,y) - \varphi_2(x,y)]} \\ &\quad + a_1(x, y) a_2(x, y) e^{i[\phi_2(x,y) + \varphi_2(x,y) - \varphi_1(x,y)]} \end{aligned}$$

Here, random nature of the phases $\varphi_1(x, y)$ and $\varphi_2(x, y)$ makes the last two terms to behave as random noise and hence these two terms can be assumed as part of

noise. Hence, the reconstructed moiré field can be represented as

$$\Gamma(x,y) = a_1^2(x,y)e^{i\phi_1(x,y)} + a_2^2(x,y)e^{i\phi_2(x,y)} + \eta(x,y) \tag{6.5}$$

Hence the problem of digital holographic moiré boils down to the estimation of phase maps from a multi-component complex signal.

State Space Model

The reconstructed interference moiré field of digital holographic Moiré with variable amplitude embedded in noise can be expressed by equation (6.5) [Gorthi and Rastogi (2009c)] as:

$$\Gamma(x,y) = \alpha_1(x,y)e^{i\phi_1(x,y)} + \alpha_2(x,y)e^{i\phi_2(x,y)} + \eta(x,y) \tag{6.6}$$

where $\alpha_i(x,y)$ are the real valued amplitude and $\phi_i(x,y)$ are the real valued interference phase of the complex signal and $\eta(x,y)$ is the zero mean complex Additive White Gaussian Noise (AWGN). Here x and y are the rows and columns of the N×N complex field. For any arbitrary row, equation (6.6) can be written as

$$\Gamma_x(y) = a_{1x}(y)e^{i\phi_{1x}(y)} + a_{2x}(y)e^{i\phi_{2x}(y)} + \eta_x(y) \tag{6.7}$$

In proposed method, both the phase components are assumed to be continuous and differentiable functions. Hence we can define the Taylor series expansion of the phase function $\phi_{1x}(y)$ and $\phi_{2x}(y)$ in equation (6.7) as:

$$\phi_x(y+1) = \phi_x(y) + \frac{1}{1!}\phi'_x(y) + \frac{1}{2!}\phi''_x(y) + w_0(y) \tag{6.8}$$

subsequently we can calculate the $\phi'_x(y+1)$ and $\phi''_x(y+1)$ as

$$\phi'_x(y+1) = \phi'_x(y) + \frac{1}{1!}\phi''_x(y) + w_1(y) \tag{6.9}$$

$$\phi''_x(y+1) = \phi''_x(y) + w_2(y) \tag{6.10}$$

Here, $w_0(y)$, $w_1(y)$, $w_2(y)$ are the Higher Order Terms which can be considered in

process noise. The amplitude can be modelled as random walk and represented as:

$$a_x(y+1) = a_x(y) + w_x(y) \tag{6.11}$$

Now, above equations can be written in matrix form as:

$$\begin{bmatrix} a_x(y+1) \\ \phi_x(y+1) \\ \phi'_x(y+1) \\ \phi''_x(y+1) \end{bmatrix} = \begin{bmatrix} 1 & 0 & 0 & 0 \\ 0 & 1 & \frac{1}{1!} & \frac{1}{2!} \\ 0 & 0 & 1 & \frac{1}{1!} \\ 0 & 0 & 0 & 1 \end{bmatrix} \begin{bmatrix} a(y) \\ \phi_x(y) \\ \phi'_x(y) \\ \phi''_x(y) \end{bmatrix} + \begin{bmatrix} w_x(y) \\ w_0(y) \\ w_1(y) \\ w_2(y) \end{bmatrix} \tag{6.12}$$

Applying same analysis to both the phase components and augmenting the state vector as in equation given below,

$$\mathbf{x} = \begin{bmatrix} a_{1x} & \phi_{1x} & \phi'_{1x} & \phi''_{1x} & a_{2x} & \phi_{2x} & \phi'_{2x} & \phi''_{2x} \end{bmatrix}^T$$

$$\mathbf{F} = \begin{bmatrix} 1 & 0 & 0 & 0 & 0 & 0 & 0 & 0 \\ 0 & 1 & \frac{1}{1!} & \frac{1}{2!} & 0 & 0 & 0 & 0 \\ 0 & 0 & 1 & \frac{1}{1!} & 0 & 0 & 0 & 0 \\ 0 & 0 & 0 & 1 & 0 & 0 & 0 & 0 \\ 0 & 0 & 0 & 0 & 1 & 0 & 0 & 0 \\ 0 & 0 & 0 & 0 & 0 & 1 & \frac{1}{1!} & \frac{1}{2!} \\ 0 & 0 & 0 & 0 & 0 & 0 & 1 & \frac{1}{1!} \\ 0 & 0 & 0 & 0 & 0 & 0 & 0 & 1 \end{bmatrix}$$

$$\mathbf{w}(y) = \begin{bmatrix} w_{1x} & w_{10} & w_{11} & w_{12} & w_{2x} & w_{20} & w_{21} & w_{22} \end{bmatrix}$$

So, in matrix form we can write:

$$\mathbf{x}(y+1) = \mathbf{F}\mathbf{x}(y) + \mathbf{w}(y) \tag{6.13}$$

here, the vector $\mathbf{x}(y)$ denotes the state vector, the matrix $\mathbf{F}$ is the transition matrix representing the relation between the present and the next state of the field and $\mathbf{w}(y)$ denotes the process noise. This forms our process model.

Using state vector we can generate the measurement signal with the relation

$$\Re[\mathbf{f}(y)] = a_{1x}(y)cos(\phi_{1x}(y)) + a_{2x}(y)cos(\phi_{2x}(y))$$
$$\Im[\mathbf{f}(y)] = a_{1x}(y)sin(\phi_{1x}(y)) + a_{2x}(y)sin(\phi_{2x}(y))$$

Hence from above equations, the function used for prediction of observation from state vector $h(\cdot)$ can be written as:

$$\mathbf{h}(\mathbf{x}(n)) = \begin{bmatrix} x_1 cos(x_2) + x_5 cos(x_6) \\ x_1 sin(x_2) + x_5 sin(x_6) \end{bmatrix} \tag{6.14}$$

where x_i is the i^{th} element in the state vector $\mathbf{x}$. As the measurement signal is a complex field, noise is also complex. We assume the measurement (observation) noise to be additive white Gaussian noise with zero mean and variance of σ_ν^2. The noise $\nu(y)$ is given by

$$\nu(y) = \begin{bmatrix} \Re[\eta(y)] \\ \Im[\eta(y)] \end{bmatrix} \tag{6.15}$$

the noise covariance $\mathbf{R}$ can be estimated effectively from the measured signal as

$$\mathbf{R} = k_R \frac{\sigma_v^2}{2} \mathbb{I} \tag{6.16}$$

where k_R is a scaling constant used for tuning the filter and $\mathbb{I}$ is 2×2 identity matrix. Hence observation model can be written as

$$\mathbf{z}(y) = \mathbf{h}(\mathbf{x}(y)) + \nu(y) \tag{6.17}$$

6.2.2 Simulation Results

An reconstructed interference moiré field of size 512×512 was simulated in MATLAB. The signal then corrupted by using AWGN at signal to noise ration (SNR) of 20 dB using MATLAB's *awgn* function.

With the state space model derived, UKF is used to estimate the state containing amplitude and phase maps corresponding to each component from the complex measurement field. To analyse the performance of the proposed method, we sim-

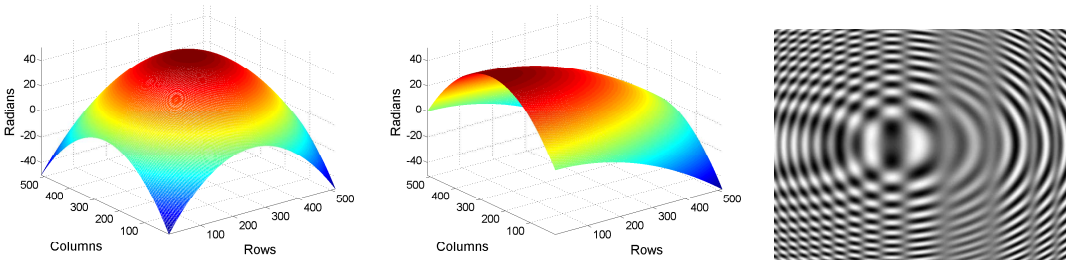

(a) Phase map I (b) Phase map II (c) Fringe Pattern

Figure 6.10: True phase maps and corresponding fringe pattern

ulated the reconstructed interference field using two phase maps shown in figure 6.10(a) and 6.10(b), respectively. AWGN was then added to the field at SNR of 20 dB. Corresponding fringe pattern in shown in figure 6.10(c). The reconstructed interference field is then processed using unscented Kalman filter based phase estimation algorithm. Estimated phase maps are shown in figure 6.11(a) and 6.11(b), whereas error in phase estimation are shown in 6.11(c) and 6.11(d), respectively.

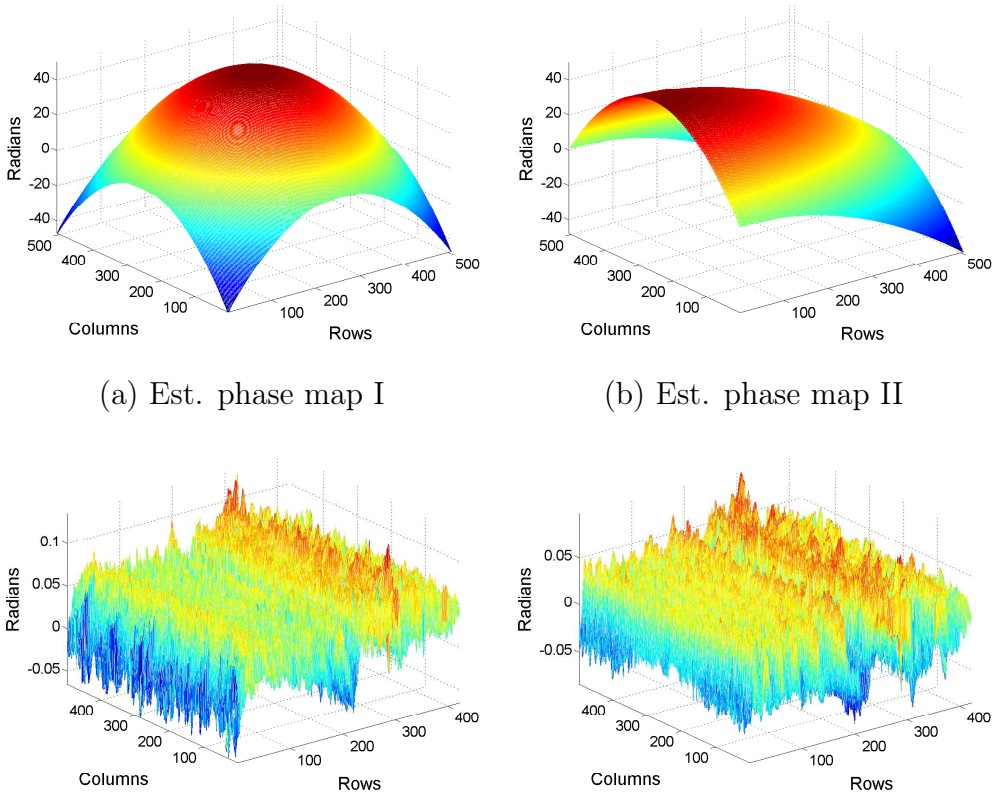

(a) Est. phase map I (b) Est. phase map II

(c) Error in phase map I (d) Error in phase map II

Figure 6.11: Simulation analysis of multi-component phase estimation

As Kalman Filter and its variants are not an optimal estimator in non-linear scenarios, hence sufficient care must be taken while initializing the Kalman filter parameters like initial error covariance, process noise covariance and the measurement noise covariance. We have successfully shown in the figure 6.11 that the UKF based method efficiently tracks the phase components if the initialization done properly. Here, we have used true values of the phase components for initialization which will not be accessible in real-time scenarios.

6.2.3 Summary

We provide insights on extending the signal tracking approach for tracking multiple phases of a multi-component complex signal, embedded in AWGN noise. Proper tuning of parameters and initialization can potentially turn this method into a powerful tool that aids in performing simultaneous measurement of in-plane and out-of-plane displacements from a single record in holographic moiré.

6.3 Fringe projection profilometry

The fringe projection profilometry, which are used for extracting the 3D features of the object, is one of the active research area in the optical metrology. This

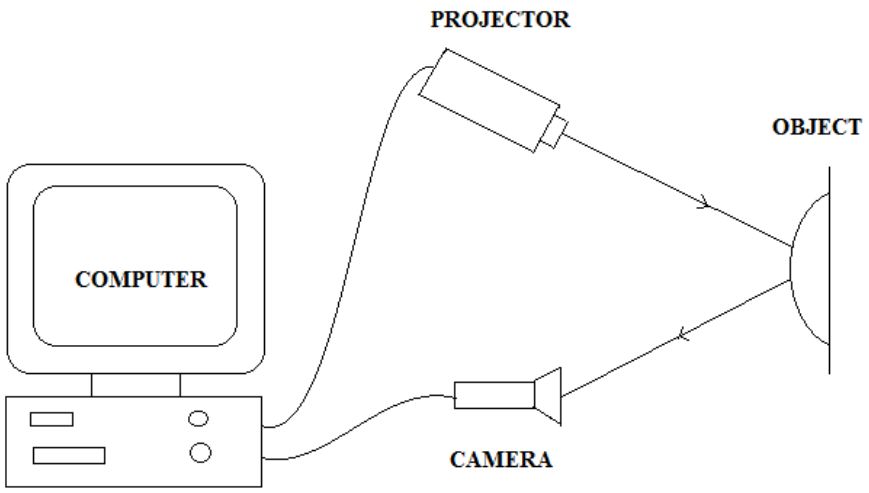

Figure 6.12: Fringe Projection Profilometry

technique caters numerous applications in the fields like biomedical applications, namely, 3D intra-oral dental measurement, [Chen and Huang (2005)], human body shape measurement for shape guided radiotherapy treatment [Lilley et al. (2000); Moore et al. (2006)]; industrial and scientific applications, namely, characterization of MEMS components [Quan et al. (2002); He et al. (2006)], quality control of printed circuit board manufacturing [Yen et al. (2006)]; 3D face recognition systems [Yagnik et al. (2007)] and many more. The major feature of the fringe projection technique is in their ability to generate the high resolution 3-dimensional reconstruction of the object via non-contact and non-destructive process. This feature has helped fringe projection methods to create their own space in new areas like security systems, object scanning and virtual reality. Fringes or grating analysis have been widely used in analysing the 3D shapes. The fringe projection basically uses the non-interfering lighting and image processing technique to obtain the 3D shape. A typical fringe projection profilometry setup is shown in the figure 6.12.

This technique involves projecting the sinusoidal fringe patterns on the object surface. The depth of the object is transformed into the phase changes of these projected fringes i.e., initially projected zero phase fringes undergoes phase modulation due to the depth of the object. The phase of these modulated fringes are estimated using various fringe analysis techniques like Fourier transform methods [Takeda and Mutoh (1983)], windowed Fourier transform methods [Kemao (2004)], phase shift grating projection [Fu and Luo (2011)], etc. The phase estimated by most of these techniques is wrapped phase and noisy, and hence a phase unwrapping algorithm is required to obtain the unwrapped and continuous phase which is proportional to the depth distribution.

The major limitation of the phase unwrapping algorithms is that their performance is influenced by noise present in the fringe pattern. We propose use of signal tracking approach, which is realized using the wrapped statistics based filter. This method provides accurate, unwrapped and continuous phase directly without need of additional unwrapping procedure. In this technique, a complex fringe is generated by projecting sine and cosine fringes separately on the object, recording the deformed fringes and finally combine them by taking cosine fringes as real and sine fringes as imaginary part of the complex fringes. The complex

fringes are then analysed by signal tracking approach to get the unwrapped phase.

Once the complex field is generated, the direct phase estimation is also possible by piecewise polynomial approximation approach [Gorthi and Rastogi (2009c)]. These approaches are efficient, provided that the polynomials used for phase approximation is smaller; otherwise a small errors in the coefficients will lead to larger errors in the phase estimation. Since interference fringe pattern has sinusoidal fringes, naturally phase map will have larger dynamic range, owing to multiple cycles of sinusoidal fringes.

We propose a signal tracking approach to estimate the phase directly from the noisy interference fringes. The UKF and particle filter based realizations of signal tracking approach works when either the phase map is larger dynamic range and fringe pattern is moderately noisy (SNR$>$ 20 dB) or the slowly varying phase with severely noisy fringe pattern. But when larger dynamic range of phase is hidden in severely noisy fringe pattern, only wrapped statistics based realization of the signal tracking approach produces accurate unwrapped phase. Thus, we use wrapped statistics based phase estimation method for analysis of these fringe patterns.

6.3.1 Theory

Generation of Complex Fringe

A deformed fringe pattern is represented in the mathematical form as

$$z(m,n) = a(m,n) + b(m,n)\cos(2\pi f x + \psi(m,n)) \tag{6.18}$$

where $a(m,n)$, $b(m,n)$ and $\psi(m,n)$ are respectively the background intensity, the amplitude modulation of the fringes and the phase to be measured at the location (m,n) in a fringe pattern. A complex fringe is generated by combining a cosine and sinusoidal fringe as shown below,

$$z_1(m,n) = a(m,n) + b(m,n)\cos(2\pi fx + \psi(m,n)) \quad (6.19)$$

$$z_2(m,n) = a(m,n) + b(m,n)\sin(2\pi fx + \psi(m,n)) \quad (6.20)$$

By combining equations 6.19 and 6.20, we can obtain the fringe in exponentials forms as below,

$$\Gamma(m,n) = z_1(m,n) + iz_2(m,n) \quad (6.21)$$

Generation of complex interference fringe pattern using the fringe projection profilometry setup, is depicted in the figure 6.13.

With the assumption that the $a(m,n)$ and $b(m,n)$ are constant throughout the complex field, we can represent equation 6.21, in polar form as

$$\Gamma(m,n) = b(m,n)exp^{j(2\pi fx+\psi(m,n))} \quad (6.22)$$

The phase of the complex fringe is estimated using the signal tracking approach by the wrapped Kalman filter followed by removal of the carrier frequency component to obtain the actual depth of the object.

6.3.2 Simulation Results

To validate the performance of proposed method (WKF) for the 3D reconstruction of the object using fringe projection, sine and cosine fringes were simulated using MATLAB. The simulations were performed on Windows 7 OS based workstation with intel(R) Xeon(R) CPU at 3.20GHz with 16GB of primary memory. The complex fringe pattern was simulated using equations 6.19, 6.20 and 6.21. The wrapped statistics based realization of signal tracking approach was then applied on the complex field to get the complete phase map (i.e., along with phase corresponding to carrier frequencies of the fringe pattern). Frequency of the deformed fringe pattern is calculated by taking Fourier transform of the fringe pattern. This frequency is used to generate the phase component corresponding to the carrier frequency of the fringes. Final phase map, which directly corresponds to the 3D

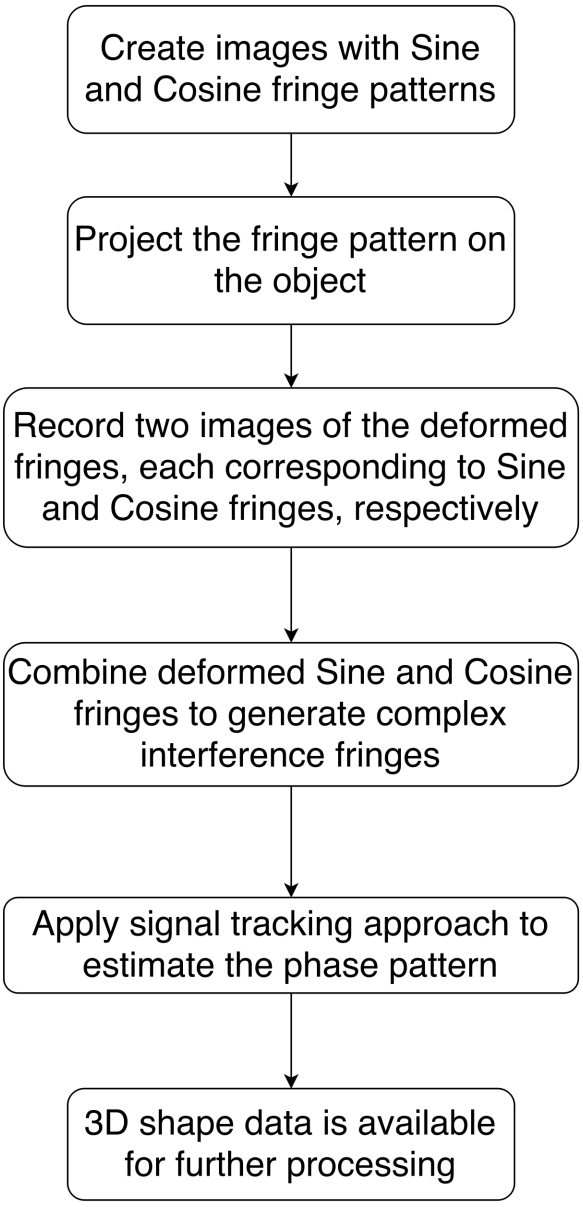

Figure 6.13: Flow Chart of Fringe Projection Profilometry

shape of the object, is produced by subtracting the carrier phase component. As a part of simulation, the wrapped statistics based phase estimation algorithm method was compared with Fourier transform profilometry and windowed Fourier transform Profilometry.

In the Fourier transform profilometry, the idea is to extract the phase information from the fringes by separating the side lobes (phase information) in the frequency domain. When the phase map is rapidly varying, two side lobes get mixed into each other making the separation of them difficult. This case is depicted in figure 6.14(b). A phase map with larger dynamic range was generated using the peaks function. The complex fringes are then generated according to

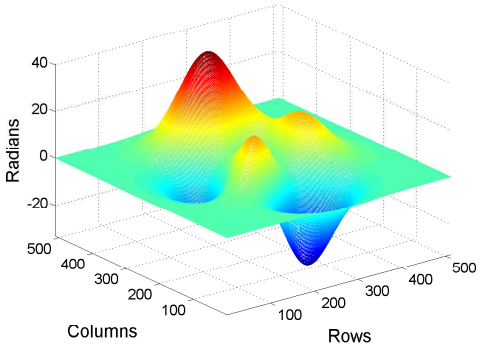

(a) True phase

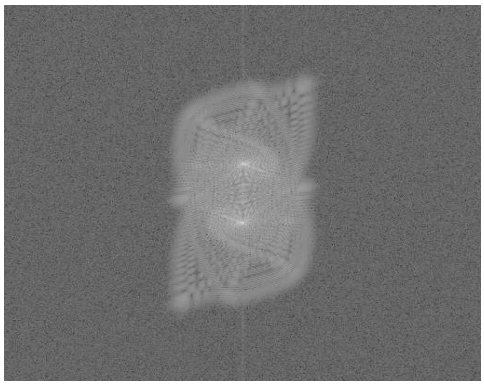

(b) Log of FT of fringes

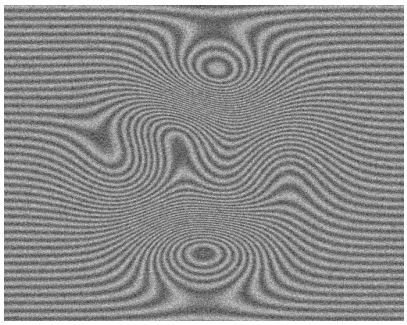

(c) Sine fringes

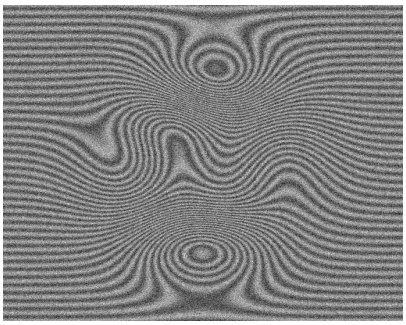

(d) Cosine fringes

Figure 6.14: Simulation of larger dynamic range phase map depicting non-separability of the side lobes in Fourier Transform (FT) domain at SNR of 6 dB

equations 6.18. The complex white Gaussian noise was then added to it in order to generate the noisy fringes. The original phase map and the noisy sine and cosine fringe pattern are shown in the figure 6.14(a), 6.14(c) and 6.14(d), respectively.

The proposed method (WKF) was compared with Windowed Fourier Trans-

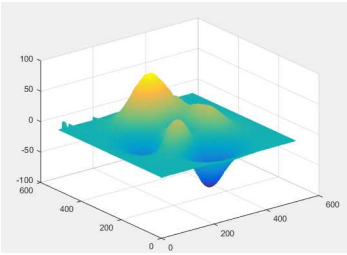

(a) WFT

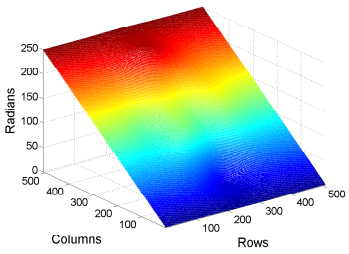

(b) With carrier fringes

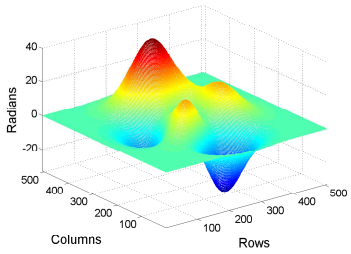

(c) Without carrier fringes

Figure 6.15: Estimated phase maps using different methods for larger dynamic range and SNR = 6dB

form(WFT) and it was observed that the when the SNR is changed there is no noticeable difference in the phase reconstructed for WFT while in the case of the proposed method (WKF), the root mean square error (RMSE) of the estimated phase reduces as SNR of the fringe pattern increases. It was also observed that when the dynamic range of the phase increases, fringes corresponding to the part of higher slope (where the phase is changing rapidly) produces densely spaced fringes. Windowed Fourier transform based method discards those fringes assuming them to be noise. This leads to the erroneous phase map generation. Estimated phase maps generated using Fourier transform profilometry, windowed Fourier transform profilometry, and the proposed method (WKF) are shown in figure 6.15.

We conducted fringe projection experiment which validates real-time applicability of our proposed approach. In this experiment, Lab chair was used as an object. Fringe pattern, which is showing deformation due to dents of the back support of the chair, is shown in the figure 6.16

The complex fringe pattern was generated using deformed sine and cosine fringes. This fringe pattern was then processed using wrapped statistics based phase estimation algorithm to estimate the phase patter along with the phase component corresponding to carrier frequency, as shown in figure 6.17(a). This phase component is generated y finding the carrier frequency of the fringe pattern using Fourier transform. Estimated phase map after removal of carrier frequency is shown in figure 6.17(b), which shows the dents of the chair clearly. This analysis substantiate the applicability of the proposed approach (WKF) in the real-time experiments for estimation of phase and thereby 3D shape reconstruction of the

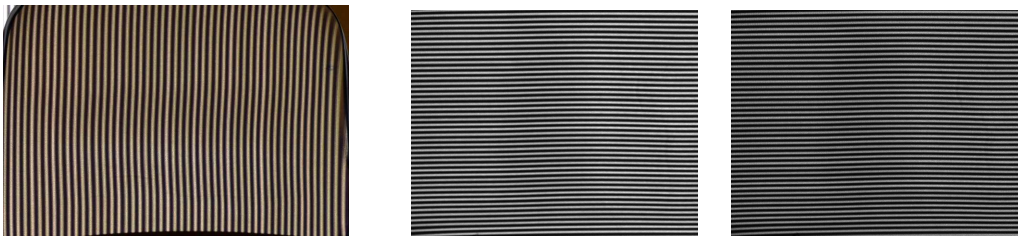

(a) Fringes projected on chair (b) sine fringes (c) cosine fringes

Figure 6.16: Experimental data. The fringe patterns (sine and cosine) were projected in the lab chair [fig (a)] and deformed fringe pattern recorded using camera are shown in (b) and (c).

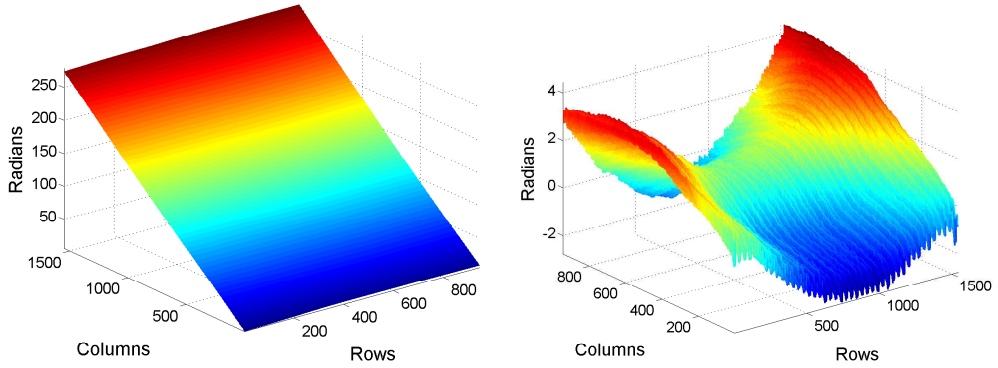

(a) Phase with Carrier (b) Phase without Carrier

Figure 6.17: Experimental results. (a) Estimated phase with carrier frequency and (b) without carrier frequency

object.

In summary, we propose a novel approach for generation of complex interference field in fringe projection profilometry and use of wrapped statistics based phase estimation algorithm for the estimation of phase from those complex fringes. The proposed approach (WKF) can estimate the phase from the interference pattern for a larger dynamic range. Our method gives better performances as compared to the state-of-the-art fringe analysis techniques. Simulations and experimental analysis advocates the possible application the proposed method in real-time scenarios. This work can also be taken forward to generate whole field 3D reconstruction by generating depth map of the object from different view points..

6.4 Thermal expansion study using DHI

Previous sections showed the application of signal tracking in different scenarios such as simultaneous estimation of phase and derivatives of arbitrary order, estimation of multiple components of phase using single record of reconstructed interference field, 3D reconstruction of the object shape via fringe projection profilometry. In this section, we discuss another application of the signal tracking approach using digital holographic interferometry for thermal expansion analysis of the surface. When the conducting material is heated at single point, the heat disperses through the object and that causes non-uniform expansion on the surface

of the object.

In present application, we used an Aluminium as the material for expansion study. The test object made up of Aluminium (2 mm in thickness) was clamped from four corners on the custom made mount at the optical table. The object was then illuminated by object beam generated from a laser source (He-Ne laser, 632.8nm), and the interference of scattered beam from the object with the reference beam generated from the same laser source was recorded by a CMOS sensor (DMK72BUC02 Imaging Source). The test object was heated using heating iron from backside of the object and the holograms were recorded at every 30 seconds during heating process. Recorded holograms were reconstructed to retrieve the complex object wave corresponding to the holograms. Reconstructed interference field was calculated, with first hologram as a reference state of the object, by multiplying current object wave-field with the complex conjugate of the reference object wave-field. Figure 6.18 shows the noisy reconstructed interference field, whereas figure 6.19 shows the 3D mesh plot of estimated phase map corresponding to one instance of the hologram recording after 5 minutes of heating the object.

From the Figure 6.18, we understand that the major requirements of the fringe analysis algorithm is to be able to handle severely corrupted fringe pattern, and at the same time it should be capable of handling larger dynamic range. The noisy interference field is processed using wrapped statistics based realisation of signal tracking approach for phase estimation. Figure 6.19 shows the estimated phase

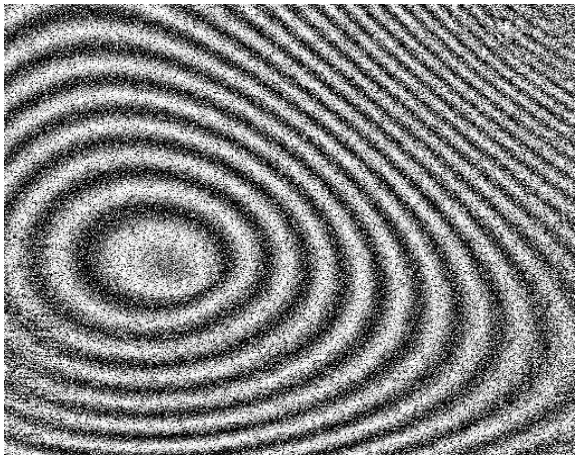

Figure 6.18: Experimental results for phase estimation using signal tracking approach

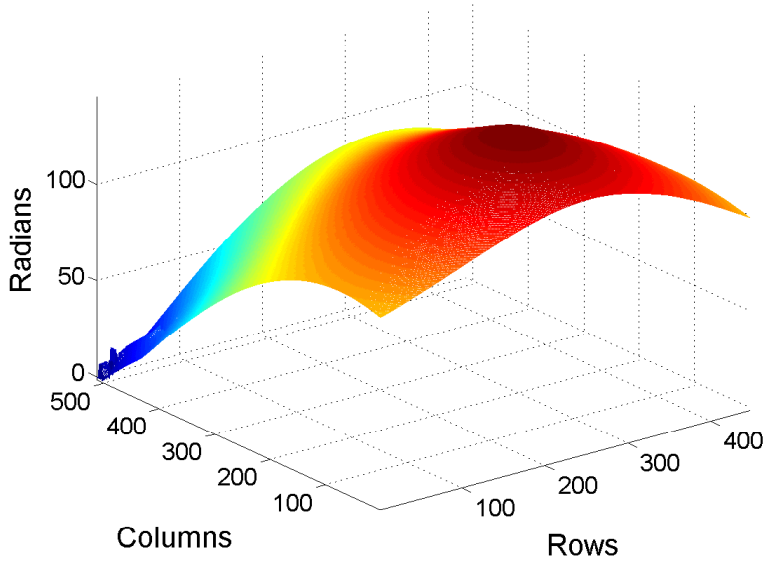

Figure 6.19: Experimental results for phase estimation using signal tracking approach

map using signal tracking approach. This proves the applicability and credibility of the proposed signal tracking approach as a fringe analysis in the real time environment, especially when the fringe pattern is extremely noisy and the underlying phase map is of larger dynamic range.

CHAPTER 7

Conclusions and Future Scope

The research work carried out in this thesis is mainly motivated by the requirement of development of an approach with the capability of handling larger dynamic range of the phase and severe noise in the interference field, simultaneously. The signal tracking approach proposed for fringe analysis has the potential to (1) estimate phase and phase derivatives simultaneously from the single record of interference field, and (2) handle extremely noisy fringes and produce an accurate, unwrapped and continuous phase map. It involves two important parts: State space model and Tracking algorithm. State space model is based on Taylor series expansion of phase map as state model and polar to Cartesian conversion as measurement model.

We have proposed and tested different tracking algorithmic frameworks for estimation of phase based on the proposed state space model. Our first choice of tracking algorithm was extended Kalman filter (EKF) owing to ease of implementation. It is observed that the EKF algorithm works effectively, even outperforms the state-of-the-art phase estimation algorithms, when the interference field is not corrupted by noise. It is capable of handling rapidly varying phase with larger dynamic range. Since EKF uses linearisation to linearise the non-linear measurement model, its performance gets affected when the measurements become noisy.

To overcome this issue, we explored to approximate the measurement model (non-linear polar to Cartesian conversion) by different techniques. We used sigma points (UKF) and randomly generated particles (PF) to approximate the non-linear transformation. It is observed that the UKF and PF framework based methods can handle extreme noise and larger dynamic range but separately. When the interference field is extremely noisy, and the underlying phase is rapidly varying with larger dynamic range, aforementioned approximation becomes unreliable.

In order to resolve this issue, we extended our state space model using the wrapped dynamical system as the measurement model instead of polar to Carte-

sian conversion based model. This, as against the our earlier work, bypasses the 2D non-linear rotating vector model and wrapped dynamical system are best approximated by wrapped Gaussian distribution. It was observed that the wrapped statistics based filter satisfied all of our goals providing the efficient solution of phase estimation problem when the interference fringes are extremely noisy and at the same time underlying phase map is having larger dynamic range. Since the state vector used for signal tracking approach consists of phase and phase derivatives components, proposed algorithms can be used for simultaneous estimation of phase and phase derivatives of arbitrary order from a single record of the reconstructed interference field, which are helpful for analysis of stress/strain, curvature and twist in the deformed objects.

Finally, we presented different applications of the proposed signal tracking approach such as multiple phase component estimation, 3D reconstruction of an object via fringe projection profilometry and estimation of phase for thermal expansion study. We demonstrated through thermal expansion study that the proposed approach makes the best suitable candidate for fringe analysis.

Further research needs to be focussed on applications of these algorithms for real-time applications in different interferometric methods such as InSAR phase unwrapping, demodulation of Radar echo, estimation of out-off plane and in plane deformation etc. Also. one can look into the inherent issues of Kalman filtering such as initialization of state vector, tuning of parameters etc., which keeps limitations on the performance of the state estimation algorithm. There is further need to model different parameters in the state space model such as object discontinuities, speckle noise, missing or unrecorded observations, amplitude variations. The research also can be diverted towards 360^o 3D reconstruction of the object using fringe projection profilometry, simultaneous surface topography and slope estimation in SAR interferometry, etc.

REFERENCES

1. Alvarez, A. S., Manuel, H. D., Santoyo, F. M., and Anaya, T. S. (2014a). Strain determination in bone sections with simultaneous 3d digital holographic interferometry. *Optics and Lasers in Engineering*, *57*, 101–108.

2. Alvarez, A. S., Manuel, H. D., Santoyoa, F. M., Tonatiuh, S., and Donato, R. R. (2014b). Simultaneous 3d digital holographic interferometry for strain measurements validated with fem. *Optics and Lasers in Engineering*, *52*, 178–183.

3. Arulampalam, M. S., Maskell, S., Gordon, N., and Clapp, T. (2002). A tutorial on particle filters for online nonlinear/non-gaussian bayesian tracking. *IEEE Trans. on Signal Processing*, *50*, 174–188.

4. Asundi, A., and Wensen, Z. (1998). Fast phase-unwrapping algorithm based on a gray-scale mask and flood fill. *Appl. Opt.*, *37*, 5416–5420.

5. Baldi, A. (2003). Phase unwrapping by region growing. *Appl. Opt.*, *42(14)*, 2498–2505.

6. Barbarossa, S., and Petrone, V. (1997). Analysis of polynomial-phase signals by the integrated generalized ambiguity function. *Signal Processing, IEEE Transactions on*, *45*, 316–327.

7. Barkat, B., and Boashash, B. (1999). Instantaneous frequency estimation of polynomial fm signals using the peak of the pwvd: statistical performance in the presence of additive gaussian noise. *Signal Processing, IEEE Transactions on*, *47*, 2480–2490.

8. Boashash, B. (1992a). Estimating and interpreting the instantaneous frequency of a signal – part 1: Fundamentals. *Proceedings of the IEEE*, *80(4)*, 520–538.

9. Boashash, B. (1992b). Estimating and interpreting the instantaneous frequency of a signal – part 2: Algorithms and applications. *Proceedings of the IEEE*, *80(4)*, 540–568.

10. Bone, D. J. (1991). Fourier fringe analysis: the two-dimensional phase unwrapping problem. *Appl. Opt.*, *30*, 3627–3632.

11. Chen, L., and Huang, C. (2005). Miniaturized 3d surface profilometer using digital fringe projection. *Measurement Science and Technology*, *16(5)*, 1061–1068.

12. Douc, R., and Cappé, O. (2005). Comparison of resampling schemes for particle filtering. In *Image and Signal Processing and Analysis, 2005. ISPA 2005. Proceedings of the 4th International Symposium on* (pp. 64–69). IEEE.

13. Fan, Z., Pang, H., Wang, W., and Ning, C. (2009). Three dimensional deformation measurements with digital holography. In *Image and Signal Proc., 2009. CISP '09. 2nd Intl. Cong. on* (pp. 1–5).

14. Flynn, T. (1996). Consistent 2-d phase unwrapping guided by a quality map. In *Geoscience and Remote Sensing Symposium, 1996. IGARSS'96.'Remote Sensing for a Sustainable Future, International,* (pp. 2057–2059). IEEE volume 4.

15. Flynn, T. J. (1997). Two-dimensional phase unwrapping with minimum weighted discontinuity. *J. Opt. Soc. Am. A*, *14(10)*, 2692–2701.

16. Fu, Y., and Luo, Q. (2011). Fringe projection profilometry based on a novel phase shift method. *Opt. Express*, *19*, 21739–21747.

17. Gal, J., Campeanu, A., and Nafornita, I. (2007). Estimation of chirp signals in gaussian noise by kalman filtering. In *ISSCS 2007*.

18. Gal, J., CAmpeanu, A., and NafornitA, I. (2008). Identification of polynomial phase signals by extended kalman filtering. In *EUSIPCO 2008*.

19. Ghiglia, D. C., and Pritt, M. D. (1998). *Two Dimensional Phase Unwrapping: Theory, Algorithms and Software*. John Wiley & Sons.

20. Ghiglia, D. C., and Romero, L. A. (1996). Minimum l p-norm two-dimensional phase unwrapping. *JOSA A*, *13*, 1999–2013.

21. Goldstein, R. M., Zebker, H. A., and Werner, C. L. (1988). Satellite radar interferometry: Two-dimensional phase unwrapping. *Radio science*, *23*, 713–720.

22. Gorthi, S. S., and Rastogi, P. (2009a). Estimation of phase derivatives using discrete chirp fourier transform based method. *Opt. Lett.*, *34*, 2396–2398.

23. Gorthi, S. S., and Rastogi, P. (2009b). Improved high-order ambiguity-function method for the estimation of phase from interferometric fringes. *Opt. Lett.*, *34*, 2575–2577.

24. Gorthi, S. S., and Rastogi, P. (2009c). Piecewise polynomial phase approximation approach for the analysis of reconstructed interference fields in digital holographic interferometry. *Journal of Optics A: Pure and Applied Optics*, *11*, 065405–065410.

25. Gorthi, S. S., and Rastogi, P. (2009d). Simultaneous measurement of displacement, strain and curvature in digital holographic interferometry using high-order instantaneous moments. *Opt. Express*, *17*, 17784–17791.

26. Gorthi, S. S., and Rastogi, P. (2010a). Fringe projection techniques: whither we are? *Optics and Lasers Eng.*, *48*, 133–140.

27. Gorthi, S. S., and Rastogi, P. (2010b). Phase estimation in digital holographic interferometry using cubic-phase-function based method. *Journal of Modern Optics*, *57*, 595–600.

28. Gutmann, B., and Weber, H. (2000). Phase unwrapping with the branch-cut method: Role of phase-field direction. *Appl. Opt.*, *39*, 4802–4816.

29. He, X., Sun, W., Zheng, X., and Nie, M. (2006). Static and dynamic deformation measurements of micro beams by the technique of digital image correlation. *Key Engineering Materials*, *26(3)*, 326–328.

30. Huang, M. J., and Sheu, W. (2005). Histogram-data-orientated filter for inconsistency removal of interferometric phase maps. *Optical Engineering*, *44(4)*, 1–11.

31. Hunt, B. R. (1979). Matrix formulation of the reconstruction of phase values from phase differences. *J. Opt. Soc. Am. A*, *69(3)*, 393–399.

32. Huntley, J. (1989). Noise-immune phase unwrapping algorithm. *Appl. Opt.*, *28(16)*, 3268–3270.

33. Immerkar, J. (1996). Fast noise variance estimation. *Computer Vision and Image Understanding*, *64*, 300–302.

34. Jiang, M., Chen, W., Zheng, Z., and Zhong, M. (2012). Fringe pattern analysis by s-transform. *Optics Communications*, *285*, 209–217.

35. Julier, S., and Uhlmann, J. (2004). Unscented filtering and nonlinear estimation. *Proc. of the IEEE*, *92*, 401–422.

36. Kalman, R. E. (1960). A new approach to linear filtering and prediction problems. *Transactions of the ASME–Journal of Basic Engineering*, *82*, 35–45.

37. Katkovnik, V. (1997). Nonparametric estimation of instantaneous frequency. *IEEE Trans. on Information Theory*, *43-1*, 183–189.

38. Kemao, Q. (2004). Windowed fourier transform for fringe pattern analysis. *Appl. Opt.*, *43*, 2695–2702.

39. Kemao, Q. (2015). Applications of windowed fourier fringe analysis in optical measurement: A review. *Optics and Lasers in Engineering*, *66*, 67–73.

40. Kitagawa, G. (1996). Monte carlo filter and smoother for non-gaussian nonlinear state space models. *Journal of Computational and Graphical Statistics*, *5*, 1–25.

41. Kulkarni, R., and Rastogi, P. (2014). Estimation of phase derivatives using discrete energy separation algorithm in digital holographic interferometry. *Opt. Lett.*, *39*, 3722–3724.

42. Lee, J.-S., Papathanassiou, K. P., Ainsworth, T. L., Grunes, M. R., and Reigber, A. (1998). A new technique for noise filtering of sar interferometric phase images. *IEEE Trans. on Geoscience and Remote Sensing*, *36*, 1456–1465.

43. Li, T., Bolic, M., and Djuric, P. M. (May 2015). Resampling methods for particle filtering: Classification, implementation, and strategies. *IEEE Signal Processing Magazine*, *32*, 70–86.

44. Li, Y., Zhu, J., and Shen, W. (2008). Phase unwrapping algorithms, respectively, based on path-following and discrete cosine transform. *Optik - International Journal for Light and Electron Optics*, *119(11)*, 545–547.

45. Lilley, F., Lalor, M. J., and Burton, D. R. (2000). Robust fringe analysis system for human body shape measurement. *Optical Engineering*, *39(1)*, 187–195.

46. Lim, H., Xu, W., and Huang, X. (1995). Two new practical methods for phase unwrapping. In *Geoscience and Remote Sensing Symposium, 1995. IGARSS'95.'Quantitative Remote Sensing for Science and Applications', International* (pp. 196–198). IEEE volume 1.

47. Liu, W. (2013). Auto term window method and its parameter selection. *Measurement*, *46*, 3113–3118.

48. Mardia, K. V., and Jupp, P. E. (1999). *Directional Statistics*. Wiley:New York, NY.

49. Moore, C. J., Burton, D. R., Skydan, O., Sharrock, P. J., and Lalor, M. (2006). 3d body surface measurement and display in radiotherapy part i: Technology of structured light surface sensing. In *Proc. International Conference on Medical Information Visualisation - BioMedical Visualisation* (pp. 97–102).

50. O'Shea, P. (2002). A new technique for instantaneous frequency rate estimation. *Signal Processing Letters, IEEE*, *9*, 251–252.

51. Palacios, F., Gonçalves, E., Ricardo, J., and Valin, J. L. (2004). Adaptive filter to improve the performance of phase-unwrapping in digital holography. *Optics communications*, *238*, 245–251.

52. Paul Kumar, U., Somasundaram, U., Kothiyal, M., and Krishna Mohan, N. (2013). Single frame digital fringe projection profilometry for 3-d surface shape measurement. *Optik - International Journal for Light and Electron Optics*, *124*, 166–169.

53. Peleg, S., and Friedlander, B. (1995). The discrete polynomial-phase transform. *Signal Processing, IEEE Transactions on*, *43*, 1901–1914.

54. Qian, K., Seah, H. S., and Asundi, A. (2005). Fault detection by interferometric fringe pattern analysis using windowed fourier transform. *Measurement Science and Technology*, *16*, 1582–.

55. Quan, C., Tay, C. J., He, X. Y., Kang, X., and Shang, H. M. (2002). Microscopic surface contouring by fringe projection method. *Optics and Laser Technology*, *34(7)*, 547–552.

56. Rajshekhar, G., Gorthi, S. S., and Rastogi, P. (2009). Strain, curvature, and twist measurements in digital holographic interferometry using pseudo-wigner ville distribution based method. *Review of Scientific Instruments*, *80*, –.

57. Rajshekhar, G., Gorthi, S. S., and Rastogi, P. (2010a). Estimation of displacement derivatives in digital holographic interferometry using a two-dimensional space-frequency distribution. *Opt. Express*, *18*, 18041–18046.

58. Rajshekhar, G., Gorthi, S. S., and Rastogi, P. (2010b). Estimation of the phase derivative using an adaptive window spectrogram. *J. Opt. Soc. Am. A*, *27*, 69–75.

59. Rajshekhar, G., Gorthi, S. S., and Rastogi, P. (2011a). Estimation of dynamically varying displacement derivatives using fringe projection technique. *Appl. Opt.*, *50*, 282–286.

60. Rajshekhar, G., Gorthi, S. S., and Rastogi, P. (2011b). Simultaneous multidimensional deformation measurements using digital holographic moiré. *Appl. Opt.*, *50(2)*, 4189–4197.

61. Rajshekhar, G., Gorthi, S. S., and Rastogi, P. (2012). Estimation of multiple phases from a single fringe pattern in digital holographic interferometry. *Opt. Express*, *20(2)*, 1281–1291.

62. Rajshekhar, G., and Rastogi, P. (2011). Application of complex-lag distributions for estimation of arbitrary order phase derivatives in digital holographic interferometry. *Opt. Lett.*, *36*, 3738–3740.

63. Rajshekhar, G., and Rastogi, P. (2012). *Phase Gradient Estimation Techniques in Fringe Analysis*. Ph.D. thesis EPFL, Lausanne.

64. Rajshekhar, G., and Rastogi, P. (2013). Phase estimation using a state-space approach based method. *Optics and Lasers in Engineering*, *51*, 1004–1007.

65. Sai Subrahmanyam, G. R. K. (2008). *Recursive Image Estimation And Inpainting In Noise Using Non-Gaussian MRF Prior*. Ph.D. thesis Indian Institute of Technology, Madras (India).

66. Schnars, U., and Japtner, W. P. O. (2002). Digital recording and numerical reconstruction of holograms. *Meas. Sci. Technol.*, *13*, R85–R101.

67. Schofield, M. A., and Zhu, Y. (2003). Fast phase unwrapping algorithm for interferometric applications. *Opt. Lett.*, *28*, 1194–1196.

68. Steinchen, W., Yang, L., Schuth, M., and Kupfer, G. (1995). Application of shearography to quality assurance. *Journal of Materials Processing Technology*, *52*, 141–150.

69. Sun, Y. (2009). Application of digital holography in displacement measurement. In *CISP '09. 2nd Intl. Cong. on* (pp. 1–5).

70. Takeda, M., Ina, H., and Kobayashi, S. (1982). Fourier-transform method of fringe-pattern analysis for computer-based topography and inteferometry. *J. Opt. Soc. Am.*, *43(1)*, 156–160.

71. Takeda, M., and Mutoh, K. (1983). Fourier transform profilometry for the automatic measurement of 3-d object shapes. *Appl. Opt.*, *22*, 3977–3982.

72. Traa, J., and Smaragdis, P. (2013). A wrapped kalman filter for azimuthal speaker tracking. *IEEE Signal Processing Letters*, *20*, 1257–1260.

73. Volkov, V., Zhu, Y., and De Graef, M. (2002). A new symmetrized solution for phase retrieval using the transport of intensity equation. *Micron*, *33*, 411–416.

74. Watkins, L. R., Tan, S. M., and Barnes, T. H. (1999). Determination of interferometer phase distributions by use of wavelets. *Opt. Lett.*, *24(13)*, 905–907.

75. Xia, X.-G. (Nov 2000). Discrete chirp-fourier transform and its application to chirp rate estimation. *IEEE Transactions on Signal Processing*, *48*, 3122–3133.

76. Xie, X., and Li, Y. (2014). Enhanced phase unwrapping algorithm based on unscented kalman filter, enhanced phase gradient estimator, and path-following strategy. *Appl. Opt.*, *53*, 4049–4060.

77. Xu, W., and Cumming, I. (1999). A region-growing algorithm for insar phase unwrapping. *IEEE Trans. on Geoscience and Remote Sensing*, *37(1)*, 124–134.

78. Yagnik, J., Gorthi, S. S., Ramakrishnan, K. R., and Rao, L. K. (2007). 3d shape extraction of human face in presence of facial hair: A profilometric approach. In *Proc. IEEE Region 10 Annual International Conference*.

79. Yaroslavsky, L. (2007). Space-variant and adaptive transform domain image restoration methods. *Advances in Signal Transforms*, (pp. 201–240).

80. Yen, H., Tsai, D., and Yang, J. (2006). Full-field 3-d measurement of solder pastes using lcd-based phase shifting techniques. *IEEE Trans. on Electronics Packaging Manufacturing*, *29(1)*, 50–57.

81. Zappa, E., and Busca, G. (2008). Comparison of eight unwrapping algorithms applied to fourier-transform profilometry. *Optics and Lasers in Engineering*, *46(2)*, 106–116.

82. Zhong, J., and Weng, J. (2004). Spatial carrier-fringe pattern analysis by means of wavelet transform: wavelet transform profilometry. *Appl. Opt.*, *43*, 4993–4998.

83. Zhou, X., Yang, T., Zou, H., and Zhao, H. (2012). Multivariate empirical mode decomposition approach for adaptive denoising of fringe patterns. *Opt. Lett.*, *37*, 1904–1906.

APPENDIX A

Parameter Estimation from the State Vector

In polynomial phase approximation approach (i.e., parameter estimators) used for state-space based approach, the phase is approximated by second order polynomial. The phase polynomial with a_2, a_1, a_0 being coefficients of the polynomials is represented as:

$$\phi(n) = a_2 n^2 + a_1 n + a_0 \tag{A.1}$$

By differentiating the phase polynomial shown in equation A.1, we get

$$\phi'(n) = 2a_2 n + a_1 \tag{A.2}$$

$$\phi''(n) = 2a_2 \tag{A.3}$$

Now, for state space based approaches, we combine these equations along with the amplitude term $\mathbf{A}(n)$ to form the state vector $x[n] = \begin{bmatrix} \mathbf{A}(n) & \phi(n) & \phi'(n) & \phi''(n) \end{bmatrix}$.

At the initial condition (or for first pixel of column/row), i.e., n=0, we get

$$\phi(0) = a_0$$

$$\phi'(0) = a_1$$

$$\phi''(0) = 2a_2$$

Above equations along with amplitude $\mathbf{A}(n)$ of the interference field, above equations can be represented in the matrix form as:

$$\begin{bmatrix} \mathbf{A}(n) \\ \phi(0) \\ \phi'(0) \\ \phi''(0) \end{bmatrix} = \begin{bmatrix} 1 & 0 & 0 & 0 \\ 0 & 1 & 0 & 0 \\ 0 & 0 & 1 & 0 \\ 0 & 0 & 0 & 2 \end{bmatrix} \begin{bmatrix} \mathbf{A}(n) \\ a_0 \\ a_1 \\ a_2 \end{bmatrix}$$

i.e.,

$$\mathbf{x}(0) = C^{-1}\theta(n)$$

where, $\theta(n) = \begin{bmatrix} a_0 & a_1 & a_2 \end{bmatrix}^T$ represents the parameter vector. Hence, we can write the parameter vector in relation with initial state vector $\mathbf{x}(n)$ as:

$$\theta(n) = C\mathbf{x}(0) \tag{A.4}$$

where $C = \begin{bmatrix} 1 & 0 & 0 & 0 \\ 0 & 1 & 0 & 0 \\ 0 & 0 & 1 & 0 \\ 0 & 0 & 0 & 0.5 \end{bmatrix}$, i.e. a diagonal matrix with elements 1, 1, 1, 0.5.

Now, current state (i.e., $\mathbf{x}(n)$ is back-propagated to initial condition using inverse of state transition matrix. The process update equation $\mathbf{x}(n) = \mathbf{F}\mathbf{x}(n-1)$ is written as:

$$\mathbf{x}(n-1) = \mathbf{F}^{-1}\mathbf{x}(n) \tag{A.5}$$

The initial state vector is, then, written as

$$\mathbf{x}(0) = \mathbf{F}^{-n}\mathbf{x}(n) \tag{A.6}$$

Finally, we combine equations A.4 and A.6 that derives the relation between current state vector and the parameters of the phase polynomial, which is then used to reconstruct the phase map. The relation is represented as:

$$\theta(n) = C\mathbf{F}^{-n}\mathbf{x}(n) \tag{A.7}$$

LIST OF PAPERS BASED ON THESIS

Papers in Refereed Journals

1. **Rahul G. Waghmare**, Deepak Mishra, Sai Subrahmanyam G. R. K., Earu Banoth, and Sai Siva Gorthi., "Signal tracking approach for phase estimation in digital holographic interferometry," *Appl. Opt.*, **53(19)**:4150–4157, 2014.

2. **Rahul G. Waghmare**, P. Ram Sukumar, Sai Subrahmanyam G. R. K., Rakesh Kumar Singh, and Deepak Mishra, "Particle-filter-based phase estimation in digital holographic interferometry", *J. Opt. Soc. Am. A*, **33(3)**:326–332, 2016.

3. **Rahul G. Waghmare**, Deepak K Mishra, and Sai Subrahmanyam G. R. K., "Wrapped Statistics based Phase Retrieval form Interference Fringes", *J. Mod. Opt*, Taylor & Francis, **63**:1384-1390, 2016

Presentations in Conferences

1. **Rahul G. Waghmare**, Deepak K. Mishra and Sai Subrahmanyam G. R. K. "UKF based Multicomponent Phase Estimation in Digital Holographic Moiré," *4^{th} national conference on Computer Vision, Pattern Recognition, Image Processing and Graphics (NCVPRIPG 2013), In proceedings*, 2013.

2. **Rahul G. Waghmare**, Deepak Mishra, Sai Subrahmanyam G. R. K.and Sai Siva Gorthi. "Extended kalman filter based phase estimation in digital holographic interferometry," *Eighth international conference on signal and image processing (ICSIP 2014), In proceedings*, 2014. (won **the Best Paper** award)

3. **Rahul G. Waghmare**, Deepak Mishra, Sai Subrahmanyam G. R. K. "Signal tracking approach for simultaneous estimation of phase and instanta-

neous frequency," *Signal Processing, Informatics, Communication and Energy Systems (SPICES), 2015 IEEE International Conference on*, 1:5, 19-21 Feb. 2015

4. **Rahul G. Waghmare**, Deepak K. Mishra and Sai Subrahmanyam G. R. K. "Signal Tracking Approach based Phase Estimation for Analysis of Thermal Expansion by Digital Holographic Interferometry", in *Imaging and Applied Optics 2016*, OSA Technical Digest (online) (Optical Society of America, 2016), paper JW4A.15.